

University of Nottingham
UK | CHINA | MALAYSIA

Interpretation of Small Specimen Creep Test and Recommendations on Standardisation of Impression Creep Test Method

Charles N. C. Dyson, BEng (Hons)

Thesis submitted to the University of Nottingham for the degree of Doctor of Engineering

September 2018

Abstract

In-service monitoring of power plant components toward later stages of plant life requires several methods for evaluation. Strain monitoring, metallography and ultrasonic techniques are the most common for inspection. Sampling and mechanical testing are novel techniques that can be used alongside the tools mentioned above. Sampled material is mechanically tested using non-standard small specimens, generating creep data for components that operate in the creep range. Non-standard small specimen creep test methods include sub-size uniaxial, small punch, impression, small ring and two bar creep test techniques.

The impression creep test is the focus of this thesis, consisting of a square specimen loaded by a flat-ended rectangular indenter, of which the recommended dimensions are 10x10x2.5mm. Conversions to equivalent uniaxial creep strain and stress are obtained through reference stress techniques. 'Round Robin' testing between several independent labs using different test rig set-ups has been used to provide feedback for the progression to standardization of the test technique. It is also shown how the test method can be used to determine the creep strength of high temperature components. Furthermore, the test method is used to characterise pre-strained materials at several strain levels to assess the impact on creep strength.

Scoop sampling is integral to using the small samples for component risk management. Therefore, the impact of sampling on the component is assessed using creep continuum damage mechanics, a by product of which was the development of two new test specimens along with a novel validation method for the material model.

Progress has been made on the standardisation of the impression creep test technique, with recommendations made based on the analysis in this thesis. A procedure for creep strength determination of components is suggested and component-sampling tolerances are outlined too based on finite element analysis.

List of Publications

1 C. Dyson, W. Sun, C. J. Hyde, S. J. Brett and T. H. Hyde (2016) Use of small specimen creep data in component life management: a review, Materials Science and Technology, 32:15, 1567-1581, DOI: 10.1080/02670836.2015.1132536

2 C. Dyson, W. Sun, S. J. Brett, T. H. Hyde, C. J. Hyde, J. Shingledecker and D. Purdy (2016) Impression creep testing and its role in component integrity management, Proceedings of 8th Int. Conf. On Advances in Materials Technology for Fossil Power Plants, Oct 11-14, Albufeira, Portugal, pp 517-530

3 S. J. Brett, C. Dyson, D. Purdy, J. Shingledecker, J. Rantala, J. Eaton-Mckay and W. Sun (2017) Impression creep test of a P91 steel: a round robin programme, Materials at High Temperatures, Vol. 35, No. 6, 529–534 DOI: 10.1080/09603409.2017.1410330

4 S. J. Brett, C. Dyson **,** A. Bridges, S. Maskill, W. Sun Pre-straining effect on the creep behaviour of impression creep tests for a P91 steel at 600^{o}C (to be submitted)

Acknowledgements

I would firstly like to thank my supervisors Professor Wei Sun, Dr Chris Hyde and Dr James Rouse, without whom this thesis would have not been possible in the slightest. I would also like to thank the retired Professor Tom Hyde for his advice and support during the early stages of my project.

The centre for Carbon Capture, Storage and Cleaner Fossil Energy (CCSCFE) for making this project possible under its materials development theme. Its partnership with the Engineering and Physical Sciences Research Council provided primary financial support to my project and so both bodies deserve my thanks. The CCSCFE doctoral training programme gave me a firm grounding in knowledge of the energy sector allowing for a broad understanding of the impact of my research and its position in the wider world. Links with the Biomass and Fossil Fuel Research Alliance (BF2RA) allowed for their industrial input and financial support, along with opportunities to network during their annual energy science lectures.

I would also like to extend my thanks to the staff at the Materials Division at EPRI (Dr John Shingledecker, Daniel Purdy and Alex Bridges), who have offered continuous support throughout the duration of my studies through our regular correspondence and experimental participation. Further to that, the industrial support of Dr Steve Brett who provided meaningful practitioners advice and helped drive a significant portion of the work. AMEC FW and VTT Technical Research Centre also deserve thanks for the provision of their test data and feedback about their test rigs and procedures.

For the majority of my experimental work I have none other than Shane Maskill to thank for his technical assistance and expertise, his flexibility helped greatly when I was not quite sure where to extract my specimens from. The technical staff in the Wolfson Building and NMRC offered training in analysis techniques and so are deserving of thanks too.

Finally but yet importantly, I have to thank my friends and family who offered much needed emotional support outside of working hours and offered an energy release in the form of sporting activities when I needed it.

Nomenclature

A_f	Area on which force acts
a	Major axis dimension of small ring creep test
a_p	Receiving hole radius, small punch test
B	Kachanov creep damage law material constant
B'	Replacement material constant in Norton's law, for small punch conversion
b	Minor axis dimension of small ring creep test
b_i	Length of impression specimen
b_t	Bar width, two bar specimen
C	Monkman-Grant constant
C_{LM}	Constant in the Larson-Miller relationship
D	Diameter of small punch specimen
D_{LM}	Liu-Murukami damage law constant
D_r	Reference multiplier in the reference stress method
d_i	Width of impression creep indenter
d_{GL}	Diameter of gauge length of sub-size uniaxial specimen
E	Young's modulus, material stiffness constant
F	Applied force
G	Shear modulus
GL	Gauge length of sub-size uniaxial specimen
h	Thickness of impression specimen
I_x	Second moment of area about x-axis
K	Plastic hardening multiplier
K_{sp}	Small punch correlation factor
k	Dimension of two bar specimen
k_1	Constant in Wilshire equations
k_s	Pipe system loading factor
l	Gauge length
l_e	Small specimen equivalent gauge length
n	Norton and creep damage law stress exponent
M_x	Applied moment about x-axis

m	Plastic hardening exponent
m_1	Creep time hardening exponent
P	Applied load
P_{LM}	Larson-Miller parameter
p	Liu-Murakami creep damage law material constant
$\bar{p}$	Impression creep mean indenter pressure
Q^*_c	Apparent activation energy in Wilshire equations
q_2	Liu-Murakami creep damage law material constant
R	Ideal gas constant
R_s	Radius of small punch ball/hemispherical punch head
R_i	Pipe inner radius
R_o	Pipe outer radius
S_{ij}	Deviatoric stress tensor
T	Temperature
t_0	Initial thickness of small punch specimen
t_f	Time to failure
u	Constant in Wilshire equations
w	Width of impression specimen
α	Scaling factor in the reference stress method
α_m	Multiaxiality constant
β	Reference stress parameter
$\dot{\Delta}$	Displacement rate
$\dot{\Delta}_{ss}$	Steady-state displacement rate
Δ^c	Creep displacement
Δ_i	Initial displacement
Δl	Change in gauge length
Δ_t	Total displacement
δ_{ij}	Kronecker deltta
ε	Uniaxial strain
$\dot{\bar{\varepsilon}}^{pl}$	Equivalent plastic strain rate
ε_{ij}	Strain tensor
ε_{tr}	Transverse strain

ε_t	True strain
$\dot{\varepsilon^c}$	Creep strain rate
ε^c	Creep strain
$\dot{\varepsilon_0}$	Initial creep strain rate
η	Reference stress parameter
γ	Shear strain
λ	Plastic hardening coefficient
ν	Poisson's ratio
σ	Applied stress
$\sigma_1, \sigma_2,$	
σ_3	Principal stresses
σ_{AX}^{A}	Allowable axial stress
σ_{AX}^{CE}	Closed end axial stress
σ_{AX}^{MAX}	Maximum axial stress
σ_{eq}	von Mises equivalent stress
σ_{ij}	Stress tensor
σ_{MDH}	Mean diameter hoop stress
σ_{nom}	Nominal stress
σ_{ref}	Reference stress
σ_{UTS}	Ultimate tensile stress
σ_y	Yield stress
τ	Shear stress
τ_{max}	Maximum shear stress
Φ	Plastic strain rate ratio
φ	Failure plane angle
χ	Kachanov damge law material parameter
Ω	Omega method material creep damage susceptibility parameter
ω	Creep damage parameter

Contents

Abstract i

List of Publications ii

Acknowledgements iii

Nomenclature iv

Chapter 1 1

Introduction 1

1.1 Background 1

1.2 Aim and Objectives 3

1.3 Layout 3

Chapter 2 5

Theoretical Background and Literature Review 5

2.1 Introduction 5

2.2 Constitutive Equations 7

2.2.1 Elasticity 7

2.2.2 Material Yield 9

2.2.3 Plasticity and Hardening 10

2.2.4 Creep 12

2.3 Non-standard Small Specimen Creep Testing 18

2.3.1 Currently Used Small Specimen Creep Test Methods 20

2.3.2 Data Conversion 28

2.4 Current Practice Using Small Specimen Data for Power Plant Components 32

2.4.1 General Procedure 32

2.4.2 Main Applications – How to Use the Small Specimen Data 40

2.4.3 Current Practice 43

2.4.4 Applications in Life Management: Case Studies 44
2.4.5 Representative Examples 45
2.4.6 The Need for Standardisation of Impression Creep Testing 49
2.5 Concluding Remarks 50
Chapter 3 52
Methodology 52
3.1 Experimental Methodology 52
3.1.1 Mechanical Testing 52
3.1.2 Electron Backscatter Diffraction (EBSD) 57
3.2 Modelling Methodology 58
3.2.1 Materials Constants Determination 58
3.2.2 Numerical Simulations 58
Chapter 4 60
Round Robin Impression Creep Testing 60
4.1 Introduction 60
4.2 Impression Creep Test and Basic Requirements 61
4.2.1 Impression Creep Test Using a Rectangular Indenter 61
4.2.2 Basic Requirements 62
4.3 Round Robin Impression Creep Test Programme 65
4.3.1 Background and Motivation 65
4.3.2 Material and Test Conditions 65
4.3.3 Equipment Specifications 66
4.3.4 Test Results 68
4.4 Discussion 72
4.4.1 Data Variation and Applicability 72
4.4.2 Requirement for Future Extension Life of Power Plant Components 72

4.5 Conclusions....74
Chapter 5....80
Pre-Straining Effect on the Creep Behaviour of Impression Creep Tests for a P91 Steel at 600°C....80
5.1 Background/Motivation....80
5.1.1 Small Scale Creep Testing – Impression & Small Punch....81
5.1.2 P91 Steel – Normal and Aberrant Microstructural Conditions and Implications for Operating Power Plant....82
5.2 Material and Experimental Set-Up....83
5.2.1 Material and Heat Treatment....83
5.2.2 Large Uniaxial Specimen and Hot Tensile Testing....84
5.2.3 Removal of Impression Specimen and Creep Test Conditions....85
5.3 Experimental Results....86
5.3.1 Uniaxial Tensile Test at 600°C....86
5.3.2 EBSD and Hardness Mapping of Tested Tensile Specimen....88
5.3.3 Impression Creep Tests at 600°C Using Un-Strained and Pre-Strained Specimens....89
5.4 Modelling of Large Uniaxial Tensile Test....91
5.4.1 Finite Element Modelling of the Uniaxial Tensile Test....91
5.5 Discussion....94
5.5.1 Capability of Impression Creep Testing....94
5.6 Conclusions....95
Chapter 6....97
Scooping Effect of Power Plant Pipes Using Continuum Damage Mechanics....97
6.1 Introduction....97
6.2 Materials and Method....100
6.2.1 Material Composition....100

6.2.2 Material Behaviour Model 100
6.2.3 Pipe Geometry and Loading 102
6.2.4 FE Modelling 104
6.2.5 Life Prediction 105
6.3 Preliminary Results 105
6.3.1 Illustrative Behaviour 105
6.3.2 Parametric Behaviour 106
6.4 Validation of Pipe Results 110
6.4.1 FE Simulations 110
6.4.2 Experimental Testing 116
6.5 Discussion 119
6.6 Conclusions 121
Chapter 7 122
Discussion, Conclusions and Future Work 122
7.1 Discussion 122
7.1.1 Small Specimen Creep Testing and Life Management 122
7.1.2 Pre-Straining and Impression Creep Testing 124
7.2 Conclusions 125
7.3 Future Work 125
References 127
Appendix 138

List of Figures

Figure 1: Graphical representation of the Tresca and von Mises Yield surfaces in 3 dimensions 10
Figure 2: Stress- strain curve for examples of real and modelled behaviour 11
Figure 3: Schematic of creep behaviour 12
Figure 4: Ashby map of creep mechanisms [5].....13
Figure 5: (a) Time hardening model with increasing stress, strain interpolation is vertical and (b) strain hardening model with decreasing stress, strain interpolation is horizontal 14
Figure 6: Shapes and dimensions of small creep test specimens: (a) conventional sub-size uniaxial specimen (GL≈5-12mm; d_{GL}≈1-3mm); (b) Small punch creep test specimen (D≈8mm; t_0≈0.5mm); (c) Impression creep test specimen (w≈ 10mm; b_i≈ 10mm; d_i≈ 1mm, and depth b_o≈ 2mm); (d) elliptical small ring creep test (a≈ 15mm, b≈ 7.5mm, d≈ 1mm; h≈ 2.5mm); (e) two bar specimen (L_0≈ 13mm, b_t≈ 2mm, D_i≈ 5mm and k≈ 6.5mm) adapted from [13].....21
Figure 7: Schematics of small specimen loading modes, adapted from [13] 21
Figure 8: (a) Comparison of impression creep strain rate data to that of uniaxial data for 316 stainless steel at 600°C and 2.25CrMo weld metal at 640°C [21] (b) Creep deformation of impression creep tests for the 0.5Cr0.5Mo0.25V steel at 565°C [22].....23
Figure 9: (a) Typical small punch curves from the fine grained heat affected zone (FGHAZ), the weld material (WM), the coarse grained heat affected zone (CGHAZ), service exposed material (SE) and the base/parent material (BM) of a 9Cr1Mo1V weldment under the same test conditions, 250N, 600°C (b) Uniaxial and small punch weld metal rupture tis 600°C [32].....26
Figure 10: Schematic diagram illustrating the use of FE analysis to obtain reference parameters [26].....29
Figure 11: Scoop sampling in progress [52] 33
Figure 12: (a) Tested impression specimen (width w ≈ 10mm) [64], (b) tested elliptical ring specimen (major axis, a ≈ 20mm) [65], (c) ruptured small punch

specimen (diameter $D \approx 8$mm) [37] and (d) ruptured two bar specimen (length, $L_0+2k \approx 26$mm) [65]....38
Figure 13: (a) Minimum creep strain rate data for P91 steel at 650°C, small ring test and (b) two bar test creep rupture data alongside uniaxial for P91 steel at 600°C [65]....38
Figure 14: Minimum creep strain rate corresponding to mean and lower bound [88] strength levels at 600°C....46
Figure 15: Distribution of impression creep strength of specimens (a) as-sampled (b) corrected to start of life [18]....47
Figure 16: Blade root, with specimens removed by spark erosion and (b) Log-log plot of stress as a function of minimum strain rate, for a small ring and uniaxial tests at 800°C [34]....48
Figure 17: Wilshire plot for time to rupture as a function of stress for CMSX-4. SP represents small punch, alongside uniaxial data [61]....49
Figure 18: (a) Impression creep specimen dimensions and (b) loading arrangement....52
Figure 19: Twin screw impression creep test rig....53
Figure 20: Specimen removal locations (top) and detailed drawing of specimen....54
Figure 21: Square specimens without notch....56
Figure 22: Schematic of specimen drawings showing notch types, circular (left) elliptical (right)....56
Figure 23: Micro hardness tester used....57
Figure 24: Nottingham stepped stress test results BAR 257 along with loads in MPa at each step....69
Figure 25:Converted impression strain rates (i.e. into equivalent uniaxial strain rate) from all labs at 600°C against the converted applied stress, with the strain rate predicted using the ECCC grade 91 mean and mean -20% minimum strain rate (determined from rupture data), where ImpMG is the Impression Monkman-Grant curve....70
Figure 26: Maximum strain rate fluctuation at 600°C averaged from all stress levels evaluated here....71

Figure 27: Converted strain rates for all labs at 104 MPa and 600°C, showing a general decreasing trend across the final 100 hrs for the 104 MPa test step.(t/te = time over time to the end of the step)....71
Figure 28: Impression creep (IC) traces at 118MPa....73
Figure 29: EPRI stepped stress results....75
Figure 30: Nottingham stepped stress results alternative rig....75
Figure 31: VTT stepped stress results....76
Figure 32: AMEC stepped stress results....76
Figure 33: 89MPa step impression creep (IC) strain comparison....77
Figure 34: 98 MPa step impression creep (IC) strain comparison....77
Figure 35: 104MPa step impression creep (IC) strain comparison....78
Figure 36: 98Mpa strain rates....78
Figure 37: 118MPa strain rates....79
Figure 38: Best fit and calibration line for future test rigs and standard deviations at each stress level....79
Figure 39: Top left impression specimen, top right impression loading arrangement, bottom left small punch specimen and bottom right small punch loading arrangement....82
Figure 40: Oversize uniaxial specimen (dimensions in mm)....84
Figure 41: Engineering and true strain curves for aberrant material at 600°C..87
Figure 42: Engineering and true strain curves for martensitic material at 600°C....87
Figure 43: Hardness map of failed aberrant specimen (left) and SEM-EBSD images showing granular distortion orientation map (right)....88
Figure 44: Impression creep test results for pre-strained P91 at 600°C a) indentation traces and b) equivalent creep strain rates....89
Figure 50: Martensitic pre-strain indentation cases....90
Figure 51: Martensitic strain rates....90
Figure 47: Un-deformed uniaxial mesh and boundary conditions....92
Figure 48: Study used to select the appropriate mesh....93
Figure 49: Plastic equivalent strain contours....93
Figure 50: Tensile test at 600°C and true vs engineering strain finite element results and power law fitting....94

Figure 49: Derivation of the phi parameter for aberrant and martensitic cases at 98MPa 600°C 95
Figure 52: FE Model and Boundary Conditions 104
Figure 53: Life estimations, comparison of different methods. 106
Figure 54: a), b) Geometric effects on failure life 107
Figure 55: Life reduction caused by different loadings, cut depth h=3mm 109
Figure 56: Accumulated damage (ω) due to extent of loading 109
Figure 57: FE model set-ups for spherical and elliptical specimens 110
Figure 58: Liu and Murakami model fitting to P91 uniaxial data at 600C 112
Figure 59: Specimen Notch sensitivities 113
Figure 60: (Top) Angles and orientation of failure plane (Bottom) Example plot θ = 45° 114
Figure 61: Fit of failure plane dependence 116
Figure 61: Elliptical notch top and spherical notch bottom 116
Figure 63: Segment taken from Alicona measurements of spherical dimple 117
Figure 64: Fourier transform of surface roughness of spherical dimple 117
Figure 64: Creep rupture tests for the P91 notched bars at 600°C 118
Figure 66: Comparison of Experimental and modelling failure times alpha 0.288 118
Figure 66: Model and specimen failure 140MPa (net section stress), aspect ratio a/b = 1.6 alpha 0.288. 119
Figure 68: Generic procedure for component life assessment according to EPRI [48], with stage incorporating small specimen testing. 123

CHAPTER 1
INTRODUCTION

1.1 BACKGROUND

Power plants and chemical plants that operate at elevated temperature will have components that are susceptible to failure due to a mechanism referred to as creep, the time dependant deformation of materials subjected to a load. Specially designed materials have been developed in order to resist the deformation usually by the inclusion of alloying elements that form precipitates within the metal matrix serving as barriers in order to reduce the rate of deformation. These materials are used to construct high temperature steam carrying components, which subject them to extreme thermal and mechanical loading conditions. Chrome is usually used as an alloying element providing strength and corrosion resistance, for example it has been used as an alloying element in P22 and CrMoV ferritic steels used in boiler components and steam pipelines. More advanced steels include 9CrMo and a more successful steel the modified version P91. Grade 91 is part of the class of steels referred to as creep strength enhanced ferritic (CSEF) steels, which apart from including more chromium as a weight percentage, have MX type carbo-nitride precipitation due to inclusions of (V,Nb and N) and have been heat treated by quenching and tempering so that they have a martensitic microstructure rather than a ferritic one. This allows for the construction of components with smaller wall thicknesses than the ferritic steels but with equal creep resistance and increased thermal loading resistance due to reduced thermal gradients within the structures. Further to that are grade 92 steels which have an even greater creep strength and are the candidate steels to be used in advanced power plants with ultra-supercritical steam conditions (temps > 600^{o}C).

Throughout the life of the plant as the material degrades it tends to form cavities, micro cracks and then fully fledged macro cracks, at which point catastrophic failure would occur. It is therefore the structural engineer's job to correctly judge

damage levels so that they do not reach dangerous levels or predict at which point they may occur. This is done through periodic checks of the components over the lifetime of the plant by consistently monitoring the component strain and plant temperatures and pressures. Non-destructive methods of evaluation include strain monitoring of the components using strain gauges to judge creep ductility and the use of ultrasound or x-rays for crack detection. A power plant consists of thousands of components, which can be narrowed down and prioritised for inspection due to the severity of the conditions that they experience. However the components that undergo these conditions are still plentiful including hundreds of metres of main steam and hot reheat pipelines as well as high temperature headers containing many branches. Further filtering is needed if management of the components is to be done in a safe and economical manner. Mechanical testing of small specimens using scoop samples serves to address this problem. The samples are removed non-invasively from the surface of the component, taking advantage of the excess material usually present in the thickness of the component (as per design codes). This may leave behind a notch and a potential site for a stress riser, which may be reduced by polishing and deburring the sampled region. One of the test methods that is ready for widespread commercial use is the impression creep test method, which has demonstrated by the ability to produce equivalent secondary minimum creep strain rates. Therefore it has been used successfully in ranking power plant pipeline materials by creep strength [1]. Minimum requirements of the test rigs and settling down of test dimensions and a reference material need to be decided if the material is to be a standalone test. The impression creep test along with other small specimen creep tests have the potential to be used alongside other tools to assess component vulnerability and solidify any ambiguity in assessment results.

1.2 AIM AND OBJECTIVES

The overall aim of the work is to aid in the reduction of metallurgical risk of failure for ageing power plant components. For which the specific objectives are:

1] The development of a power plant material, component and service database (CrMoV or P91 or P22);

2] The development of a small specimen creep test database (impression creep tests);

3] The development of improved theoretical data interpretation methods;

4] The implementation of an experimental programme for validation/demonstration purposes (possibly Gr 91 and Gr 22 steels);

5] The development of a recommendation for standardization of the impression creep test method;

6] The development of a ranking, remnant life management/assessment methodology for power plant applications.

1.3 LAYOUT

This thesis begins with a general theoretical background pertaining to creep and small specimen creep testing methods and their conversion parameters, chapter 2. A general introduction into the current state of small specimen test techniques and their use in the power plant industry is discussed. Chapter 3 includes the experimental and modelling methodologies used in this work including all test specimens and test rigs used. The theoretical background of the models used in this work are described along with an explanation as to why they were used instead of similar models available. Chapters 4 and 5 include the work done to standardise the impression creep test through collaboration with industrial partners, and then discussed how the technique fits within a general power plant life management framework as a metallurgical risk reduction procedure. The later chapter includes application of impression creep testing to pre-strained materials. Chapter 6 is an outline of the scoop sampling procedure of power plant straight pipes and the resulting damage that may be incurred during sampling, a guide is presented as to how much material may be removed taken from

continuum damage mechanics modelling. The discussion, conclusions and future work sections then round off the thesis in Chapter 7.

CHAPTER 2
THEORETICAL BACKGROUND AND LITERATURE REVIEW

2.1 INTRODUCTION

A general mechanical background is introduced in this chapter as a basis for the description for models used in subsequent chapters. Fundamental equations of elasticity and plasticity are described in their static forms and then for the description of high temperature components rate dependant plasticity is described, also referred to as creep.

Creep is a time dependant phenomenon where materials deform under stress when operating at high temperatures for extended periods. The situation in many countries is that the coal fired power plants operate well beyond their design lives (~25 years). For example the last dedicated coal fired plant in the UK was built over 40 years ago [2]. In these time frames, creep damage becomes a significant and dominant failure mode for high temperature components. Due to the current economic climate the extension of the life of plants is in demand, especially in a manner that allows the continued operation of an examined component using, non-destructive testing methods. Small specimen testing is a 'non-invasive' test technique that is realised through the testing of material taken from small, button-shaped scoop samples obtained from in-service components. The tests are still in the process of development and refinement but have attracted attention owing to their abilities to produce minimum creep strain rate and creep rupture data from small amounts of material compared to full size uniaxial tests. The associated test techniques and the data interpretation methods however rely on comparisons with uniaxial test data for validation. Current tests still depend on some form of uniaxial data tested on a material or component of choice, although in some cases once the data is obtained the small specimen creep tests can then operate independently using the uniaxial data as a

reference point. Due to the small amounts of material required, small specimens have the potential to be used in novel alloy development [3], [4].

The ability to extract mechanical data from a non-destructive test is unmatched by any other life management method, hence the requirement for small specimen methods. This chapter reviews the methods currently employed for the use of small specimen testing in life management, prediction and remaining life assessment. Power plant steels mentioned in this study are detailed in Table 1.

2.2 CONSTITUTIVE EQUATIONS

2.2.1 Elasticity

The basis of structural mechanics modelling hinges on the concept of stress and strain. At room temperature when a material is mechanically loaded it first undergoes a linear response in tension/compression which is referred to as the elastic part of loading because once the load is removed from the material it should return to its original shape provided it has not exceeded its yield point or fractured (non-ductile materials). In a uniaxial condition the resulting stress σ on the system can be calculated using the well-known relationship:

$$\sigma = \frac{F}{A_f} \qquad (2.1)$$

where F is the force applied and A_f is the area on which it acts, the resulting strain ε:

$$\varepsilon = \frac{\Delta l}{l_0} \qquad (2.2)$$

l_0 is the original gauge length of the bar/material and Δl is its change in length. The relationship between stress and strain also known as Hooke's law in a uniaxial condition with then determine the materials stiffness or Young's Modulus (E) to give:

$$E = \frac{\sigma}{\varepsilon} \qquad (2.3)$$

Given an isotropic uniaxial bar in tension loaded elastically the material will elongate and its cross section will contract according to the materials poisson's ratio ν, where

$$\nu = -\frac{\varepsilon_{tr}}{\varepsilon} \qquad (2.4)$$

ε_{tr} is the transverse strain. So far the stiffness and deformation have been discussed in a manner where the loading is axial, if the material is loaded in any other way such that it may exhibit shear, the extent of deformation is determined by another material property referred to as the shear modulus G:

$$G = \frac{\tau}{\gamma} \qquad (2.5)$$

where, τ and γ are the shear stress and strain respectively, the shear modulus and the bulk modulus are related by :

$$G = \frac{E}{2(1+\nu)} \quad (2.6)$$

Using the basic concepts outlined above a more generalised formulation of the concept of elastic stress and strain can be elucidated, so that it may be applied effectively in 3 dimensions. So that the stress and strain tensors can be represented as symmetric matrices:

$$\sigma_{ij} = \begin{pmatrix} \sigma_{11} & \sigma_{12} & \sigma_{13} \\ \sigma_{21} & \sigma_{22} & \sigma_{23} \\ \sigma_{31} & \sigma_{32} & \sigma_{33} \end{pmatrix} \quad (2.7)$$

$$\varepsilon_{ij} = \begin{pmatrix} \varepsilon_{11} & \varepsilon_{12} & \varepsilon_{13} \\ \varepsilon_{21} & \varepsilon_{22} & \varepsilon_{23} \\ \varepsilon_{31} & \varepsilon_{32} & \varepsilon_{33} \end{pmatrix} \quad (2.8)$$

The 'i' and 'j' subscripts represent the face and the direction respectively. The diagonal components in the matrices can be referred to as the principal components of the tensor meaning they act normal to faces on which they sit as opposed to forces acting parallel to faces, which represent shear components. Hooke's law can then be generalised for an isotropic material to calculate each component in the strain tensor:

$$\varepsilon_{11} = \frac{1}{E}[\sigma_{11} - \nu(\sigma_{22} + \sigma_{33})], \qquad \varepsilon_{12} = \frac{(1+\nu)}{E}\sigma_{12} \quad (2.9)$$

$$\varepsilon_{22} = \frac{1}{E}(\sigma_{22} - \nu(\sigma_{11} + \sigma_{33})], \qquad \varepsilon_{23} = \frac{(1+\nu)}{E}\sigma_{13}$$

$$\varepsilon_{33} = \frac{1}{E}[(\sigma_{33} - \nu(\sigma_{11} + \sigma_{22})], \qquad \varepsilon_{23} = \frac{(1+\nu)}{E}\sigma_{23}$$

The symmetry in the strain tensor means that the 6 shear strain components are mirrored and so expressions for only three are needed. The suite of equations can be compressed even further to make one general neat expression:

$$\varepsilon_{ij} = \frac{1}{E}\left[(1+\nu)\sigma_{ij} - \nu\delta_{ij}\sigma_{kk}\right] \quad (2.9)$$

Where $\sigma_{kk} = \sigma_{11} + \sigma_{22} + \sigma_{33}$ and δ_{ij} is the kronecker delta and is described as :

$$\delta_{ij} = \begin{cases} 0 & i \neq j \\ 1 & i = j \end{cases} \quad (2.10)$$

σ_m is the hydrostatic stress obtained by taking the average of the trace of the stress tensor ($\frac{\sigma_{kk}}{3}$). The key material properties therefore are the Young's Modulus and the Poisson's ratio, with these two parameter it is possible to predict the elastic deformation of materials in any stress state. The component of the stress tensor that determines the mode of deformation is the deviatoric stress 'S_{ij}', which is found by subtracting the hydrostatic stress from the stress tensor.

$$S_{ij} = \sigma_{ij} - \frac{1}{3}\sigma_{kk}\delta_{ij} \quad (2.11)$$

2.2.2 **Material Yield**

For isotropic ductile materials, which are the materials studied in this thesis, with increased load magnitude the material will exceed its linear elastic response at a critical stress i.e. the yield stress 'σ_y'. From this point onwards the material deforms in a non-linear manner and the strain on the material starts to become unrecoverable. This is the state referred to as plasticity, in this non-linear region there is excessive deformation for a relatively small increase in stress as compared to the elastic region. Calculating the material yield in a multiaxial stress state can be done by one of two methods, the Tresca yield criterion, which states that a material shall yield once the maximum shear stress exceeds a limiting value, which is the uniaxial yield stress such that,

$$\tau_{max} = \frac{\sigma_1 - \sigma_3}{2} \quad (2.12)$$

where σ_1, σ_2 and σ_3 are the principal stresses acting on the system and $\sigma_1 > \sigma_2 > \sigma_3$, according to the criterion the material will yield if

$$\sigma_1 - \sigma_3 \geq \sigma_y \quad (2.13)$$

The second criterion is the von Mises yield criterion, which states that a material will yield if the maximum shear strain energy per unit volume is exceeded. The equivalent stress σ_{eq} according to this criterion can be calculated as:

$$\sigma_{eq} = \frac{1}{\sqrt{2}}\sqrt{(\sigma_{11} - \sigma_{22})^2 + (\sigma_{22} - \sigma_{33})^2 + (\sigma_{11} - \sigma_{33})^2 - 6(\sigma_{12}^2 + \sigma_{23}^2 + \sigma_{13}^2)} \quad (2.14)$$

as well as predicting whether the material will yield this criterion is also effective in determining the magnitude and location of the critical stress in the system. The principal shear components are represented by the τ symbol in the above

relationship. If plotted on the principal stress coordinate system, the shape of the yield surfaces according to both criteria can be visualised. They fall on the π plane, also known as the deviatoric plane, as this is the plane through which the deformation/shear stresses act as seen in Figure 1. The von Mises yield criterion can be described using principal stresses as $(\sigma_1 - \sigma_2)^2+(\sigma_2 - \sigma_3)^2+(\sigma_3 - \sigma_1)^2 \geq 2\sigma_y^2$.

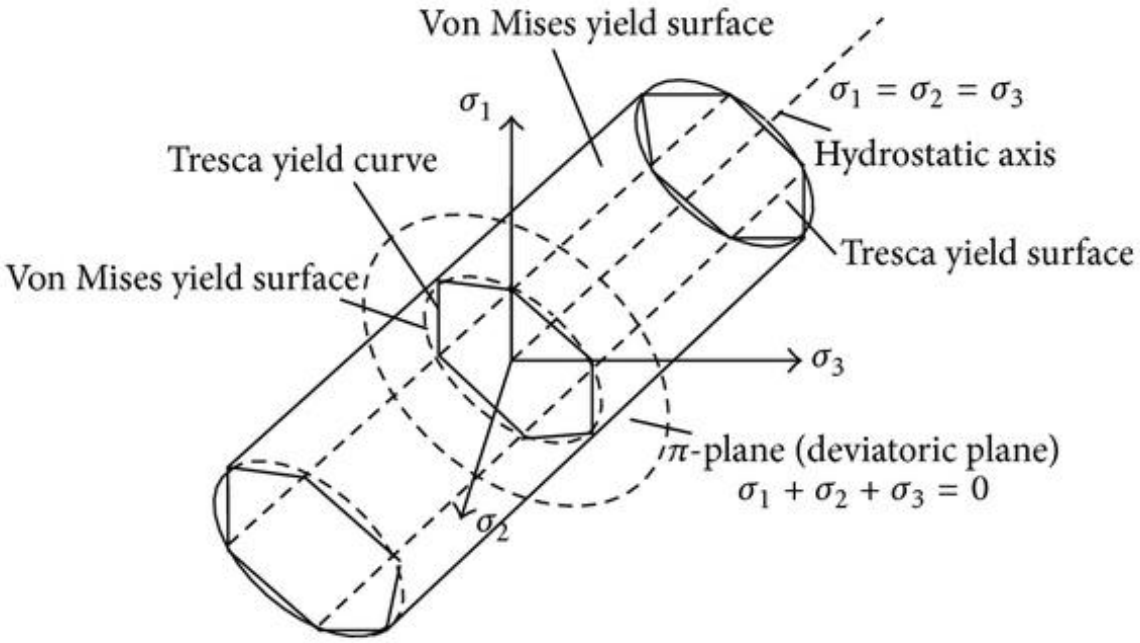


Figure 1: Graphical representation of the Tresca and von Mises Yield surfaces in 3 dimensions [5]

2.2.3 **Plasticity and Hardening**

Once the material has exceeded its yield state, in the case of all ductile isotropic materials the behaviour is non-linear and differs based on material, temperature and rate of loading. On a structural level, the lattice has transformed from being stretched to the physical movement of dislocations (irregularities in the lattice structure) and the local shear of atoms as they slide past each other. This has an effect on the poissons ratio of the material which in an elastic state is around 0.3 but increases to 0.5 during plasticity which alludes to the fact that although the material is elongating it still occupies the same space (constant volume). Material behaviour models in this case can only approximate the true material behaviour. A schematic of the stress and strain of a real uniaxially loaded bar shows the elastic and plastic portions, along with graphical models that attempt to

represent the real behaviour, Figure 2. The graphical models represent the different approaches to interpreting the theory of plasticity.

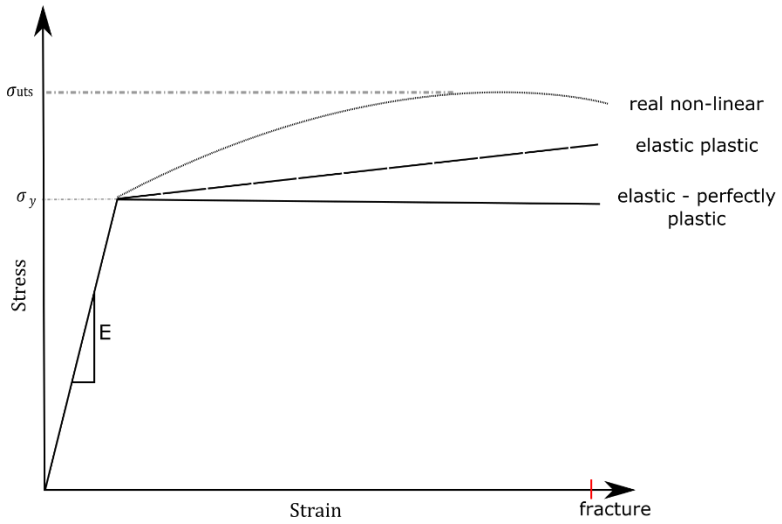


Figure 2: Stress- strain curve for examples of real and modelled behaviour

According to the theory of plastic flow in order for a material to continue to deform a uniform load must be applied to it which is scaled according to the momentary plastic strain. The stress required to maintain plastic flow is known as the flow stress and is an important concept in non-linear material behaviour. According to Reuss it is directly proportional to the plastic strain increment:

$$d\varepsilon_{ij}^{p} = S_{ij}\mathrm{d}\lambda \qquad (2.15)$$

ε_{ij}^{p} is the plastic strain accumulated in the direction of the deviatoric stress tensor and scaled by the hardening coefficient λ which is recalculated at every increment in strain. For an elastically perfectly plastic material λ would be assumed to be constant and so a horizontal plastic region would be observed.

Once the material has reached its maximum load carrying capacity (ultimate tensile strength 'σ_{UTS}') deformation after this point in an engineering sense will be due to a reducing stress, this is due to the necking phenomenon, where the cross-sectional area of the specimen starts to reduce in a localised area and a notch starts to form. The true stress in that region is actually higher than the engineering stress. The relationship between the engineering stress and strain can be easily derived.

$$\varepsilon_t = \int_{l_0}^{l_t} \frac{dl}{l} = \ln\left(\frac{l_t}{l_0}\right) = \ln\left(\frac{\mathrm{A}}{A_0}\right) = \ln(1+\varepsilon_{eng}) \qquad (2.16)$$

And the true stress σ_t:

$$\sigma_t = \sigma_{eng}(1 + \varepsilon_{eng}) \tag{2.17}$$

These relationships hold up until the ultimate tensile stress of the material from which point the material is said to obey the simple isotropic hardening law:

$$\sigma_t = K\varepsilon_t^m \tag{2.18}$$

The constants *K* and *m* can be obtained by taking the logs of the true stress-strain curve and taking the intercept and gradient respectively. As the material is loaded to failure the strain in the necked region of a uniaxial sample will be non-uniform, as the ratio of cross-sectional area is reduced the strain is increased and so for a perfectly ductile material that would neck until a point the strain in that region would theoretically be infinite.

2.2.4 **Creep**

The phenomenon of creep is a time dependant process that occurs to materials subject to loading at temperatures greater than $\sim 0.3T_{melt}$(T in K). The result is unrecoverable deformation which occurs in three distinct phases, primary, secondary and tertiary. At constant stress primary is characterised by a decreasing rate of strain, which leads to secondary, the longest phase, during which a constant rate of strain occurs and finally tertiary creep where the rate increases and the material eventually fails, Figure 3.

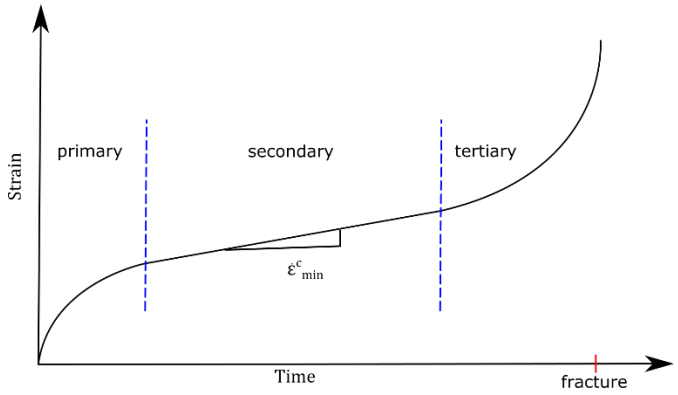


Figure 3: Schematic of creep behaviour

In ductile materials the phenomenon occurs by two general mechanisms, diffusion and dislocation creep, Figure 4 [6]. Diffusion creep occurs at lower

stresses and is temperature dependant - at lower temperatures it occurs through the diffusion of vacancies through the materials lattice subsequently distorting the grains, at higher temperatures it occurs through grain boundary sliding also known as coble creep. At higher stresses, which is the focus of most engineering work, creep occurs through the movement of dislocations (irregularities in lattice) via glide and climb down a stress gradient. Climb of dislocations refers to the movement of dislocations past barriers within the lattice which usually come in the form of interstitials and inclusions.

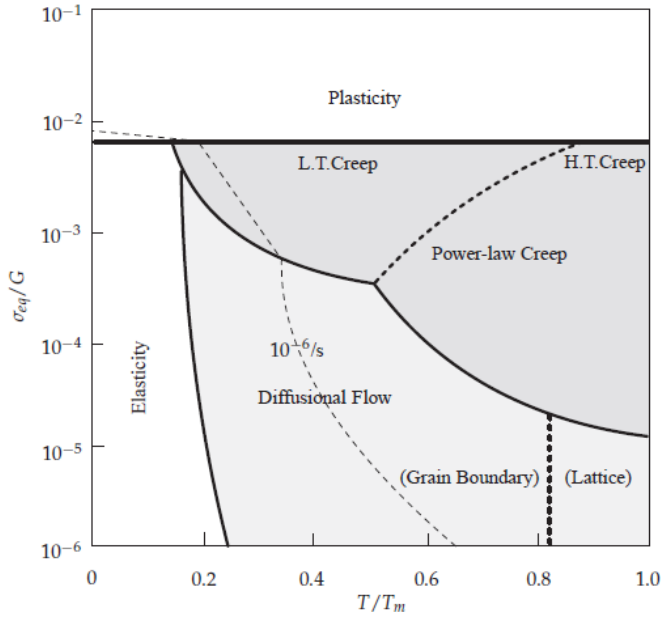


Figure 4: Ashby map of creep mechanisms [6]

As can be seen in the map, increasing stress tends to deformation which is closer to the deformation mechanisms present in plasticity i.e. local shear stress dominated dislocation movement. The stress used also has an impact on the failure mechanism incurred. Higher stress will tend towards ductile fracture, showing signs of transgranular fracture, necking and weak to no void nucleation. This is primarily due to the strain induced damage brought about by the higher stresses. The lower stresses bring about lower strains at failure, but generally fail by a brittle mode, characterised by intergranular fracture which is driven by the coalescence and nucleation of voids at the grain boundaries [7]. Voids, link up to form micro and then macro cracks at points of stress concentration.

2.2.4.1 Steady State Creep

During dislocation creep the material obeys a power law relationship which has been described by Norton and Bailey as:

$$\dot{\varepsilon^c} = A\sigma^n \tag{2.19}$$

A and *n* are temperature dependant materials constants and can be determined through isothermal testing of the candidate material. As creep is a time dependant phenomenon a function of time may be added to give:

$$\dot{\varepsilon^c} = A\sigma^n t^{m_1} \tag{2.20}$$

This relationships holds for a system with constant stress, however in cases where there may be a change in stress, a time hardening model may be adopted (Equation 2.21). The strain rate at the change in stress state will be taken from the strain rate of the new stress at the equivalent time interval to give:

$$\dot{\varepsilon^c} = A\sigma^n m_1 t^{m_1 - 1} \tag{2.21}$$

An alternative is the strain hardening model [8], where the new strain rate will be taken from point of equivalent strain in the new stress level:

$$\dot{\varepsilon^c} = A^{\frac{1}{m_1}} \sigma^{\frac{n}{m_1}} m_1 (\varepsilon^c)^{(m_1-1)/m_1} \tag{2.22}$$

A graphical comparison of the two models can be seen in Figure 5. In practice a combination of the two approaches may be used i.e. combined hardening.

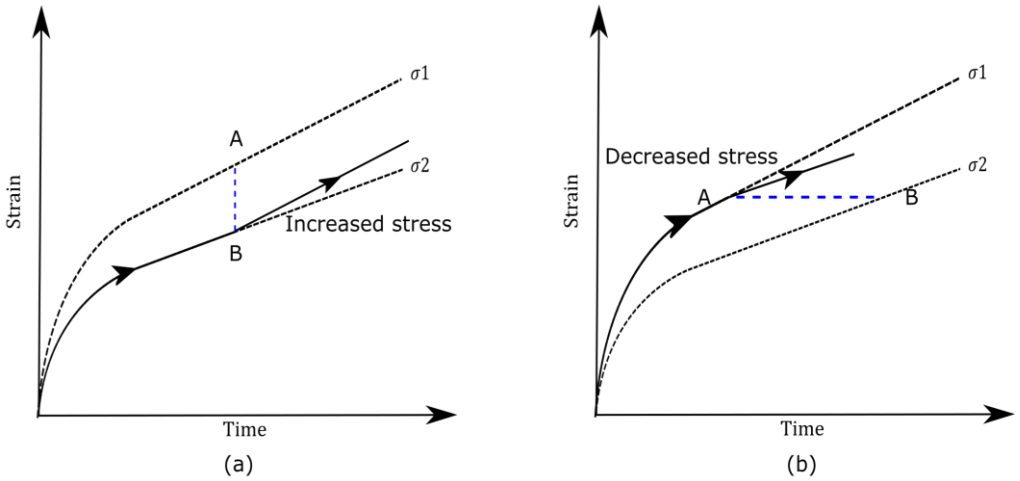


Figure 5: (a) Time hardening model with increasing stress, strain interpolation is vertical and (b) strain hardening model with decreasing stress, strain interpolation is horizontal

A more general formulation of the Norton-Bailey law can be derived from the application of the flow rule to creep deformation where the material satisfies the constant volume requirement:

$$\varepsilon_{11} + \varepsilon_{22} + \varepsilon_{33} = 0 \tag{2.23}$$

and so the increment in the creep strain tensor according to the flow rule is given as:

$$d\varepsilon_{ij}^{c} = \frac{\partial \psi}{\partial \sigma_{ij}} d\lambda \tag{2.24}$$

where ψ is the plastic potential function and λ as for plasticity is hardening constant that changes during loading history and is related to the scalar equivalent strain. The partial derivative of the plastic potential function and the stress tensor is the deviatoric and the plastic potential function may be related to the equivalent stress by $\psi = 2/3\ \sigma_{eq}$ which leads to the expression for the creep strain rate tensor:

$$d\dot{\varepsilon}_{ij}^{c} = {}^{3}/_{2}\, d\varepsilon_{eq}^{c}\ \frac{S_{ij}}{\sigma_{eq}} \tag{2.25}$$

applying the Norton-Bailey constants gives:

$$\varepsilon_{ij}^{c} = {}^{3}/_{2}\, A\ \frac{S_{ij}}{\sigma_{eq}^{n}} \tag{2.26}$$

A and *n* have their usual meanings.

2.2.4.2 Creep Failure and Continuum Damage Mechanics

The steady state models effectively model the relationship between strain hardening and recovery during creep, but fail to incorporate any form of material degradation and hence fail to model the tertiary stages of creep and eventual failure. What results is an infinitely long secondary stage. It was Kachanov and with further additions by Rabotnov [9] who were first to incorporate the effects of material degradation during creep, by introducing a damage parameter into the model. The material damage is modelled on the accumulation of voids within the material which is associated with a reduction in surface area through which the normal stress is applied. The damage parameter ω is described as the ratio of the area of the voids A to the total area A_0:

$$\omega = 1 - \frac{A}{A_0} \tag{2.27}$$

and the rate of damage according to Kachanov and Robotnov in uniaxial form is:

$$\frac{d\omega}{dt} = B\frac{\sigma_{eq}^{\chi}}{(1-\omega)^{\chi}}t^{m_1} \tag{2.28}$$

where B, m_1 and χ are temperature dependant constants. The rate of damage is driven by the magnitude of the equivalent stress and is coupled to the creep strain rate via:

$$\frac{d\varepsilon^{c}}{dt} = A\frac{\sigma_{eq}^{n}}{(1-\omega)^{n}}t^{m_1} \tag{2.29}$$

where A and n are the Norton constants and are determined in the same way. The multiaxial formulation as presented by Leckie and Hayhurst [10]:

$$\frac{d\omega}{dt} = B\frac{\sigma_{r}^{\chi}}{(1-\omega)^{\chi}}t^{m_1} \tag{2.28}$$

creep strain rate tensor :

$$\frac{d\varepsilon_{ij}^{c}}{dt} = \frac{3}{2}A\frac{\sigma_{eq}^{n}}{(1-\omega)^{n}}\frac{S_{ij}}{\sigma_{eq}}t^{m_1} \tag{2.29}$$

The damage rate is a function of the rupture stress rather than equivalent stress; it is a combination of the maximum principal stress and the equivalent stress. The relative influence of the two stress components is determined by a material parameter α_m, which represents the materials triaxiality and varies from 0 to 1 such that:

$$\sigma_r = \alpha_m\sigma_1 + (1-\alpha)\sigma_{eq} \tag{2.30}$$

Integrating the uniaxial damage rate equation between the bounds of zero time and time to rupture and solving for the time to rupture gives:

$$t_r = \frac{1}{B(\chi+1)\sigma_{eq}^{\chi}} \tag{2.31}$$

Constants B and χ may then be determined from uniaxial rupture data. The α_m value is determined by conducting a Bridgman notch test to failure and then simulating the test using the finite element method using the known values of A, n, B and χ, derived from uniaxial tests until an α_m value that gives a failure time the same as the experimental value is found [11]. The time to rupture equations can be used along with the steady state analysis in life prediction, by finding the rupture stress using equation 2.30 and replacing the equivalent stress with the

rupture stress in equation 2.31 to give an estimate of failure life in multiaxial stress states [11].

The Kachanov- Robotnov equations have limitations in their formulation, to reach a damage value of 1 when the rate must have an infinite gradient and so the maximum damage is often capped to ~0.99 to induce failure [12]. Stress concentrations also result in lengthy computational times which is again due to the damage rate gradient being extremely large inducing tiny time increments and stress sensitivity [13]. This problem was addressed by Liu and Murakami [14] who removed the damage term from the denominator of the creep strain equations and placed it with an exponential function derived from micromechanical creep crack development theory, so that the creep strain rate would be expressed in its general form as:

$$\frac{d\varepsilon_{ij}^{c}}{dt} = \frac{3}{2} A \sigma_{eq}^{n} \frac{S_{ij}}{\sigma_{eq}} \exp\left[\frac{2(n+1)}{\pi\sqrt{(1+3/n)}} \left(\frac{\sigma_1}{\sigma_{eq}}\right) \omega^{3/2}\right] \tag{2.32}$$

and the damage term was modified so that:

$$\frac{d\omega}{dt} = D_{LM} \frac{(1 - e^{q_2})}{q_2} \sigma_r^{p} e^{q2\omega} \tag{2.33}$$

integrating using the same procedure as for the Kachanov-Robotnov equations gives the relationship for time to rupture:

$$t_{rLM} = \frac{1}{D_{LM} \sigma_r^{p}} \tag{2.34}$$

The Liu-Murakami equations are better suited to crack growth problems than the Kachanov equations [13] due to decreased stress localisation and mesh dependence and so are used in this work.

2.3 NON-STANDARD SMALL SPECIMEN CREEP TESTING

Small specimen creep testing methods have gained a lot of interest in recent years due to the need to use small samples of simple geometry to produce rupture data and aid in the remnant life assessment of high temperature components. They mainly consist of the conventional sub-size uniaxial creep test, the impression creep test, the small punch creep test, the small ring test and the two bar test, all shown in Figure 6 [15].

Table 1: Standard power plant steels (BS EN 10216-2) by composition (mass %) and creep rupture strength. [79]

Steel name		C	Si	Mn	P	S	Cr	Mo	Ni	Al	Cu	Nb	Ti	V	100000h Creep rupture strength 600°C (MPa)
Standard	**Colloquial**														
14MoV6-3	0.5CrMoV	0.10-0.15	0.15-0.35	0.40-0.70	0.025	0.010	0.30-0.60	0.50-0.70	≤0.30	≤0.04	≤0.30	…	…	0.22-0.28	41
10CrMo9-10	P22(2.25CrMo)	0.08-0.14	≤0.5	0.3-0.7	0.02	0.01	2.00-2.50	0.90-1.10	≤0.30	≤0.04	…	…	…	…	35
X10CrMoVNb9-1	P91	0.08-0.12	0.20-0.50	0.30-0.60	0.02	0.005	8.0-9.5	0.85-1.05	≤0.40	≤0.02	≤0.30	0.06-0.10	≤0.01	0.06-0.1	90

2.3.1 **Currently Used Small Specimen Creep Test Methods**

2.3.1.1 Conventional Sub-size Creep Test

The conventional sub-size creep test is essentially a miniaturised conventional 'uniaxial' creep test specimen. The size of the specimen is limited, due to the size of the scoop samples which are removed via non-invasive scoop sampling of power plant components comprising low alloy steels e.g. 0.5CrMoV, 2.25CrMo. Scoop samples are typically oval hemispheres with dimensions 30x20x3mm. Depending on the mean grain size of the test material the diameter of the gauge region of the test specimen may vary between 1-3mm in diameter with a 5-12mm gauge length [16]. A typical full size uniaxial specimen may have a 5-10mm gauge diameter and 30-50mm gauge length [17]. Once the preliminary cylinder is machined (Figure 6 a), in order for loading to be applied to the specimen, grips must be electron or laser beam welded to the top and bottom surfaces of the cylinder [18], [19]. These welding methods are used in order to reduce the size of the heat-affected zone. The dimensions of the specimen warrant this in order for creep mechanisms to occur primarily in the base material, effectively minimising the effects of welds. Due to the elevated temperatures and stresses during testing, samples may require the use of an inert atmosphere within the test furnace, because the impact of oxidation may be magnified on small samples. A comparison has been made which confirms that in an argon-rich environment the creep curves compare more favourably with those of conventional full size uniaxial specimens [20].

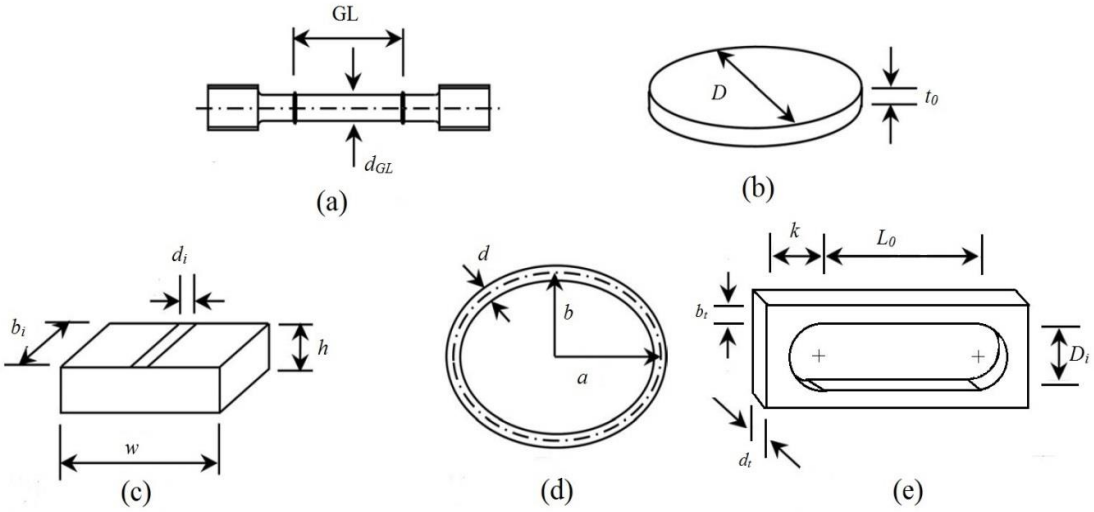


Figure 6: Shapes and dimensions of small creep test specimens: (a) conventional sub-size uniaxial specimen (GL≈5-12mm; d_{GL}≈1-3mm); (b) Small punch creep test specimen (D≈8mm; t_0≈0.5mm); (c) Impression creep test specimen (w≈ 10mm; b_i≈ 10mm; d_i≈ 1mm, and depth b_o≈ 2mm); (d) elliptical small ring creep test (a≈ 15mm, b≈ 7.5mm, d≈ 1mm; h≈ 2.5mm); (e) two bar specimen (L_0≈ 13mm, b_t≈ 2mm, D_i≈ 5mm and k≈ 6.5mm) adapted from [15].

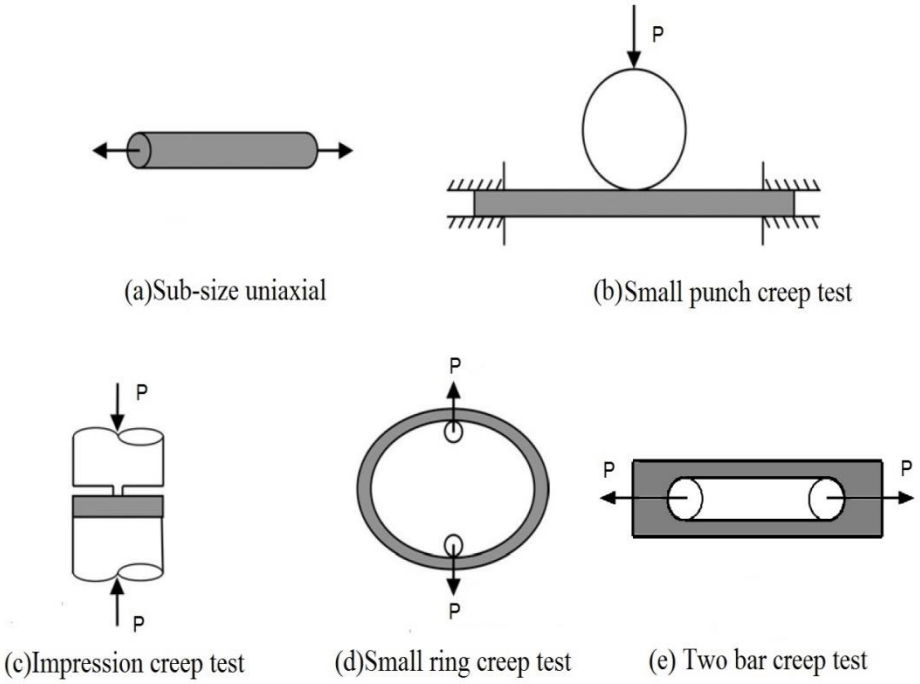


Figure 7: Schematics of small specimen loading modes, adapted from [15]

These miniature specimens are also able to produce the full creep strain curve including time to rupture and data conversion is simple as geometries and loading are the same, but considering the complexity of the manufacturing process can be costly to manufacture in comparison to other small test

specimens. The size of the specimen as with all small specimens means that finer load and temperature control are required in comparison to full size specimens to achieve the same level of repeatability. In particular the alignment of the loading arrangement is known to be a problem and may cause unwanted bending stresses [18].

2.3.1.2 Impression Creep Test Method

In the impression creep test, a 10x10x2.5mm specimen loaded by a rectangular indenter of width d_i = 1mm [21]. Where material is scarce an 8x8x2mm specimen can be used that is loaded by a d_i = 0.8mm wide indenter [22]. The indenter and specimen are defined by three ratios, *w/di, w/bi* and *h/di* as seen in Figure 6c which allows for the scaling down of the specimen size [23]. The test is compressive in nature and is only able to produce primary and secondary stages of the traditional creep curve reliably, so crucially, it is not able to produce rupture data directly. Where the impression strain rate can be shown to be the same as the uniaxial minimum creep strain rate obtained under equivalent test conditions, rupture times can be extrapolated to indirectly, using the Monkman-Grant correlation and uniaxial rupture times, expanded on later, sect 3.2.1. Due to the simplicity of the specimen geometry, preparation is relatively easy, although careful consideration must be made in grinding the contact surfaces of the specimen so as to remove any machining marks and reduce any residual stresses [24]. Furthermore the indenter must be made of a material of higher creep strength than the test material, so that creep occurs predominantly in the specimen. The aim is to maximise contact with the indenter of the specimen so it would be beneficial to have an indenter that extends across the full width of the specimen. Since the test has been used extensively to test low alloy ferritic 0.5CrMoV and high chromium martensitic P91 pipework , nickel based superalloy indenters have commonly been used to load the specimen [25] although it has been shown a ceramic indenter can also be used [26]. Tests are usually performed at constant load and constant temperature. Important data obtainable from the test are the mean indenter pressure $\bar{p}$ which can be can be

converted to the corresponding uniaxial stress σ by the reference stress approach [27]

$$\sigma = \eta\bar{p} \tag{2.35}$$

and the creep displacement Δ^c which can be converted to the uniaxial creep strain ε^c

$$\varepsilon^c = \frac{\Delta^c}{\beta d_i} \tag{2.36}$$

where η and β are conversion constants or "reference parameters" and d_i is the indenter width. Bd_i is the equivalent gauge length of the specimen, which will be expanded on later, and is the relation used to relate the geometry of the impression creep test specimen to that of a uniaxial specimen. The conversion factors allow for the comparison of the minimum creep strain rate in Figure 8a [28]. Although the test does not produce rupture data it has other benefits in that once a steady state displacement rate is reached, the load or temperature levels can be altered on a single specimen to produce multiple sets of minimum creep strain rate data from the same test specimen [25], (Figure 8b[29]). The indentation depth into the specimen should be shallow compared to the specimen thickness (<10%) and indenter width (hence the name impression) and the contact area must be large enough so that the region undergoing creep

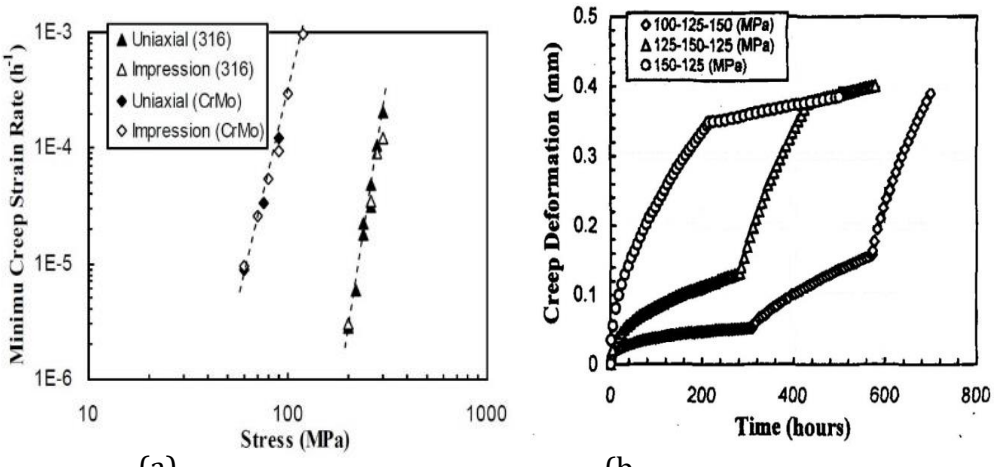


Figure 8: (a) Comparison of impression creep strain rate data to that of uniaxial data for 316 stainless steel at 600°C and 2.25CrMo weld metal at 640°C [21] (b) Creep deformation of impression creep tests for the 0.5Cr0.5Mo0.25V steel at 565°C [22].

consists of enough grains so as to ensure that bulk properties can be obtained [23].

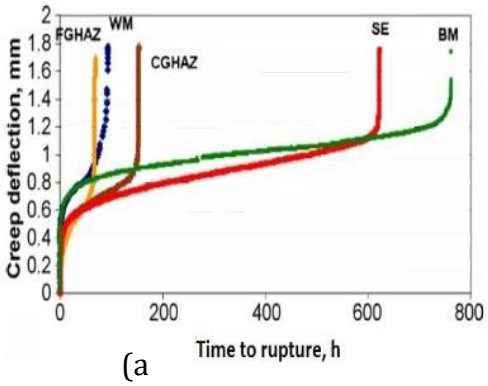
2.3.1.3 Small Punch Creep Test

Similar to the impression creep test, small punch creep test samples are of a simple geometry and are relatively easy to manufacture out of samples scooped from in-service components. Specimens are generally machined and mechanically polished, sometimes with diamond[30], to achieve a surface finish. The test specimen is a disc of diameter D = 8-10mm and thickness $t_0 \approx$ 0.2-0.5mm and is centrally loaded by a hemispherical punch head or ceramic ball of diameter 2-2.5mm [31]. The specimen may be clamped by upper and lower dies, the punch is pushed through the lower die which usually has a receiving hole radius of ≈2mm. The test can be performed in two separate ways, constant deflection rate or constant load [32]. The latter is more analogous to a full size uniaxial creep test and although a 'standard' data interpretation and correlation method does not exist. In Europe the CEN workshop agreement [33] provides a relationship between the punching force and the membrane stress for an established geometry (initial thickness = 0.5mm, punch radius = 1.25mm, receiving hole radius = 2mm), based on Charkrabarty's theory for stretch forming over a hemispherical punch head [34]

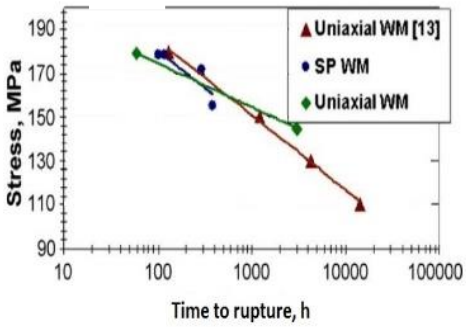
$$\frac{P}{\sigma} = 3.33 K_{sp} a_p^{-0.2} R_s^{1.2} t_0 \tag{2.37}$$

where a_p is the radius of the receiving hole, R_s is the radius of the punch indenter and t_0 is the initial specimen thickness. K_{sp} is an empirically determined material dependant correlation factor which allows the fitting of the small punch rupture data to that of uniaxial rupture data. The correlation factor is set to 1 during initial testing and by performing a recommended minimum of 5 tests at a single temperature; the correlation factor can be corrected to the actual value that allows for the alignment with uniaxial data tested on the same sample of material.

What this correlation fails to incorporate is the large initial plastic deformation [35] involved upon first contact, which has an effect on the creep properties of the material. Consequently this section is disregarded from the considered deflection ($\Delta^c = \Delta_t - \Delta_i$), otherwise a curve is produced which resembles the three stages of a conventional creep curve (Figure 9a) although it is debatable as to whether the curve represents pure creep behaviour [31]. Furthermore the progression of the test consists of the interaction of several non-linearities, which include large initial (local) plastic strains, nonlinear material behaviour, non-linear contact interactions e.g between the specimen and punch, and complex multi-axial stress/strain/damage states in the specimen which evolve in time [36]. This culminates in the differential expansion of the test-piece during loading which means that there is no unified behaviour within the material during deformation i.e. contact regions are changing with time during the test [37]. Also, depending on load levels, the specimen will tend to fracture in two separate modes, one which is around the contact edge (crown) of the punch head [38], and the other being the side wall. Otherwise rupture data tend to agree well with uniaxial rupture data (Figure 9b[39]).



(a



(b

Figure 9: (a) Typical small punch curves from the fine grained heat affected zone (FGHAZ), the weld material (WM), the coarse grained heat affected zone (CGHAZ), service exposed material (SE) and the base/parent material (BM) of a 9Cr1Mo1V weldment under the same test conditions, 250N, 600°C (b) Uniaxial and small punch weld metal rupture tis 600°C [32].

2.3.1.4 Small Ring Creep Test

The small ring creep test is a recently proposed sensitive small specimen creep test that through the use of elliptical geometry is able to produce accurate creep strain-rate data as deformations during testing are large. The merit is that the loads required are low in comparison to the impression creep test due to the relatively small strains. This is as a result of the low equivalent stress required due to the geometry [40] (Figure 6d) which has a large equivalent gauge length when converting data to reference uniaxial data. The specimen is diametrically loaded (Figure 7d) while measuring the load-line deformation of the specimen. Due to the loading and deformation modes, the loading pins required do not need to be of much greater creep strength than the tested material, so strong alloys such as those that are nickel based can be tested [41]. Hyde and Sun [42]

developed analytical conversion parameters to relate the applied load P and load line deformation rate ($\dot{\Delta}$) to the uniaxial reference stress and creep strain rate ($\dot{\varepsilon}^c$) , respectively, for which detailed derivations can be found in [42],

$$\sigma_{ref} = \eta \frac{Pa}{b_0 d^2} \tag{2.38}$$

$$\dot{\varepsilon}^c(\sigma_{ref}) = \frac{d}{4ab\beta}\dot{\Delta} \tag{2.39}$$

where η and β are reference parameters attained in a similar way to the impression creep test method and expanded on in sect 2.2.1. a and b are the major and minor axis dimensions of the elliptical specimen, b_0 is the specimen depth and d and is the thickness of the specimen (Figure 6d).

2.3.1.5 Small Two-Bar Creep Test

The latest of all the small specimen creep tests in development is the two-bar specimen. The test [43] is used to obtain rupture data from small samples without the interpretation complications that arise with the small punch creep test. The specimen is a thin rectangular bar that has had its centre machined out (Figure 6e) with semi-circular provisions into which the loading pins sit which provide a tensile axial force to the parallel bars. The load-line deformation and applied load can then be converted into corresponding uniaxial creep strain-rates and stresses. The specimen dimension ratios, L_0/D_i, k/D_i and b_t/D_i (Table 2) are designed so that η and β are close to unity (0.997 and 1.456 respectively), with recommended ratios of 2.6, 1.13 and 0.4 respectively:

Table 2: Recommended dimension ratios for the small two-bar specimen [43]

Dimension ratios	**Range**
L_0/D_i	~≥2.0-5.0
k/D_i	~≥1.0
b_t/D_i	~≥0.2-0.47

Two bar specimen constructed of P91 steel at 600°C [44] produced comparable results to full size uniaxial tests once conversions have been made. Non-simultaneous failure of the two bars, can cause bending in the intact bar [44], however, this occurs close to the termination of the test.

2.3.2 **Data Conversion**

The non-standard small specimens have unconventional geometries, which if tested in isolation would produce unfamiliar data that would have difficult to apply to engineering components. The methods below convert the data into familiar results that are comparable with full size uniaxial creep tests (Figure 9a, Figure 8a, Figure 16b).

2.3.2.1 The Reference Stress Method

The reference stress approach to data interpretation has been found to be a versatile technique that allows the interpretation of data from the latter four of the non-standard small specimen creep test techniques [27], [35], [42], [43]

Mackenzie [45], assumes that a material obeys Norton's law, $\dot{\varepsilon}^c = A\sigma^n$, where A and n are material constants, for a full size uniaxial creep tests assumed to creep at the same rate, there is a value of σ that for all values of n satisfies the Norton's law relationship above, this is called the reference stress. Then through the use of reference multipliers in conjunction with the reference creep strain rate, a relationship can be formed with the steady state displacement rate:

$$\dot{\Delta}_{ss} = D_r \dot{\varepsilon}^c(\sigma_{ref}) \tag{2.40}$$

$\dot{\Delta}_{ss}$ is the material steady state displacement rate, D_r is the reference multiplier mentioned above ($D_r=\beta d$), where β is an empirically measured constant which is multiplied by the characteristic dimension d of the test specimen. D_r is made to be independent of n by introducing a scaling factor α into the function of the

deformation rate of the creeping structure, where *dim* represents dimension quantities that pertain to the analytical solution of the structure.

$$\dot{\Delta}_{ss} = \frac{f_1(n)}{\alpha^n} f_2(dim) B(\alpha\sigma_{nom})^n \tag{2.41}$$

The reference stress is $\sigma_{ref} = \alpha\sigma_{nom}$ and η is the value of α that causes D to be independent of the stress exponent.

$$D_r = \frac{f_1(n)}{\eta^n} f_2(dim) = Constant \tag{2.42}$$

The reference stress in simple structures (i.e. beams or thick cylinders) corresponds to the skeletal point of the structure, which is the intersection of stress distributions through the structure that arise from different stress exponents n under creep conditions [27]. For more complex structures, numerical methods [46] are used to obtain η for cases where a computed creep solution has been found, by using several values of n and plotting them against $\log[\dot{\Delta}_{ss}/(A(\alpha\sigma_{nom})^n]$ for guessed α values, where η is the value of α that causes $\dot{\Delta}_{ss}/(A(\alpha\sigma_{nom})^n$ to be constant (Figure 10).

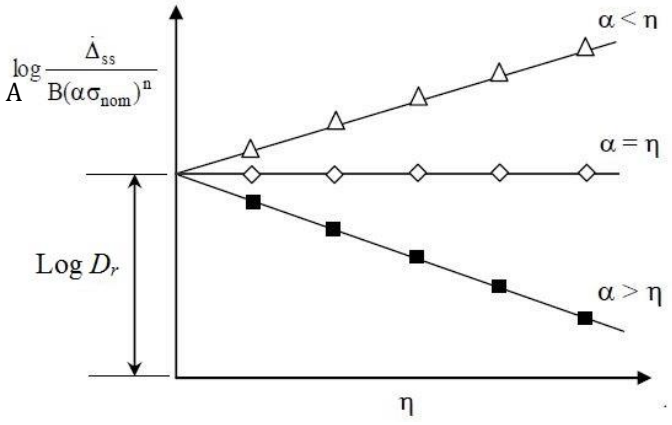


Figure 10: Schematic diagram illustrating the use of FE analysis to obtain reference parameters [28].

The method is geometry dependant, therefore in its current from can only be applied to the impression creep test, small ring creep test and two bar creep test. As the geometry of the small punch creep test changes during loading, Hyde et al.

[35] proposed a method for correlating the minimum displacement rate to the uniaxial creep strain rate by replacing A in the Norton creep law ($\dot{\varepsilon} = A\sigma^n$) with $B' = (1+\varepsilon)^n A$.

2.3.2.2 Equivalent Gauge Length

This is a tool that is used to relate the different geometries of all the individual nonstandard small specimen tests to that of the full size uniaxial test specimen. The gauge length '*l*' used in conventional uniaxial creep tests and the sub-size uniaxial creep test constitutes the creep deformation as a fraction of the working gauge length, eq. 2.44. The equivalent gauge length 'l_e 'is a quantity that is derived from the geometry of the specimen in order to create an expression that models the creep strain in the unconventionally shaped small specimen tests to the conventionally shaped specimen

$$\varepsilon^c = \frac{\Delta^c}{l} \tag{2.43}$$

where Δ^c is the elongation of the test specimen minus any elastic deformation, l the gauge length and ε^c the creep strain. A similar expression exists for small specimen geometries using the equivalent gauge length 'l_e'

$$\varepsilon^c = \frac{\Delta^c}{l_e} \tag{2.44}$$

The equivalent gauge length, if related to a reference creep strain becomes $D_r = \beta d$. Common conversion geometries along with earlier mention conversion constants have been tabulated by Hyde et al. [42] which gives a representation of how the equivalent gauge lengths are related to the analytical solutions used in the reference stress method (Table 3).

Table 3: Summary of correlation formulae [42]

Specimen	σ_{nom}	η	β	βd (l_e)
Sub-size uniaxial	$\frac{4P}{\pi d_{GL}^2}$	1	1	l
Impression	$\frac{P}{b_i d_i}$	~0.4	~2.0	$\sim 2d_i$
Small ring (elliptical)	$\frac{Pa}{b_0 d^2}$	0.892	~0.3-0.7	$\frac{4ab\beta}{d}$
Small ring (circular)	$\frac{P}{2bd}$	0.892	0.448	$\frac{4R^2\beta}{d}$
Two bar	$\frac{P}{2b_t d_t}$	~1	~1.4	βL_0
Small punch	$\frac{P}{2\pi R_s t_0}$	$\frac{0.6\pi}{K_{sp}\left({}^{a_p}/_{R_s}\right)0.2}$	…	…

*Large deformation effects, complex geometry and deformation behaviour of the small punch creep test make it difficult to define material and deformation independent parameters.

2.4 CURRENT PRACTICE USING SMALL SPECIMEN DATA FOR POWER PLANT COMPONENTS

2.4.1 General Procedure

2.4.1.1 Identification of the Components

Components at risk of creep failure are those that undergo the most severe temperature, pressure conditions and service history, and usually are the life-limiting components of a power plant. These include superheater headers, reheater headers, main steam and reheat pipe lines, turbine casings, steam chests and valve bodies [47]. Pressures in the piping components can be above 200 bar and temperatures above 500^{o}C [48], modern ultra-supercritical units have temperatures in excess of 600^{o}C [48]. With regards to piping and headers the early failures usually occur in the weldments and can be identified due to prior experience (service history), from stress analysis that reveal which areas undergo the highest system loadings and where stress concentrations are likely to occur or from visual inspection [47]. Once plants have reached a significant age weldment sections aren't the only vulnerable regions but parent material sections too [49]. The high temperatures and stresses that piping components are exposed to mean that the sections are at risk of axial creep rupture as a result of hoop stress in the parent material section.

500 MW power plants (or larger) are vast structures for which individual comprehensive assessment of every component is unfeasible. Small specimen creep testing has the potential to slot into a power plant condition assessment strategy, like for example the three stage approach developed by the Electric Power Research Institute, 'EPRI' [50],[48], [49]. Components are monitored and assessed with increasing levels of detail and sophistication depending on their condition in three separate stages. The third and final stage is the most detailed and comprehensive. This is the stage where in-situ material sampling may occur and where small specimen creep testing would be done to evaluate components. For example impression creep test results may be placed within a creep strength scatter band to assess remaining life/creep strength of the tested component.

2.4.1.2 Scoop Sampling

Small amounts of material may have to be removed for testing [51]. Sample removal should not compromise the structural integrity of the pipe, header or other component being sampled. However removed material must also have sufficient size to enable representative bulk material properties. Scoop sampling has been used on several occasions [25] on both low alloy 0.5CrMoV ferritic steels and on the newer martensitic steels such as P91 in order to perform impression creep tests. Brett [25] has used the what is called the 'SSam-2' sampler (produced by Rolls Royce) and found that for a wall thickness of 60-65mm in main steam pipes and 30-35mm in hot reheat pipes (0.5CrMoV) the maximum cutting depth should not exceed 10% of the wall thickness, which has been shown by Dedov et al. [52] to be within an allowable dimple depth as the resultant stress risers as a result of the scoop are permissible.

The 'SSam-2'[53] sampler (Figure 11) comprises a hollow hemispherical cutter of diameter 50mm with an abrasive coating that is connected to a flexible drive shaft. The cutter rotates rapidly while feeding into the surface of the material with the aid of a lever arm taking up to an hour to remove a well-polished 20-40mm diameter, and 3-4mm thick scoop samples, leaving a high surface finish on the pipe excavation site. In principle smaller samples have the potential to be removed from pipes with thinner wall sections, but this has yet to be put into practice.



Figure 11: Scoop sampling in progress [54]

EPRI [55] have documented alternative samplers such as the Low Cost Scoop Sampler also developed by Rolls Royce. Dedov et al. [52] have used the Mechanical Sampling Machine, referred to as the 'MSM-2' which operates in a similar fashion to Rolls Royce's 'SSam-2', but has a larger cutting diameter of 60mm.

Rouse et al. [56] conducted a detailed study into the stress fields created upon removal of scoop samples from power plant straight piping under steady state creep conditions. The effect of scoop sampling on three different loading conditions were tested on 0.5CrMoV piping of external diameter of 360mm and wall thickness 60mm, triaxial material constant α_m = 0.3. Internal pressure loading (closed-end condition), internal pressure loading and additional axial system loading, and internal pressure loading with bending system loading were the cases. A loading factor k_s, was used to quantify the amount of additional system loading, with 0 being none and 1 total axial stress (closed-end condition and system loading) according to the maximum allowable axial load

$$k_s = \frac{\sigma_{AX}^{A}}{\sigma_{AX}^{MAX} - \sigma_{AX}^{CE}} \tag{2.45}$$

where σ_{AX}^{A} is the additional axial load, σ_{AX}^{MAX} is the maximum allowable axial load (limited by σ_{MDH}, mean diameter hoop stress) and σ_{AX}^{CE} is the axial load as a result of the closed end condition. The effect on the long term creep strength of the pipe section in question was not considered, but this has not cause any long term complications in practice [25], [26][57]. Furthermore depending on the time of sampling it would be fair to assume that a well formed damage pattern would have accumulated elsewhere in the piping section, and that the introduction of non-invasive dimples would not drastically change those effects. However, further study and/or service experience are required before a safe conclusion can be made.

2.4.1.3 Specimen Type Selection

Due to the varying advantages and limitations of the non-standard small specimen tests (Table 4) none of them can be used as a global test for all components and material types. This is clear in the inability of some tests to produce rupture data (impression creep test, small ring creep test) but in the cases that don't, minimum creep strain rate data are of a high quality. In addition the production of samples varies significantly as some tests have basic geometries (impression creep test, small punch creep test are essentially plates) whereas others require further processes for sample preparation, the small ring and two bar specimen require electric discharge machining to remove the inner material (Figure 6d,e), and in the case of the sub-size uniaxial test, extra material is required to make the loading grips [18] which are then laser or electron beam welded to the specimen.

The impression creep test has been used extensively in industry to test the minimum creep strain rate data of power plant piping, 0.5CrMoV steels and newer martensitic P91 steels. Through stepped load/temperature tests is possible to obtain a range of minimum creep strain rates from one sample [58]. Until recently it was unable to test materials of high creep strength, as the indenter use has to be creep strength 2-3 times greater than the test sample [59]. Ceramic indenters may be used, significantly raising the creep strength of materials that can be tested [26]. This means the test may now be applied to nickel superalloys. However the small ring test also has the capability to obtain an accurate minimum creep strain rate and with its relatively large equivalent gauge lengths is able to produce highly accurate minimum creep strain rate data through loading pins of similar creep strength of the material being tested [41]. It is also possible to test brittle materials [40]. Both of the tests mentioned, however, are unable to produce rupture data directly but could be used indirectly by inputting creep strain rates into the Monkman-Grant correlation to be used with uniaxial rupture data.

The extensively tested small punch test may be used to obtain short term rupture data providing a correlation factor K_{sp} has been previously determined for the material in question, for example values for steel seem to be around 1.2-1.3 [15], [60], [61] and that the test conditions including the geometry of the sample, load line of the punch and atmosphere are kept consistent. For the current method of using the K_{sp} the need for a database of commonly used power plant materials at a range of test temperatures could aid the use of such a test for life prediction of components. As mentioned earlier characterization of the full small punch creep test curve is not fully understood which limits the test from obtaining Norton creep law constants B and n. The invention of the newer two bar specimen has the potential to produce rupture data as the test sample gauge area deforms parallel to the load line so in theory behaves in a similar fashion to a full-size uniaxial test. Furthermore it has been used successfully in determining constants in the Kachanov-Rabotnov and Liu-Murakami creep damage equations [62].

2.4.1.4 Creep Testing and Data Processing

The specimens are manufactured from scooped in-service or ex-service material by electrical discharge machining and in the case of the impression creep test and small punch creep test, a small excess of material is left on the loading surfaces for further grinding and polishing (recommended 200 grit [33]) to achieve a high quality surface finish for the removal of any residual stresses due to machining. The recommended tolerance is set to be ±0.02mm for impression creep test [24] and ± 0.5% for small punch test [33]. The small ring and two bar specimens are cut into square and rectangular plates respectively, from which they are wire spark eroded through feed holes at the centre of the plate; the wire electrode is sprayed with coolant so as to produce a better surface finish [44]. All specimens are cut to sample dimensions as shown in Figure 6.

For pneumatic, servo-hydraulic or dead weights, the test rigs must be able to hold a constant load controllable to ±1% as comparable to full size creep rigs (as in BS EN ISO 204:2009 [63]). In the case of the impression creep test, recommended indenters are made of nickel superalloys (WASPALOY or Nimonic) when testing

low alloy ferritic or martensitic steels [24] and must be ground so as to be parallel with the flat surface of the specimen. For the small punch test ceramic balls/hemispherical heads should be of sufficient hardness 55HRC so as not to deform under compression. The small ring test requires loading pins of only similar creep resistance, whereas the two bar test has loading fixtures of a much higher stiffness and are generally produced from material with greater creep resistance [43]. The load line displacements are measured using water cooled extensometers and linear variable displacement transducers although strain gauges may be used provided they are accurate to within ±1% and have sufficient resolution.

Temperature fluctuations should be kept within ±0.25% [33] or within ±4^{o}C for 600<T≤800^{o}C [63]. Temperature in most cases is determined with a thermocouple. However, with the small punch test, due to its confined loading environment, this poses difficulties. A feed hole may be drilled through the top of the upper die for thermocouple placement [64]. Due to the small sizes of the specimens, oxidation effects can be magnified, reducing overall creep strength [65] of the specimen so the use of an inert atmosphere may be required, usually in the form of metered argon flow. Tested specimens can be seen in Figure 12. For more detail regarding each of the testing procedures refs [24] and [33] provide information pertaining to the impression creep test and small punch test respectively and the ref [44] contains information regarding the small ring test and the two bar test.

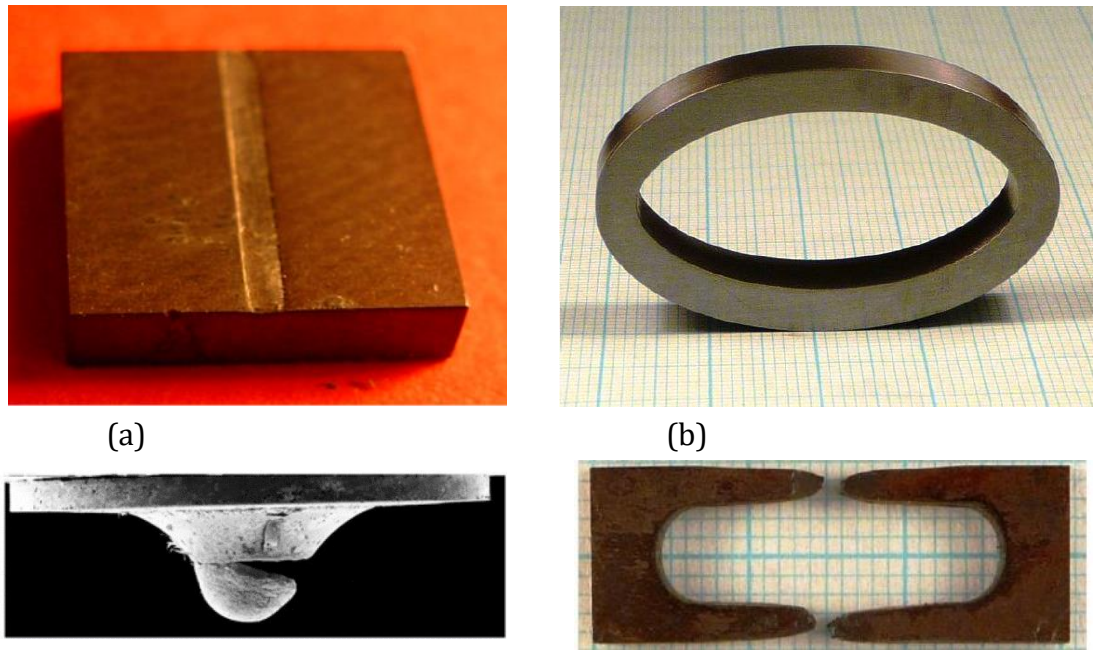


Figure 12: (a) Tested impression specimen (width $w \approx 10$mm) [66], (b) tested elliptical ring specimen (major axis, $a \approx 20$mm) [67], (c) ruptured small punch specimen (diameter $D \approx 8$mm) [39] and (d) ruptured two bar specimen (length, $L_0+2k \approx 26$mm) [67]

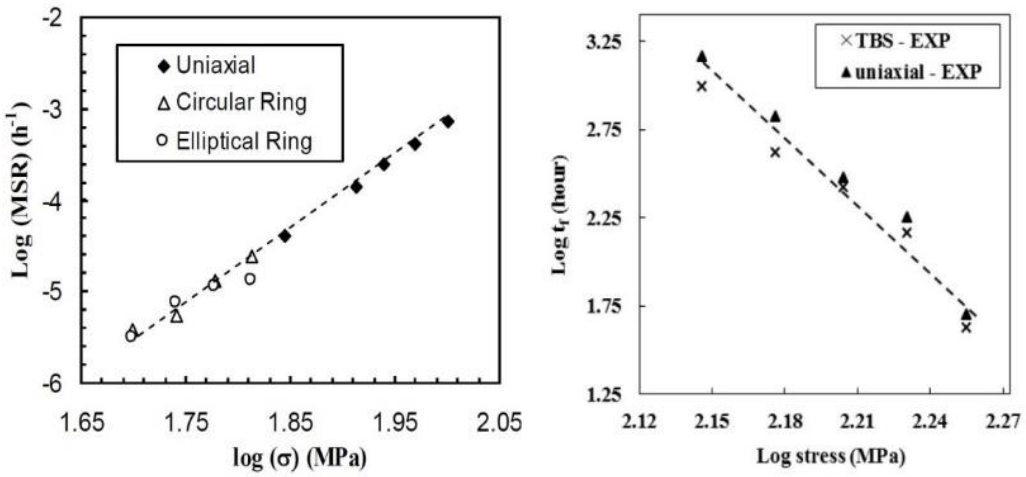


Figure 13: (a) Minimum creep strain rate data for P91 steel at 650°C, small ring test and (b) two bar test creep rupture data alongside uniaxial for P91 steel at 600°C [67]

Table 4: Summary of advantages and disadvantages of small specimen test methods.

Test method	Advantages	Disadvantages
Sub-size uniaxial [18], [19], [68]	- No complex conversion required - Uniaxial loading - Produces rupture data	- Relatively complex manufacturing method - Small gauge diameter causes difficulties during loading - Sensitive to furnace atmospheric composition
Impression creep [24], [26], [28], [29], [69], [70]	- Simple geometry - Comprehensive test database - Industrially applied - Effective strength ranking tool	- Compressive test simulating components in tension - Small deformations under loading puts strain on displacement measurement - Unable to produce rupture data
Small punch [30]–[32], [36]–[39], [71]–[73]	- Simple geometry - Large amounts of academic testing - Draft code of practice exists - Produces rupture data - Short tests useful for qualitatively assessing creep strength	- Complex Multiaxial stress-state during loading - Absence of mechanics based conversion relationship
Small ring [40]–[42]	- Accurate creep strain data as a result of a large equivalent gauge length - Can test a large range of materials	- Cannot produce rupture data - Relatively complex manufacturing procedure
Two bar [43], [67]	- Can produce rupture data - Stable uniaxial loading	- Material may creep in regions other than the gauge region - Two bars may creep at slightly different rates - Relatively complex specimen geometry

2.4.2 **Main Applications – How to Use the Small Specimen Data**

The exploitation of small scale creep testing falls into two broad categories: component specific assessment, where quantitative creep data are required to support a particular assessment, and surveying to provide creep strength ranking, where a more qualitative, relative value of creep strength may suffice. The two are not entirely separate in that ranking which can accurately place a material within a creep strength scatter band does also provide a quantitative value

2.4.2.1 Component Specific Assessment

There is a requirement for small specimen data to be used in component specific assessments in lieu of uniaxial data, for example on header sections or steam chests/casings.

In the assessment of internal fatigue cracking on steam chests and valve bodies, it has been argued that the load responsible decays through the wall thickness, thus stifling the growth of the crack before a critical length is reached. The attention is then focused on not letting the rest of the un-cracked component fail by creep with assessment based on small scale testing, thus avoiding the need for weld repair.

Extracting a pure creep curve from the small punch test is still not fully established [31]. So in the absence of an analytical approach, reliable and repeatable empirical correlations between small punch and uniaxial data at equivalent conditions are implemented. The Monkman-Grant equation ($\dot{\varepsilon}. t_f = C$) is a simple correlation in this context, but due to the absence of an identifiable steady-state creep strain rate and the fact that correcting the trend line relies on material ductility (making the test cast specific) significant testing would be required on a specific material to explore these issues. The method is better suited to either the impression creep test or the small ring creep test based on the better quality of the creep strain rate data obtained.

The phenomenological interpretation of the small punch test involves disregarding the primary and secondary regions of the creep curve and focusing only on the rupture time. This is useful if reproducible rupture times and stresses are achieved. The trends observed with small punch rupture data compare favourably with uniaxial tests and it is worth noting that the small punch test length (usually short) is comparable with uniaxial test of the same duration. Universally agreed correlation factors K_{sp} for a specific material grade and temperature range must be determined. A database can then be established.

Alternatively the two bar test has been shown to produce rupture data that compare favourably with uniaxial data for P91 at 600°C. The accelerated test data would need to be extrapolated in order to apply to service conditions. A common extrapolation method is the Larson-Miller parameter (eq. 2.46) [74] (used with the small punch creep test [75]), well known in the accelerated creep extrapolation of uniaxial tests [76]

$$P_{LM} = T.(C_{LM} + log\, t_f) \tag{2.46}$$

where T is the temperature in Kelvin, t_f is the rupture life in hours and C_{LM} is a constant originally assigned a value of 20 for all metallic materials, has now been found to vary [76]. It is derived as a result of curve fitting to experimental data and is related to the activation energy for creep fracture.

A relatively new method [77] involves the Wilshire equations, which are based on the assumption that as time to failure (hours) $t_f \rightarrow \infty$ the applied stress $\sigma \rightarrow 0$ and $t_f \rightarrow 0$ as $\sigma \rightarrow \sigma_{TS}$, the ultimate tensile stress of the material. They have already been applied to full-size uniaxial creep tests [78]

$$\sigma/\sigma_{TS} = exp\{-k_1[t_f.exp(Q_c^*/RT]^u \tag{2.47}$$

where T, R and Q_c^* are the temperature, universal gas constant and apparent activation energy respectively. Wilshire constants u and k_1 are then calculated by plotting $t_f.\exp(-Q_c^*/\mathrm{RT})$ against $\ln[-\ln(\sigma/\sigma_{TS},]$. The utility of the equations is

based on their ability to calculate an apparent activation energy 'Q_c^*' by the superimposition of different temperature data sets from temperature compensated graphs of either rupture time or minimum creep strain rate against normalised stress.

The Omega (Ω) test method [79] is based on the assumption that once the first stage of creep is over, there is a steady rise in creep strain rate. In the Ω method, strain is an indicator of damage and is represented by:

$$\dot{\varepsilon}^c(t)/\dot{\varepsilon}_0 = exp\Omega\varepsilon \tag{2.48}$$

taking logarithms gives:

$$log\dot{\varepsilon^c}(t) = log\dot{\varepsilon}_0 + \Omega\varepsilon \tag{2.49}$$

where $\dot{\varepsilon}_0$ is the initial strain rate of virgin material and $\dot{\varepsilon}^c$ is the strain rate at time *t*. Ω is the 'total damage' coefficient, which incorporates creep damage, microstructural changes and the effect of strain rate. It is obtained from the gradient of the line $d\ln\dot{\varepsilon}/d\dot{\varepsilon} = \Omega$, provided a linear relationship exists. Once Ω is obtained, the remaining life may be estimated through:

$$t_f - t = \frac{1}{\Omega\ \dot{\varepsilon}(t)} \tag{2.50}$$

The extrapolation and remnant life assessment methods mentioned are but special mentions from a host of approaches. More detail on these methods can be found in ref [76] with regards to extrapolation and in ref [11] for an analysis on continuum damage mechanics.

2.4.2.2 Material Strength Ranking

There is a somewhat different requirement for small scale test data in creep strength surveys aimed at identifying the weakest components. The ranking of component creep strength is achieved through the application of the same test to numerous samples. During initial small scale testing on a P91 header [80] enough material was removed to apply multiple small specimen tests (small punch and

impression creep), with consistent ranking. Test times were reduced by ranking based on the first part of the punch curve, prior to rupture.

The application of such tests to the US market is to older P22 pipework, as failure is more likely than in newer P91 components [81], where weld failure is the key issue [82]. However the widespread occurrences of aberrant, mis-heat treated (and therefore weaker) P91 does bring these end of life problems to the fore.

2.4.3 **Current Practice**

2.4.3.1 Impression Creep Test Data

Minimum creep strain rate data from the impression creep test have been used for strength ranking on in-service piping components and for the characterisation of weldment zones. Most data collected are for 0.5CrMoV piping for which over 170 tests [25] exist creating an effective database for comparison purposes. The method has been applied to Grade 91 [83] piping with the main concern being aberrant material, inadequately manufactured.

2.4.3.2 Small Punch Creep Test Data

Analysis of rupture life has focused on rupture data from the small punch test to extrapolate back to design temperatures, by using the Larson-Miller parameter, the Dorn equation and the Monkman-Grant correlation or simple a rupture time vs deflection relationship [30], [84]–[86]. The lack of a collated material database seems to be holding back its application to in service applications.

Izaki et al. [75] used a graphical method for converting the punch load. A Larson-Miller plot of punch loads was superimposed over a uniaxial Larson-Miller curve for equivalent test conditions. Punch loads are equivalent to uniaxial stresses if they share the same Larson-Miller parameter. The method was used on 2.25CrMoV, the dominant pipeline material in Japan.

The small punch creep test has been applied to single crystal superalloys for life assessment by Jeffs et al. [59] for the lifing of 'CMSX-4', a second generation single crystal superalloy commonly used alloy in gas turbines [87]. Tested alongside the full size uniaxial test, the load was calculated using the K_{sp} method outlined in the CEN workshop agreement, Q^* activation energy was determined for the [001] plane of the crystal and inserted into the Wilshire creep equations (eq. 2.47) for life prediction. The results compared favourably with those of a full size uniaxial test.

2.4.3.3 Use of Other Small Specimen Test Data

The small ring test has the capability of testing material of high creep strength due to its method of loading (Figure 7d) which allows the loading pins to be made of material of similar creep resistance [41] to the test material. This results in the ability of the test to be run on nickel superalloy turbine blades, such as Inconel 738 [41]. Useful minimum creep strain rate data can be analysed using strain based lifing calculations such as the Monkman-Grant or Omega method.

2.4.4 **Applications in Life Management: Case Studies**

A large proportion of the UKs coal fired plants are well past their design lives [2]. Their high temperature steam lines (main steam, hot reheat and turbine looping) are mainly constructed of 0.5CrMoV steel and the later stages of life there is a shift of focus from not only weldment failures but to parent failures as well.

P91 steel has been used to replace some 0.5CrMoV pipework and has also been seen to be used in the newer combine cycle gas turbine stations, but due to inaccurate heat treatment methods, some installed piping samples have unexpected microstructures.

Due to the sheer number (≃400) of steam line items in a typical 500MW power station [54], comprehensive testing would be uneconomical and time consuming. Impression creep testing is a reliable method for optimising inspection programmes by effectively ranking in-service creep components by creep strength so that effort is focused.

2.4.5 **Representative Examples**

2.4.5.1 Creep Strength Ranking for P91

Grade 91 martensitic steel has gradually replaced 0.5CrMoV steels in the UK for construction of main steam lines. It has better creep strength and can be constructed with thinner wall sections [88]. It is, however, more susceptible to manufacturing variations. Aberrant P91 material can be identified using hardness testing and metallographic studies. The hardness should lie in the range of 200-263HV, the aberrant material can be as low as ~151HV [89].

Once a suspect component has been identified, Brett et al. [57] have shown the capacity for the impression creep test to verify compatibility within the acceptable creep strength scatter band. Figure 14 shows the stress vs log creep strain relationship for P91 and the mean-20%, which are converted from stress rupture lines using the modified (Parker) Monkman-Grant relationship (eq. 2.51) [57] for known uniaxially tested P91 material. Creep strain rates that are found to lie to the right of the mean -20% line in Figure 14 [90] for a corresponding stress level are said to be acceptable, as they are shown to have a creep strength greater than that of the lower bound.

$$\dot{\varepsilon} = 0.1 t_f^{-1.16} \tag{2.51}$$

Where $\dot{\varepsilon}$ creep strain per hour and t_f is the uniaxial time to failure in hours.

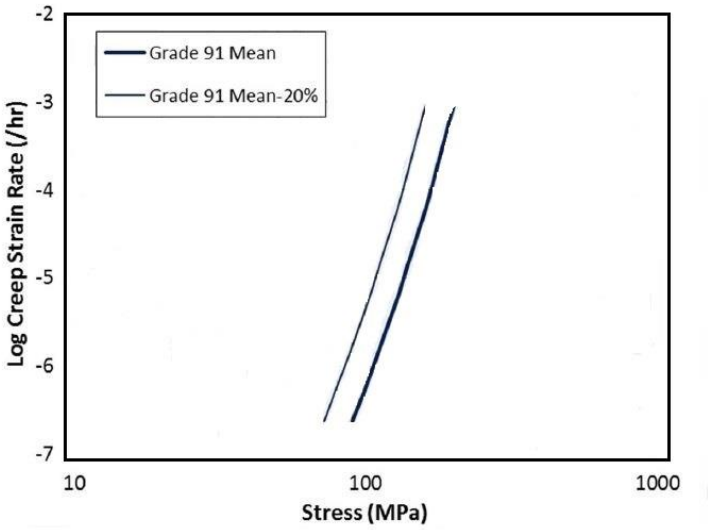


Figure 14: Minimum creep strain rate corresponding to mean and lower bound [90] strength levels at 600°C

2.4.5.2 Vulnerability Assessment of 0.5CrMoV

0.5CrMoV is an established material with regards to impression creep testing. 10x10x2.5mm specimens were tested at a proposed standard test regime of 96.7MPa and 600°C [25]. Creep strain rates are compared against a lower bound (mean-20%); creep strain rates that fall below this, represent materials of potential risk (Figure 15a). The results can then be corrected to find the estimated creep strength at start of life, which may indicate the quality of the initial manufactured product (Figure 15b).

Main steam lines, hot reheat lines, bend and straight pipe sections were tested [25] and compared with data from other power plants. A large database now exists for which creep strain measurements can be compared against.

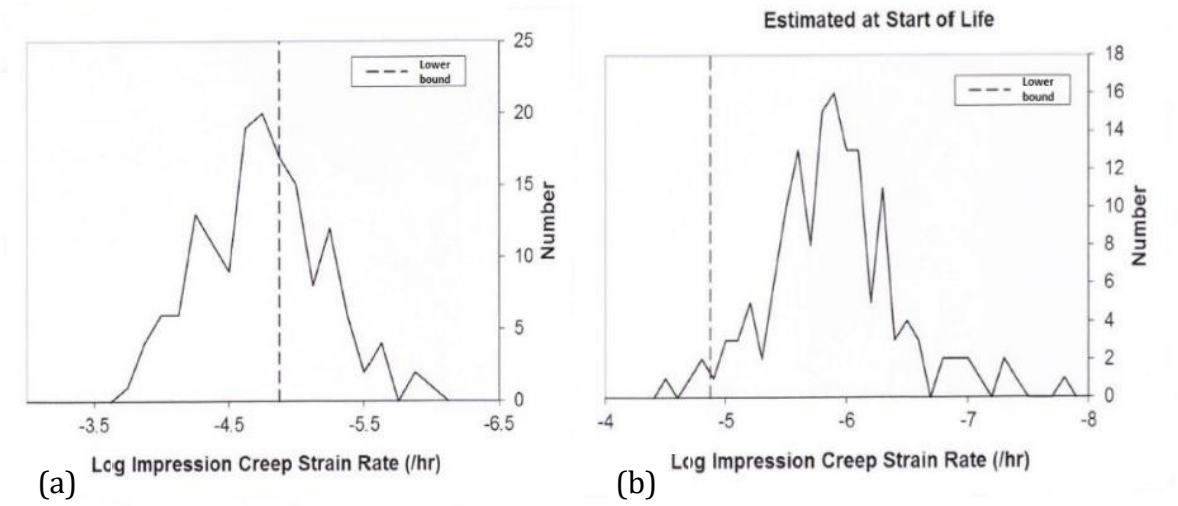
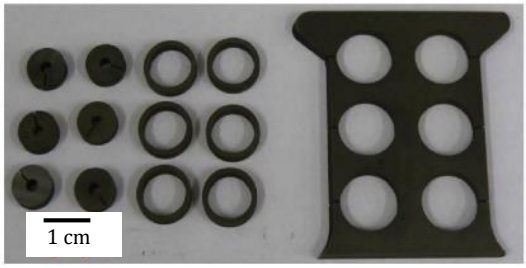


Figure 15: Distribution of impression creep strength of specimens (a) as-sampled (b) corrected to start of life [18].

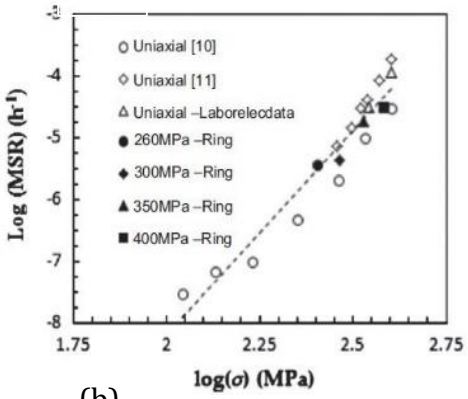
2.4.5.3 Remaining Life Assessment of Nickel-Based Turbine Blade

Evaluating turbine blades poses a unique problem as any damage caused to the geometry of the blade renders the blade useless. Furthermore the data obtained from the removed blade must be treated as representative of similar blades left in-service. The requirement is that creep tests must be performed on the material removed, but there usually is not enough material to perform full size uniaxial creep tests, let alone a comprehensive set of tests required for robust evaluation of bulk creep properties.

The development of the small ring creep test [43] allows for multiple tests on small quantities of blade material. Minimum creep strain rate data was obtained from the root of a third stage heavy duty gas turbine blade (Figure 16a) at 800^{o}C. Stress and minimum creep strain rate data were converted to equivalent uniaxial test data through the mechanics based reference stress method in conjunction with the equivalent gauge length of the material (sect 2.2.2). Data were found to fit well with the uniaxial data for Inconel 738 virgin as cast material (as it is what the blade root represents) as in Figure 16 [41].



(a)



(b)

Figure 16: Blade root, with specimens removed by spark erosion and (b) Log-log plot of stress as a function of minimum strain rate, for a small ring and uniaxial tests at 800°C [34]

Quality strain data is achievable with the small ring test. Further data interpretation procedures are necessary to obtain remnant life assessment. Available strain based methods include the Monkman-Grant relationship and Omega method. Further work is required in this area. Small punch testing on a single crystal superalloy, 'CMSX-4' [91], at 950°C and 1050°C in the [001] crystallographic orientation were done [77]. A good linear fit was found for the punch load and time to rupture. K_{sp} values of 0.6 at 950°C and 0.8 at 1050°C were found. Discrepancies were attributed to directional coarsening of γ' particles (rafting), this occurs more rapidly at higher temperatures in single crystal materials [92]. A Wilshire fit (eq.2.47) was applied to small punch stress vs time to rupture data and good agreement was found with uniaxial data (Figure 17) [77].

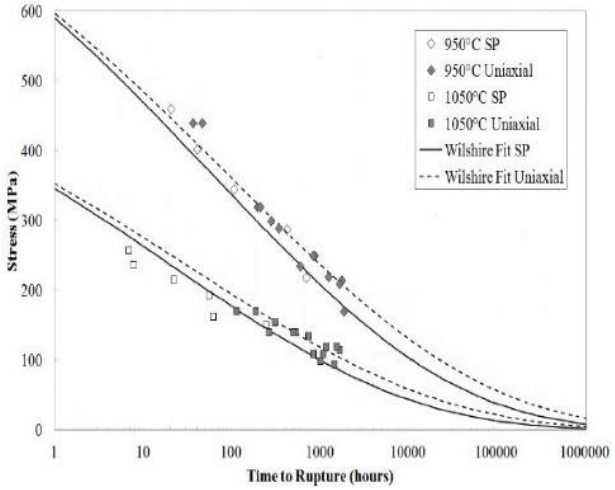


Figure 17: Wilshire plot for time to rupture as a function of stress for CMSX-4. SP represents small punch, alongside uniaxial data [61].

2.4.6 **The Need for Standardisation of Impression Creep Testing**

2.4.6.1 Background

The impression creep test has been used successfully in the creep strength ranking of in-service components for 0.5CrMoV and P91 steels as shown in earlier sections of this study, which has many benefits as it allows for the targeting of vulnerable components and allows for the focus of resources on those components. For 0.5CrMoV pipework there is a comprehensive database available for comparison of tested materials. The impression creep test is also able to produce a large volume of useful data from small amounts of material which include the ability through stepped-load and stepped-temperature tests to multiple sets of minimum creep strain rate data from a 10x10x2.5mm test specimen, useful in alloy development [3].

2.4.6.2 Work Needed

For wider implementation in power plant life management it is necessary to standardise the basic definitions of test rigs, specimen dimensions, sampling and specimen preparation, temperature and loading control and displacement measurement etc. A recommendation for most of these issues has been discussed

by Hyde et al. [24]. This would help in the production of bespoke purpose built impression creep rigs that adhere to precise load and temperature control requirements to produce consistent data across laboratories economically. A detailed description of the test can be found in the guidelines for small scale testing [77].

2.5 CONCLUDING REMARKS

Evidence for the utility of small specimen creep tests has been reviewed and cases for creep strain rate data and rupture life data of a comparable standard to uniaxial test data is present.

Limited testing and practice with the sub-size uniaxial specimen means that the issue of misalignment during the application of a load to the specimen remains unresolved. This and the acute sensitivity to the atmospheric composition of the test furnace make the test procedure difficult.

The impression creep test has been used in industry and so a database exists for strength ranking of established ferritic power plant pipeline steels [25]. A framework for the general application of the strength ranking method is needed for it to be generally applied, along with development in standardisation of the test method.

In its current form the small punch creep test can only be useful as a qualitative measure of creep strength. This is based on the absence of mechanics based conversion of strain and rupture data and the limited understanding of the deformation curve produced by the test. This is indicated by the reluctance of industry to incorporate the test into life assessment procedures.

Accurate strain rate data, the capability to test a broad range of materials and larger load line displacements than the impression creep test make the small ring creep test a strong candidate for creep strain rate measurement. The test is in its infancy, so the development of a database for a broad range of materials is in

order. Furthermore, the development of strain based lifing methods for the exploitation of the small ring test data would be beneficial for the future uptake of the test method.

Two bar rupture data shows promise when compared with uniaxial data. The immediate concern is to carry out more testing, in order to illustrate the repeatability of the test.

Small specimen creep tests should not be looked at in isolation, but should be looked at as a suite of tests that can be used in combination to test the components mentioned in this review.

CHAPTER 3

METHODOLOGY

3.1 EXPERIMENTAL METHODOLOGY

3.1.1 Mechanical Testing

3.1.1.1 Impression Creep Testing

Specimens and indenter dimensions are as follows, wxbxh are the width, breadth and height of the specimen respectively d is the width of the indenter. The candidate dimensions for standardisation are 10x10x2.5mm but dimensions 8x8x2mm may be used in cases where there isn't enough material available and are used in Chapter 5 primarily because of that reason. A schematic of the specimen may be seen in Figure 18. A flat rectangular indenter is loaded onto a square specimen at elevated temperature to create an impression on the surface of the specimen by a servo-controlled twin screw machine as seen in Figure 19 (Dead- weight rigs may be used too). The indentation depth is logged by water cooled LVDTs.

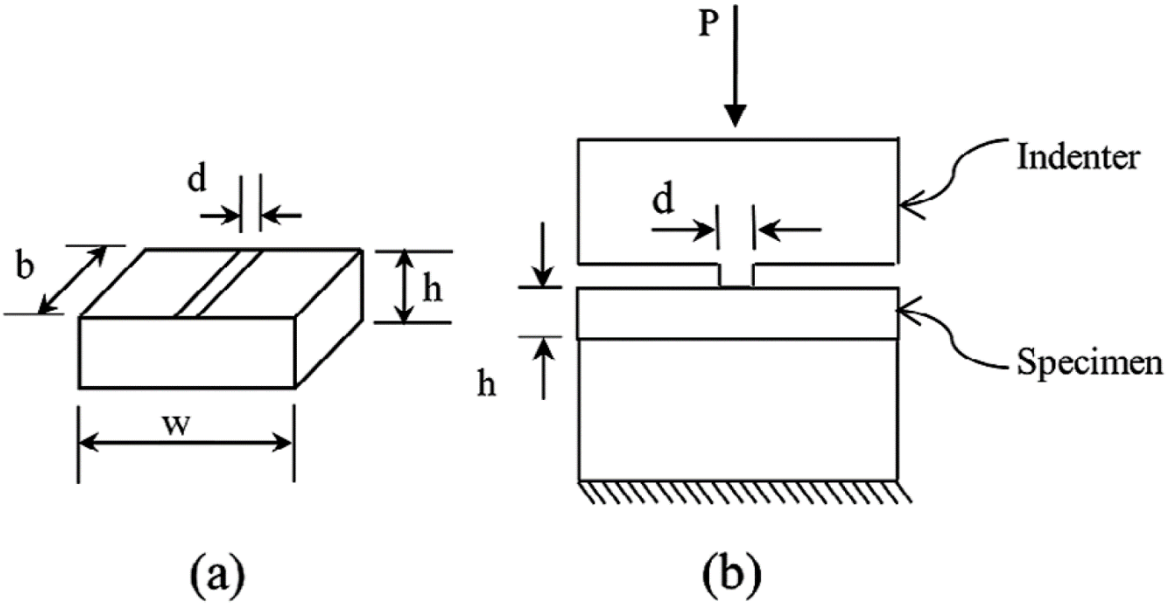


Figure 18: (a) Impression creep specimen dimensions and (b) loading arrangement

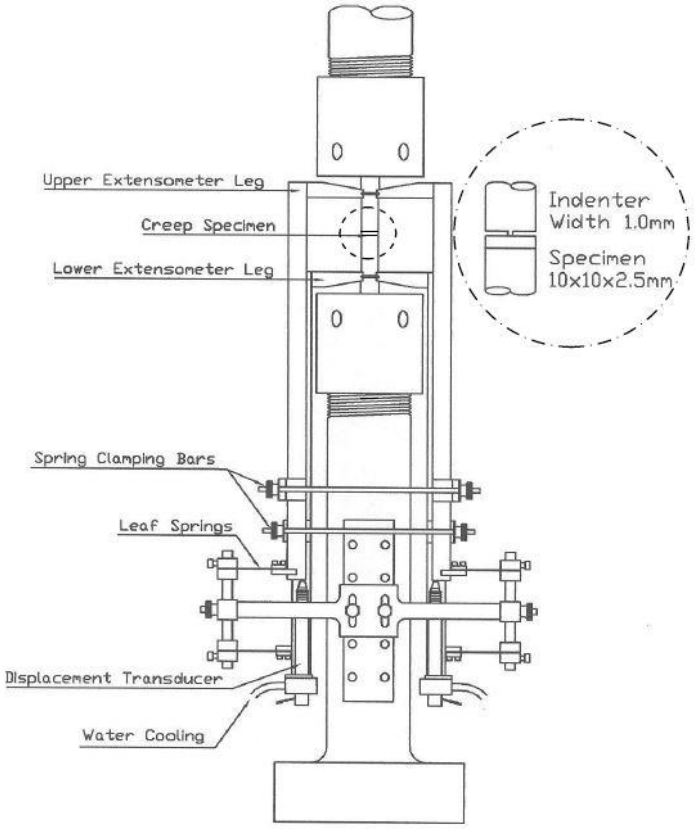


Figure 19: Twin screw impression creep test rig

3.1.1.2 Uniaxial Tensile Testing

Oversized uniaxial specimens were tested at elevated temperature to simulate the induction bending of pipes and the resultant strain on the samples for subsequent creep testing. Rather than the standard 50mm gauge length – a specimen with an 80mm gauge length and 16mm gauge diameter was taken from a section of grade 91 pipe work Figure 20. M20x2mm grips were used for the specimen to account for the increased gauge diameter. The samples once tested to failure were then used to machine impression creep test samples. A pull rate of 0.03mm/s was done on the samples. The failed material was then used to make impression samples.

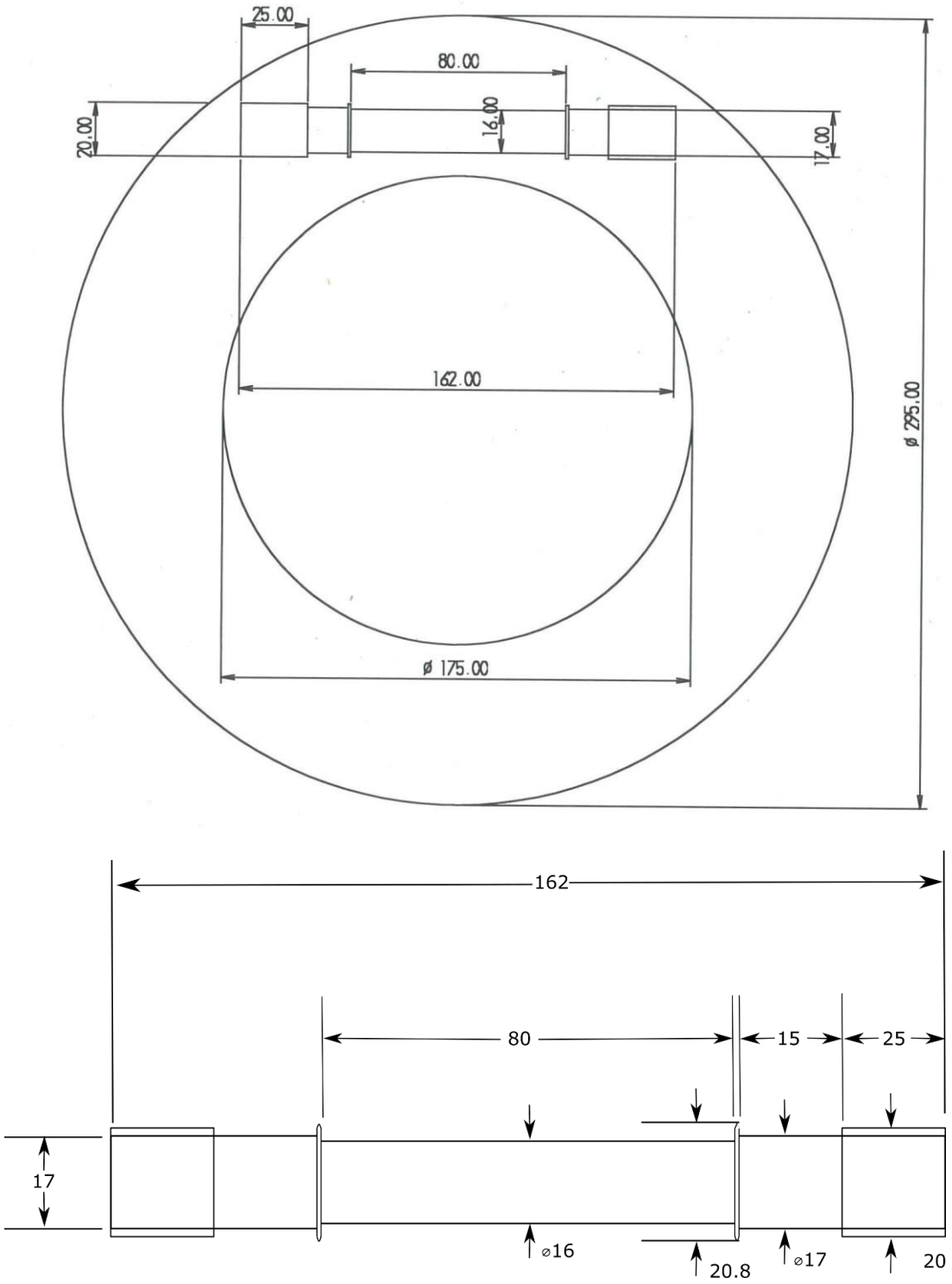


Figure 20: Specimen removal locations (top) and detailed drawing of specimen

3.1.1.3 Notch Bar Testing

Two novel asymmetric notch bar samples were used in Chapter 6 in order to validate continuum damage mechanics modelling of a scoop sampled straight pipe. The test specimens are a modification of standard uniaxial creep specimens of circular gauge to ones that have a square cross-section of 7x7mm Figure 21 & Figure 22. Notches have been carved out of one of the surfaces of the specimens. Two notch geometries have been selected for the present study, circular and elliptical cross-sections. The curvature of the spherical profile is derived from a sphere of radius 3mm, the depth of the notch is 2mm, and so the projected circle on the specimen has diameter of 5.75mm. The elliptical notches have a curvature which is derived from a prolate spheroid of major radius 6mm and minor radius 3mm and has a depth of 2mm. The projected ellipse on the surface of the specimen is tilted at an angel of 70^{o} from the normal vertical axis. The geometries of the notches were calculated by fitting a surface through the points generated from the surface characterisation of the machined specimens and then imported into an Abaqus model. The specimens were used to determine the alpha value (material triaxiality) for P91 and in the case of the elliptical notch which was designed to simulate bending and the resulting crack growth. The specimens were loaded using a dead-weight uniaxial rig.

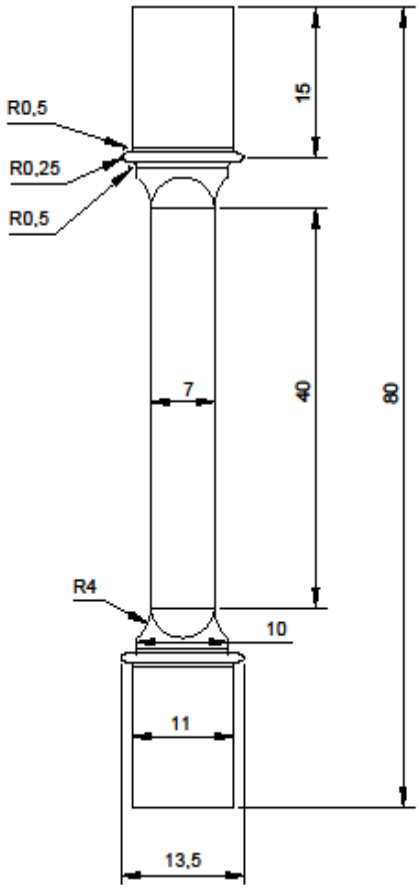


Figure 21: Square specimens without notch

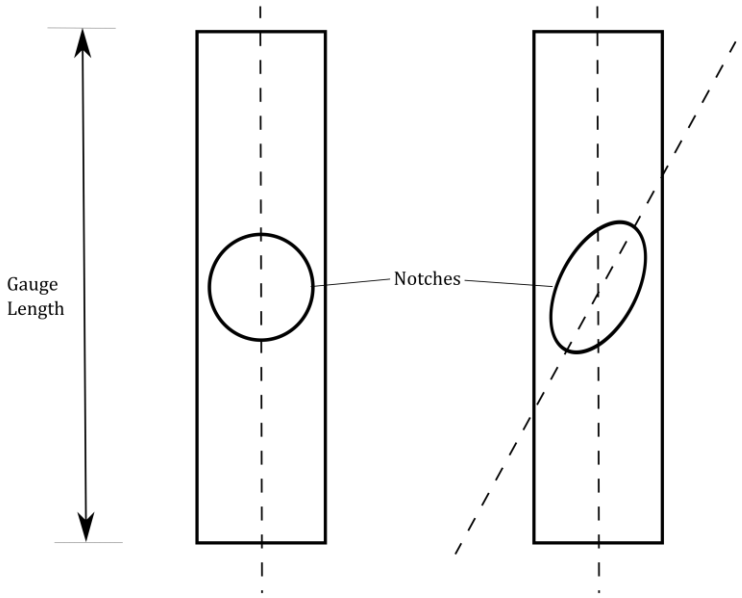


Figure 22: Schematic of specimen drawings showing notch types, circular (left) elliptical (right)

3.1.1.4 Micro Hardness Testing

Micro hardness testing was done with a micro Vickers hardness tester, 1000gf was used on the samples. A series of indentations were made along the surface of the samples, which in this case were cut offs of the oversized uniaxial specimens, before and after heat treatment.

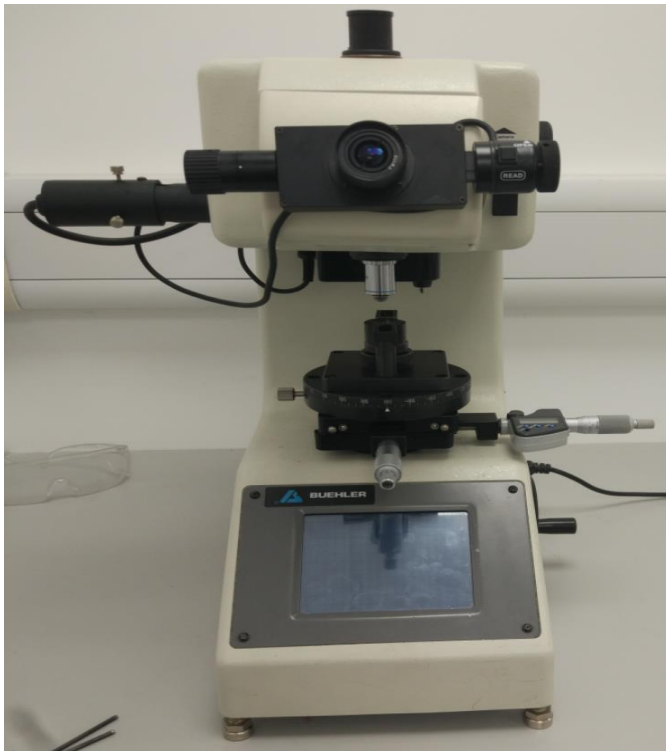


Figure 23: Micro hardness tester used

3.1.2 **Electron Backscatter Diffraction (EBSD)**

The EBSD technique was used in the detailed assessment of the deformation characteristics of crept and plastically hardened material. A JEOL 7100F field emission gun scanning electron microscope was used for this work. Standard settings for the tilt angle, emission current and voltage were used. Typically, the magnification was set at 600x with a scanning step size of 0.2-0.4μm depending on allowable time on the machine.

3.2 MODELLING METHODOLOGY

3.2.1 Materials Constants Determination

The isotropic hardening plasticity model is a simple power law model (Equation 2.18). The constants *K* and *m* are determined by taking the intercept and the gradient respectively of a linear fit of the portion of the uniaxial tensile test curve during plasticity and simultaneous hardening, that is, the plastic portion with an upward slope.

The Liu and Murakami creep damage model (Equations 2.32 & 2.33) contains several materials constants which may be determined through accelerated uniaxial creep and notched bar testing to failure along with finite element simulations. Minimum strain rates may be used to determine initial guesses of the corresponding Norton constants, a plot of the stresses against the failure lives generates initial guesses for '*m*' and '*p*'. The remaining constant needed is q_2 which can be determined through optimisation of the equations after time marching of the integrated equation. The objective function used is of the type [93]:

$$\sum_{i=1}^{k1}\left\{\left[\sum_{j=1}^{k2}\left(\varepsilon_j^{pre}-\varepsilon_j^{exp}\right)^2\right]_i+\rho_i\left|t_{fi}^{pre}-t_{fi}^{exp}\right|/t_{fi}^{exp}\right\}\rightarrow min \qquad (3.1)$$

The function can be used along with lsqnonlin in matlab to produce optimized fitting results.

3.2.2 Numerical Simulations

Finite element analysis was used in Chapters 5 and 6 to model plasticity and creep damage respectively. Abaqus is the chosen software and the in-built isotropic hardening routine was used to model a uniaxial bar in tension (P91 martensitic and ferritic) with the intention of calculating the true strain in the necked region of the sample, as no failure criterion was used the simulations were halted at the point where the engineering strain in the simulation was the

same as that in the failed experimental specimen. Details of the constitutive equations and geometrical and loading set-up can be seen in Chapter 5.

In Chapter 6 an in house Liu and Murukami creep damage routine is used to simulate the effects of creep damage on power plant straight pipes that have been subjected to scoop sampling. The CREEP subroutine used was developed by previous researchers [13]. The damage variable (ω in Equation 2.32) was halted at 0.99 to prevent the analysis being longer than necessary for the required accuracy due to small time steps. Again details of the constitutive models, geometries and loading conditions can be found in Chapter 6.

CHAPTER 4
ROUND ROBIN IMPRESSION CREEP TESTING

4.1 INTRODUCTION

The need for more detailed information in the condition monitoring of power plant components is an ongoing concern which includes high temperature headers, main steam lines, and valve bodies. The use of small specimen creep test techniques provides a method to obtain mechanical data from components. The impression creep test is such a technique, originally performed using a cylindrical indenter [94],and later using a rectangular indenter loading a square specimen from which a mechanics based interpretation technique was developed [21] . It is capable of providing data from in-service components in the form of constant-load displacement rates (converted to the corresponding uniaxial secondary creep strain rates), where specimens are machined from component surface scoop samples. In this instance, strength ranking of components may be conducted and with further development aid in remnant life assessment strategies. In the latter case, conversion of the impression creep results may be needed. While in some cases material from the surface of high temperature components may contain the greatest damage [95] in other cases temperature and stress state dependant peak damage may be present below the surface. In scenarios where material is limited, such as weldments where the separation between metallurgical zones may be small, full-size uniaxial creep testing are not feasible and so local material characterization may only be possible with small specimen creep tests. In addition to the above requirement, small specimen creep test techniques can be useful in novel alloy development [3] where material quantities and test times are scarce. Although this latter approach must recognise the dangers of mis-interpretation of behaviour where the conventional creep data is poorly characterised, or unavailable.

The present work is an evaluation of the state of the art procedures involved in testing and is in reference to prior requirements as outlined by Hyde et al [24]

who have extensive experience and have conducted hundreds of impression creep tests. It has been identified that load stability and control, temperature measurement and control, and displacement measurement are the key variable features in rig design which have a significant impact on test results, particularly displacement signal stability. The aim of this work is to investigate the effects of these different parameters through a cross lab collaboration or 'Round Robin', through which independently the different approaches may be compared.

4.2 IMPRESSION CREEP TEST AND BASIC REQUIREMENTS

4.2.1 Impression Creep Test Using a Rectangular Indenter

4.2.1.1 Test Set-up

The impression creep testing technique described herein uses rectangular indenters and involves the application of a steady load to a flat-ended indenter, placed on the surface of a specimen, at elevated temperature. The dimensions used across labs in this study are illustrated in Figure 18: (a) Impression creep specimen dimensions and (b) loading arrangement sect 3.1.1, where b=w=10 mm, h=2.5mm and d=1mm.

4.2.1.2 Conversion Relationships

The displacement-time record obtained from such a test is related to the creep properties of a relatively small volume of material in the immediate vicinity of the indenter [2]. For the rectangular type of indenter, Hyde et al [7] used a reference stress approach to convert the mean pressure under the indenter, $\bar{p}$, to the corresponding uniaxial stress, σ, i.e.

$$\sigma = \eta \bar{p} \tag{4.1}$$

and to convert the impression load-direction creep displacement, Δ^c, to the corresponding uniaxial creep strain, ε^c, i.e.

$$\varepsilon^c = \frac{\Delta^c}{\beta d} \qquad (4.2)$$

where η and β are the conversion parameters (reference parameters) and d is the width of the rectangular indenter, Figure 18. Therefore, the secondary creep properties can be obtained from impression creep test data using such conversion relationships. The technique can produce accurate results when the impression creep deformation occurring during the tests is small, compared with the indenter width or the specimen thickness. This may be done by limiting the secondary creep phase (which has a decreasing displacement rate) by allowing for a secondary creep trace that is approximately linear giving a minimum of a 100h for creep rate calculation, the test lengths are material and stress dependant. The conversion factors however are material independent. They depend on dimension ratios of indenter and specimens if the effect of the indenter deformation is neglected. η and β have been determined previously for a practical range of dimensions [21], [96].

Values for η and β are 0.430 and 2.180 [96] respectively for a standard specimen geometry (i.e w/d = 10 and h/d=2.5), if specimen dimensions are for some reason changed e.g. not enough material could be provided, ref [96] provides details on how to calculate the new values of the parameters.

4.2.2 **Basic Requirements**

4.2.2.1 Indenter and Specimen

The indenter must be made of material of significantly higher creep strength than the test material. In the case of fossil power plant pipework materials (CrMoV, P91) this means the use of nickel superalloys (Waspaloy or Nimonic 115) or ceramic indenters (Al_2O_3). This will ensure that creep occurs predominantly in the specimen; i.e. the creep strain rate present in the indenter must be negligible in comparison with the test specimen for the prescribed test conditions. The length, bs, of the indenter should also be greater than that of the specimen in order to make sure the whole length of the specimen is indented. A further

requirement is that the indenter should be ground so as to be parallel with the flat surface of the specimen. Periodic checks between tests must be made on the indenter to make sure that it is flat, including the effects of oxide and wear damage, if not the indenter may be ground so as to be made flat again, polishing of the surfaces to a recommended 200grit with a tolerance of ±0.02mm.

As shown in Figure 18, the specimen and indenter dimensions are defined by three ratios; w/d, w/b and h/d. d is the indenter width, w, b and h are the width, length and height of the specimen respectively. The recommended standard dimensions are wxbxh = 10x10x2.5mm and d = 1.0mm. If material is scarce the height of the specimen can be reduced, as long as conversion requirements are corrected. Or, the standard specimen dimensions can be reduced proportionally e.g. wxbxh = 8x8x2mm and d =0.8mm [96].

4.2.2.2 Loading, Measurement and Control

Indenter and Specimen Alignment and Load Application

Scribing lines on the sample to guide where to place the indenter is suggested. This allows for accurate alignment of the indenter to the specimen when placed on the lower loading bar. Once aligned the specimen must be held in place by the indenter with a load around 10% of the test load to secure the specimen before heating. Once the furnace has reached the test temperature the full load may be applied. The applied load should be known to an accuracy of ±1% to agree with requirements in uniaxial creep testing BS EN ISO 204 [63]. In cases where servo mechanical loading is applied there is a requirement for active control.

Displacement Measurement

Displacement measurement can be conducted through the use of water-cooled linear variable displacement transducers (LVDTs) which are connected to the bottom of two extensometers. However, strain gauges or other more advanced

methods may be used as long as measuring ranges lie within ±0.2mm with an accuracy of 0.5%.

The deformations must be monitored and are recommended to be recorded through signal conditioning and data logging software. The final displacement recorded by the data logger can be compared to an alternative measurement of the indentation depth for validation.

Temperature Control and Test Environment

The impression creep tests can be performed in air if the test temperatures are within the normal range of operating temperature for the material. Given the compressive contact between the sample and the indenter, oxidation effects on the surface are expected to be minimal even at relatively long test durations.

In the Nottingham creep laboratory, three 0.5mm dia. K type thermocouples are used to control the temperature; however there is no restriction to the use of S type or N-type thermocouples. The middle one is close to the specimen and the upper and lower thermocouples are about 25mm away from the specimen, near to the extensometer ridges. These positions may not always be held at the specified temperature due to the heat balance in the furnace. However, experience of many tests, with the temperatures checked by calibrated thermocouples and visual output, has produced a high degree of confidence in using such methods. However, increasing the proximity of the thermocouples to the specimen should be encouraged. Platinum resistance probes could be used in order to obtain a higher level of accuracy of temperature control or measurement.

BS EN ISO 204 [63] recommends a soak up period of 1 hour for full size uniaxial tests; the same recommendations are then passed on to the impression creep test method before full load is applied.

4.3 ROUND ROBIN IMPRESSION CREEP TEST PROGRAMME

4.3.1 Background and Motivation

The testing provides confidence that impression creep is capable of becoming a standardized test technique. In addition, the round-robin (RR) testing is required to show that there is sufficient expertise available to standards organisation bodies when the official standards are ready to be drafted and implemented. It is the aim that a deeper understanding of the test method may be achieved through the use of different set-ups that meet the minimum requirements.

4.3.2 Material and Test Conditions

A variant of P91 power plant steel of the same heat was tested, the material is referred to as BAR257 [97] and has a hardness toward the soft end of the normal range of P91 i.e. 204HV. The rupture strength under conventional uniaxial tensile loading of this BAR257 material has been shown to be close to 20% below the mean strength value for most P91 generally [98]. The tests done in this Round Robin were stepped stress tests. Here the load is increased once a sufficiently low secondary creep strain rate is achieved (Indenter and specimen requirements). For this particular series of tests, five stress levels were performed on the same specimen, all at 600˚C. No previous comparison of this type has been made across all testing laboratories. Loads and their converted stresses can be seen in Table 5. Equation 4.1 is used to make the conversion calculations with $\eta = 0.430$ as the conversion constant. The specimen and indenter dimensions used are those taken from the Basic Requirements Section above. An example of the output from one of the tests can be seen in Figure 24.

Table 5: Impression Creep Stepped Loads and Converted Stresses

Load (kN)	~2.07	~2.27	~2.42	~2.74	3.122
Stress (MPa)	89	98	104	118	134

4.3.3 **Equipment Specifications**

4.3.3.1 Test Rig Descriptions

Experience at Nottingham has given rise to minimum specifications [24] pertaining to load delivery and sensitivity and the same for temperature. However, there is still scope for variations in rig design as described in table 2 for the different labs. The main purpose of this exercise is to highlight the effects that variations in design have on the indentation traces and strain rates (equivalent strain rate), for which there are three major contributors according to European codes for creep testing, which are the specimen dimensions, loading cell/weights and specimen temperature [99]. Materials used for the indenters can be made of nickel based superalloys, however, ceramic indenters may be used provided the sample polishing is increased to a higher surface roughness than stipulated earlier, allowing for less noise in the initial stages of creep. However, the lower coefficients of thermal expansion, associated with many ceramics, would result in increased strain rates in comparison to nickel alloy counterparts which have a similar thermal expansion to P91. This is due to the reduction in size of indenter in comparison to the specimen after expansion which is not accounted for in the conversion relationships. It is therefore useful to not only find an indenter of higher creep strength but one with a similar thermal expansion coefficient.

4.3.3.2 Loading Application

There are two possible loading methods described by the rigs in this programme, referred to in this study as: 'normal' which involves the indenter approaching from above the specimen which is resting on a mount and 'reverse', where the indenter is facing upwards and the specimen is loaded onto the indenter.

Table 6: Test Rig Specifications

Organization	**Loading Mechanism**	**Load Accuracy**	**Indenter Contact Correction**	**Specimen – indenter Orientation**	**Heat Delivery**	**Temperature Control (°C)**	**Temperature Measurement**
AMEC	Dead-weight	5kN ±0.05kN	Not required	Normal	Coils built into furnace wall	±0.5	Two N-type thermocouples
EPRI	Servo-mechanical	25kN ±1.25kN	None	Normal	Coils built into furnace wall	±0.5	Three k-type thermocouples
NOTTS	Servo-mechanical	25kN ±1.25kN	None	Normal	Coils built into furnace wall	±0.5	Three k-type thermocouples
VTT	Servo-mechanical	10kN ±0.05kN	Floating indenter system	Reverse	Two flat coils on each loading bar	±0.3	Two R-type thermocouples

4.3.4 **Test Results**

4.3.4.1 Converted Minimum Creep Strain Rates

Generally there tends to be good agreement between the labs for the converted average impression creep strain rates (Figure 25), with data from the servo-electric and dead-weight systems giving very similar results. Indeed the dead-weight data lay at the mid-point of the servo-electric results. At each stress level within the stepped stress test as in Figure 24(other lab data at end of chapter Figure 30 - Figure 32) the final 100h of each test step are used to calculate the strain rate using a linear regression through the data. Not all step durations were the same between laboratories, but this did not appear to have a marked effect on the results as a 100h window required for calculating strain rates was present across all test data. Due to the test being indentation rather than tensile, creep tests after the primary phase are all steady state. Other methods were used which yielded results that tended to cluster around the same mean regression through the data points. These included firstly obtaining a plot of the strain rate with time, which is done by taking the slope forward and backward of each data point by either 25h or 50h. Taking the average of the resulting strain rates gave comparable results to those seen in Figure 25 and so the earlier method was used for the plot mainly due to ease of calculation. Figure 25 shows the impression strain rates for each lab compared to the minimum creep strain rate predicted using a literature Monkman-Grant relationship for Grade 91, modified for impression creep [80] at mean and mean-20% rupture life values. The uniaxial formulation of the Monkman-Grant relationship [100] is,

$$\mathrm{C} = \dot{\varepsilon}^{c}_{min} * t_f \tag{4.3}$$

where C and m are material constants, $\dot{\varepsilon}^{c}_{min}$ is the minimum creep strain rate (h^{-1}), t_f (hrs) is the time to rupture in the conventional uniaxial test. The equation can be modified to:

$$\mathrm{ICR} = 0.004575 * t_f^{-0.7391} \tag{4.4}$$

ICR is the impression creep strain rate (mmh^{-1}) and. BAR257 falls in the normal-weak range for general P91 performance and is correctly represented by the test. The Impression Monkman-Grant curves in Figure 25 deviate slightly from normal uniaxial curves, the uniaxial curve would veer more to the right and this is as a result of the decreasing converted strain rate observed in the Impression creep test.

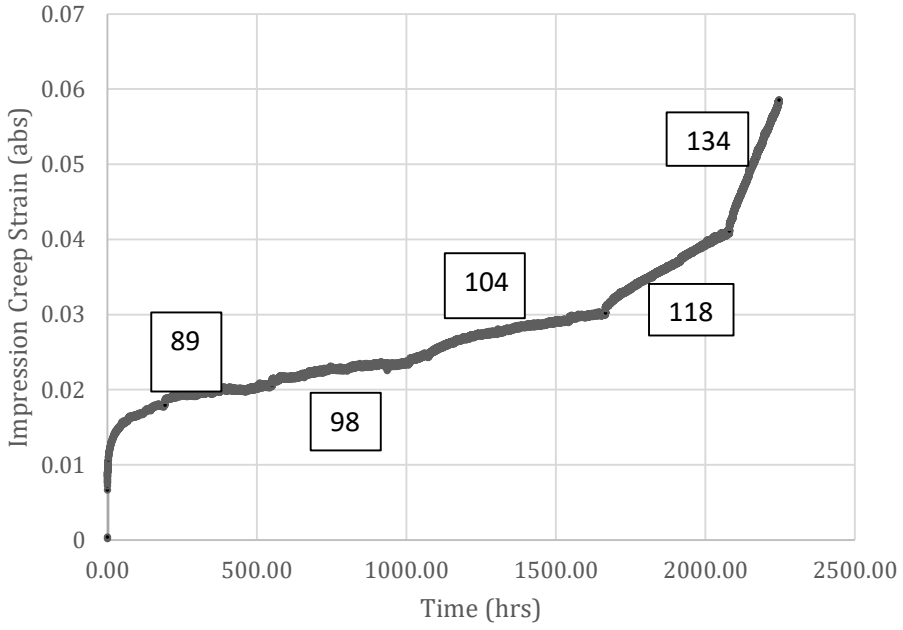


Figure 24: Nottingham stepped stress test results BAR 257 along with loads in MPa at each step.

4.3.4.2 Displacement Rate Variation

Stability and hence performance of the impression rig can be observed through the fluctuations of the displacement-time signal. For the purposes of the present study the displacement rate variation will be described as the maximum amplitude in fluctuation of the strain rate signals for each stress level in the stepped stress test. The method used to determine the plot of the strain rate is mentioned above. At each point in the final 100hrs of the step the strain rate is calculated for points 50h forwards and backwards of

that point within the stress level and will be referred to as the 100h strain rate from now on, an example plot for all labs is shown in Figure 27. The maximum amplitude in the signal is determined by detrending (removing any long term trends and focusing on short term changes) the signal and then taking the Fourier transform of the signal to identify the most prominent amplitude. This is then taken for each stress level and each lab and the averages across stress levels for each lab are compared in Figure 26. A best fit line through all the data points which may be used later for rig calibration is presented in Figure 38.

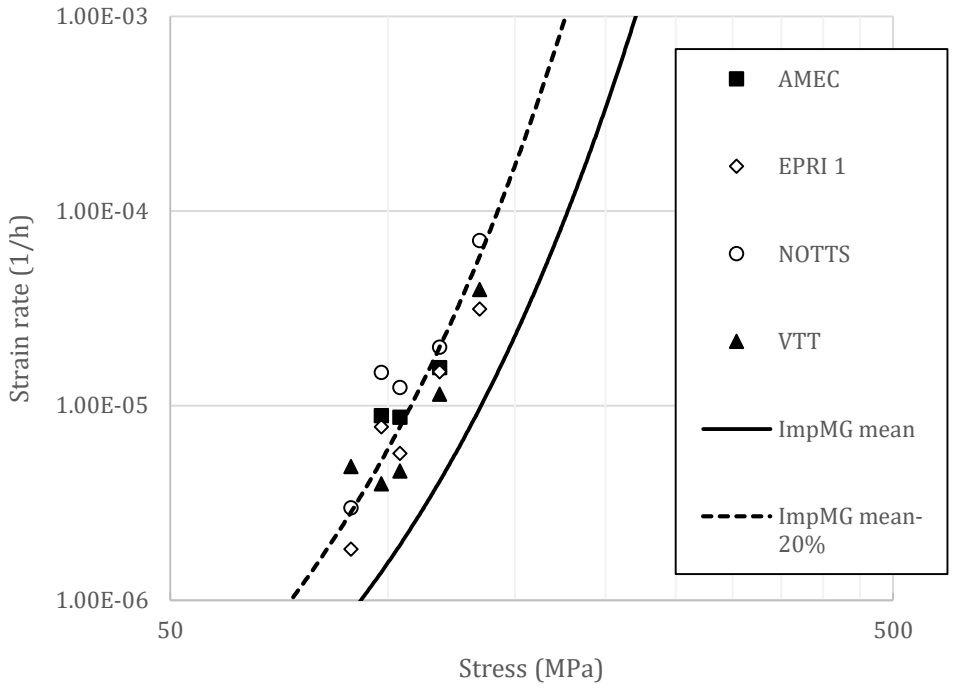


Figure 25:Converted impression strain rates (i.e. into equivalent uniaxial strain rate) from all labs at 600°C against the converted applied stress, with the strain rate predicted using the ECCC grade 91 mean and mean -20% minimum strain rate (determined from rupture data), where ImpMG is the Impression Monkman-Grant curve.

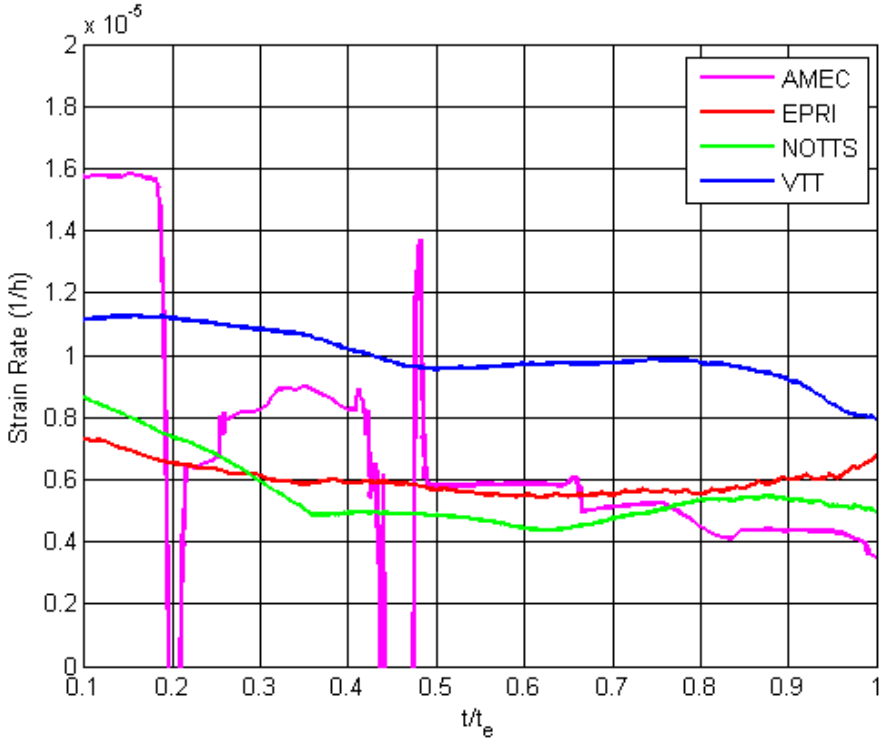


Figure 27: Converted strain rates for all labs at 104 MPa and 600°C, showing a general decreasing trend across the final 100 hrs for the 104 MPa test step.(t/te = time over time to the end of the step).

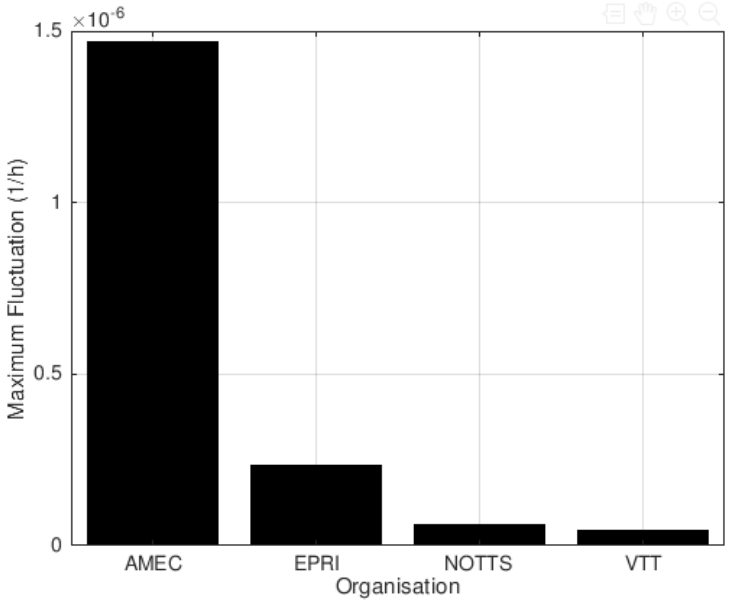


Figure 26: Maximum strain rate fluctuation at 600°C averaged from all stress levels evaluated here.

4.4 DISCUSSION

4.4.1 Data Variation and Applicability

Notable discrepancies between datasets can mainly be observed between the two loading mechanism types, that is dead-weight vs servo. The servo in combination with temperature stability lead to the ability for the load to be kept more consistent. As there is no closed loop load control with the dead-weight loading systems contact with the specimen is maintained but the expansion of the specimen as a result of fluctuations in temperature cannot be accounted for in the displacement signal, hence the larger instability in the displacement traces of the dead-weight machine. In spite of that fluctuation the average strain rates of the rig compare favourably with those of the servo operated machines. Although the data are not plentiful looking at the fluctuation of the test load across all stress levels, there is a clear trend especially when linked to the strain rate plots. The servo-mechanical systems due to their capability for active load control have a more stable signal as can be seen in Figure 28. This however is achieved at a higher cost than that of the dead-weight rig, something which is of concern to power plant operators as a test that is on par or cheaper with full-size uniaxial tests is required. VTT incorporates temperature stability in the order of ±0.3^{o}C. It has been shown that this temperature accuracy may be surplus to requirements for this particular test. However, for materials that may have higher thermal conductivities this level of accuracy may be required.

Any differences in equivalent creep strains observed between the labs (Figure 28, Figure 33-Figure 35) are attributed to the differences in step durations and initial values of LVDTs.

4.4.2 Requirement for Future Extension Life of Power Plant Components

The Impression Monkman-Grant relationship [12] has been shown to provide consistency between impression strain data produced in this

programme and the strain rate predicted from uniaxial data for the P91 material BAR257. The material used in this work may serve as a candidate material for the calibration of future test rigs, along with the fit to the data generated in Figure 28 acceptable strain rates would straddle the mean -20% curve for an acceptable rig.

An analysis of impression strain rates for other materials (preferably power plant steels) against their equivalent uniaxial tests may be useful in determining to what extent this is a general relationship.

The compressive nature of the test causes the secondary creep strain rates to decrease with time(~ $2x10^{-6}(h^{-1})$, rig dependant), the effect this has on the strain rates of subsequent loads is assumed to be reductive however this has not been quantified and so may be a useful area of investigation to be pursued.

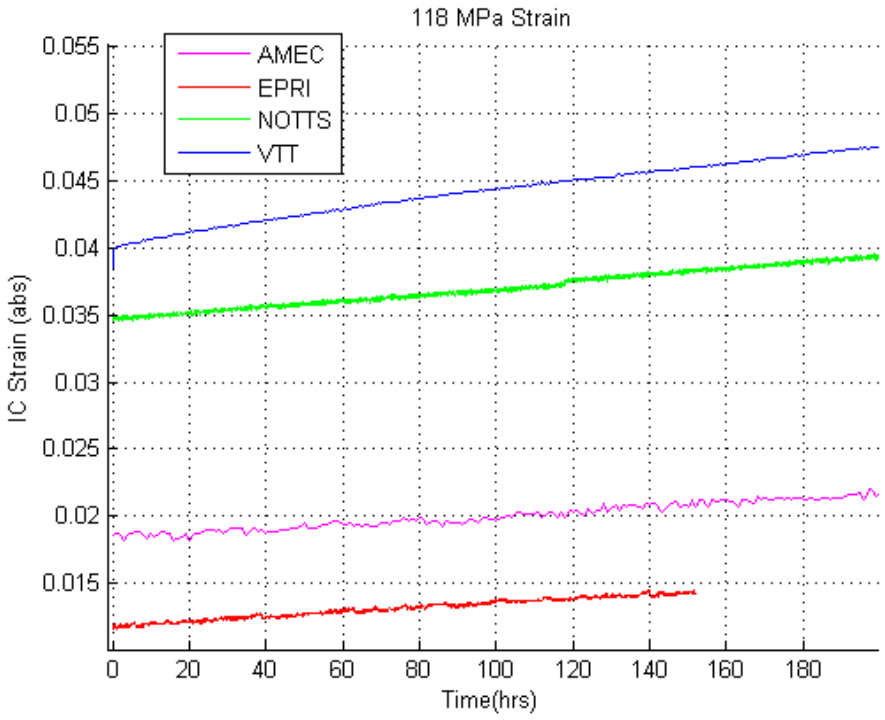


Figure 28: Impression creep (IC) traces at 118MPa

4.5 CONCLUSIONS

RR testing proved a successful benchmark of four different labs in the experimental impression creep test method, with both dead-weight and servo-electric giving similar measured strain rates under given test conditions. However, it is clear that temperature stability of the test arrangement has an impact on the stability of the displacement measurements (as with conventional uniaxial creep testing), although the averaged creep strain rate obtained appeared to be relatively insensitive in this P91 material. However, if this stability produces average strain rate comparable to that of more expensive systems, there may be an argument to use less costly equipment. However, for the purposes of precise control and accurate strain rate calculation servo mechanisms are superior but achieved at significantly higher cost.

Stepped stress test results from all labs including comparisons between labs at all stress levels along with accompanying strain rates.

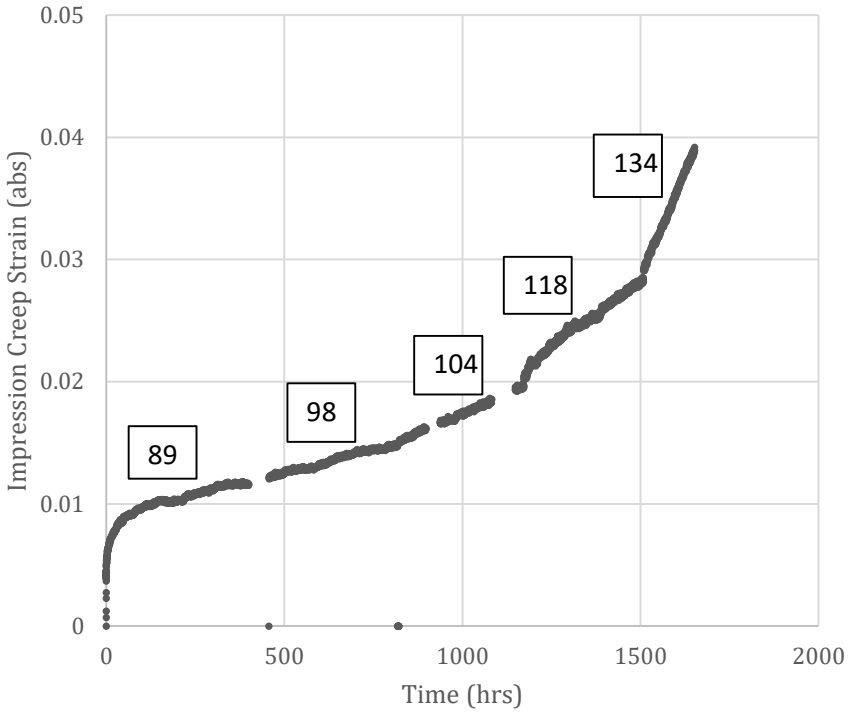


Figure 29: Nottingham stepped stress results alternative rig BAR257 600C

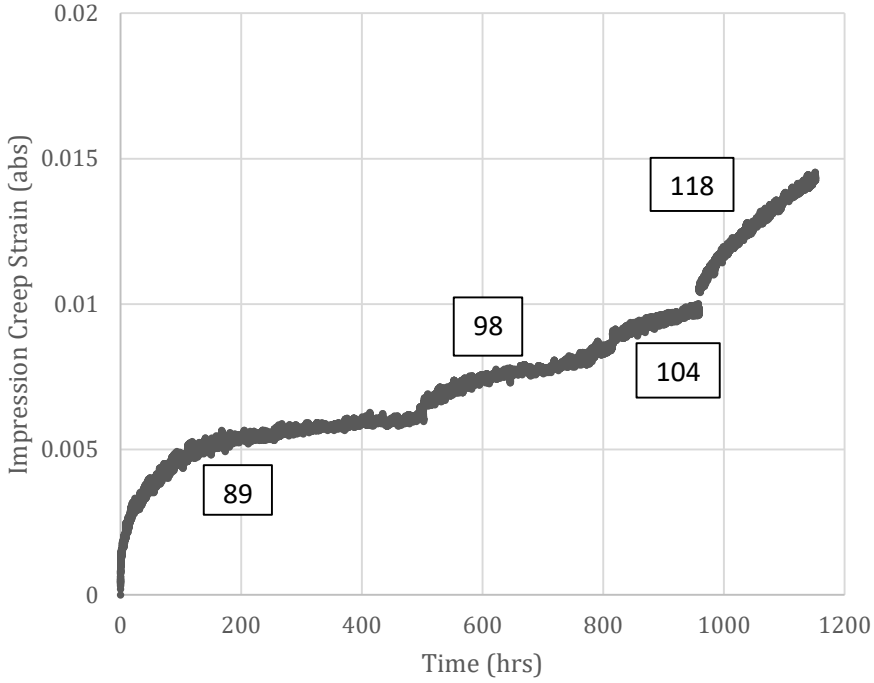


Figure 30: EPRI stepped stress results BAR257 600C

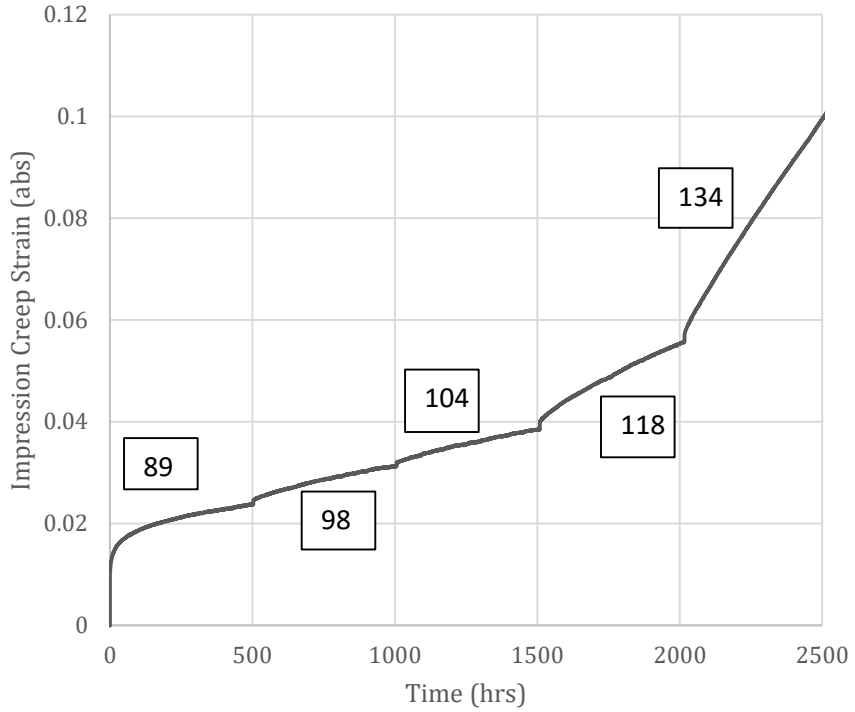


Figure 31: VTT stepped stress results BAR257 600C

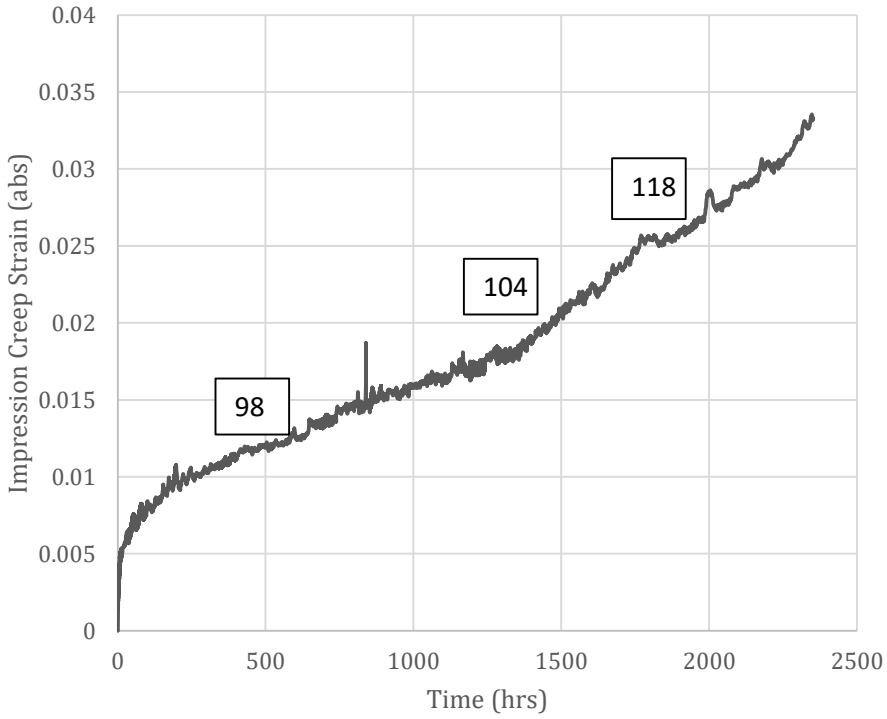


Figure 32: AMEC stepped stress results BAR257 600C

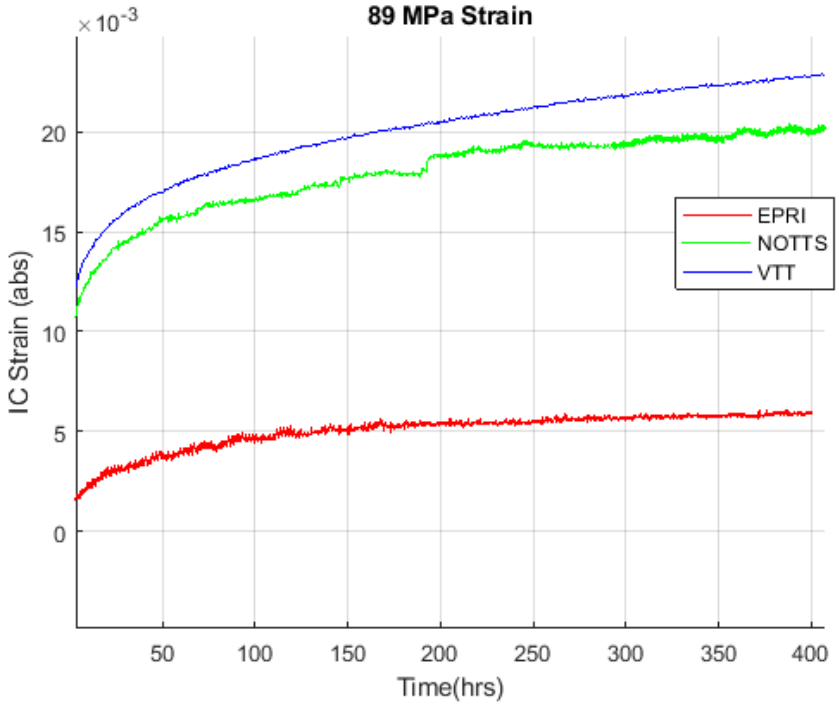


Figure 33: 89MPa step impression creep (IC) strain comparison

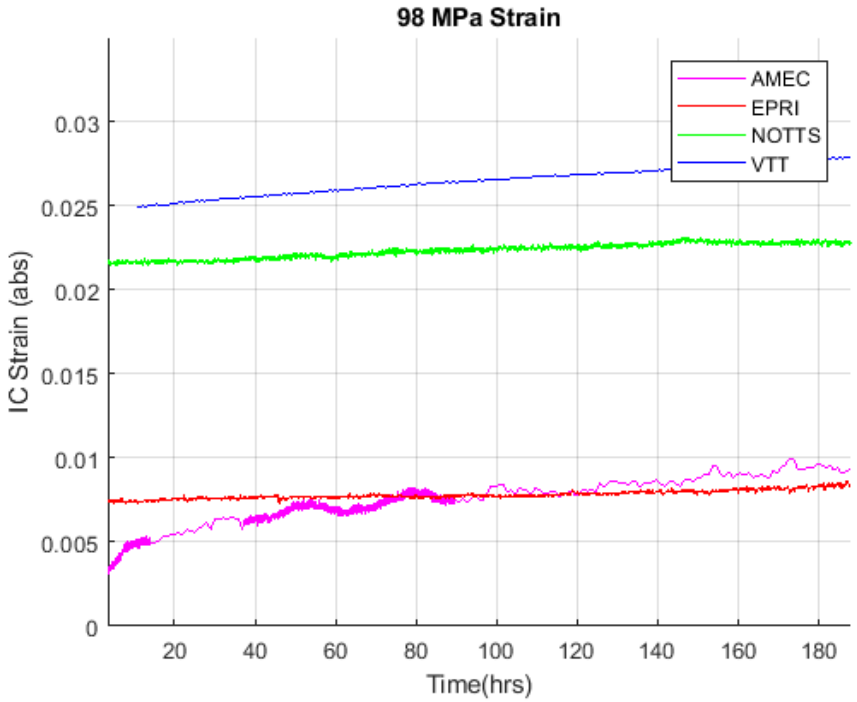


Figure 34: 98 MPa step impression creep (IC) strain comparison

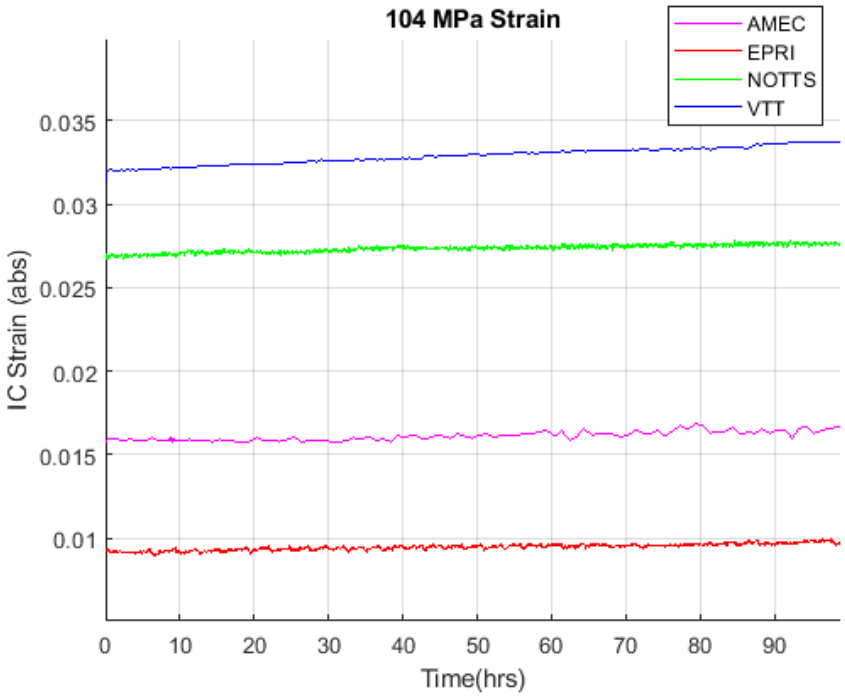


Figure 35: 104MPa step impression creep (IC) strain comparison

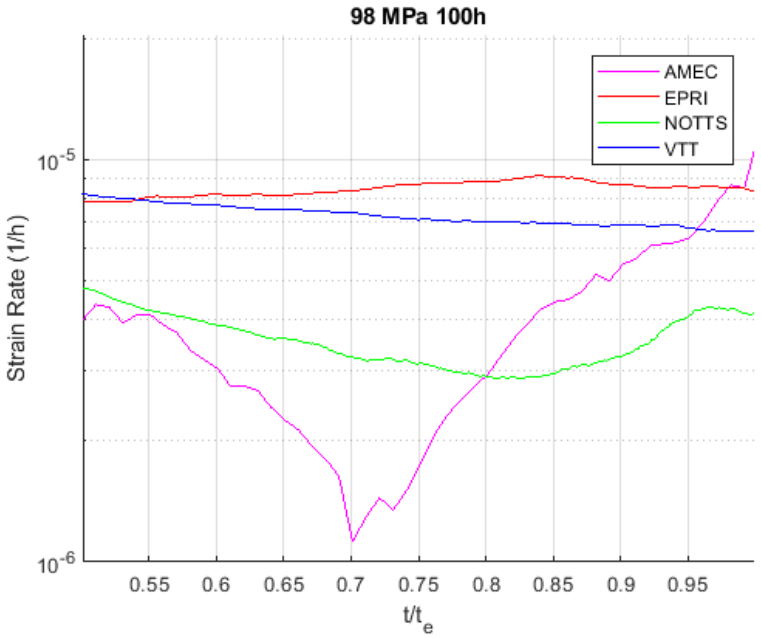


Figure 36: 98Mpa strain rates

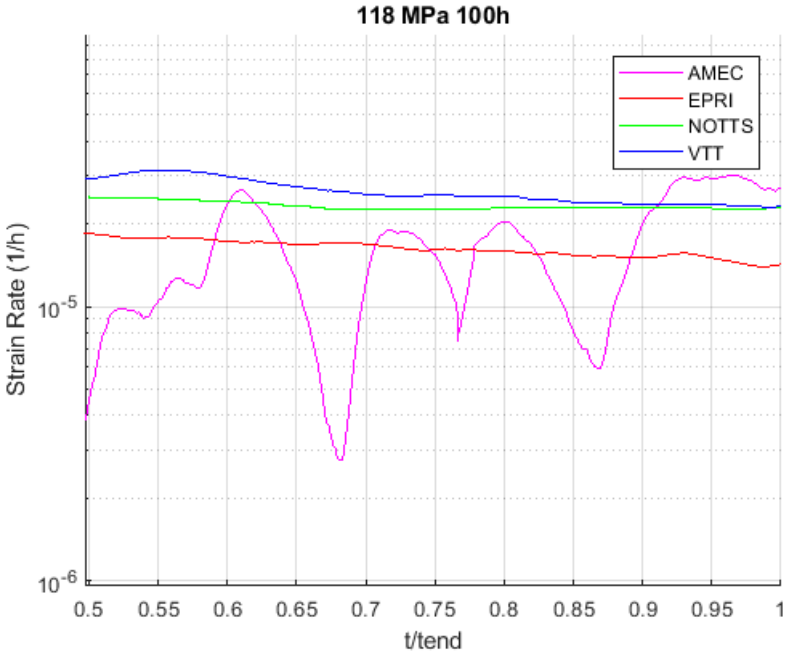


Figure 37: 118MPa strain rates

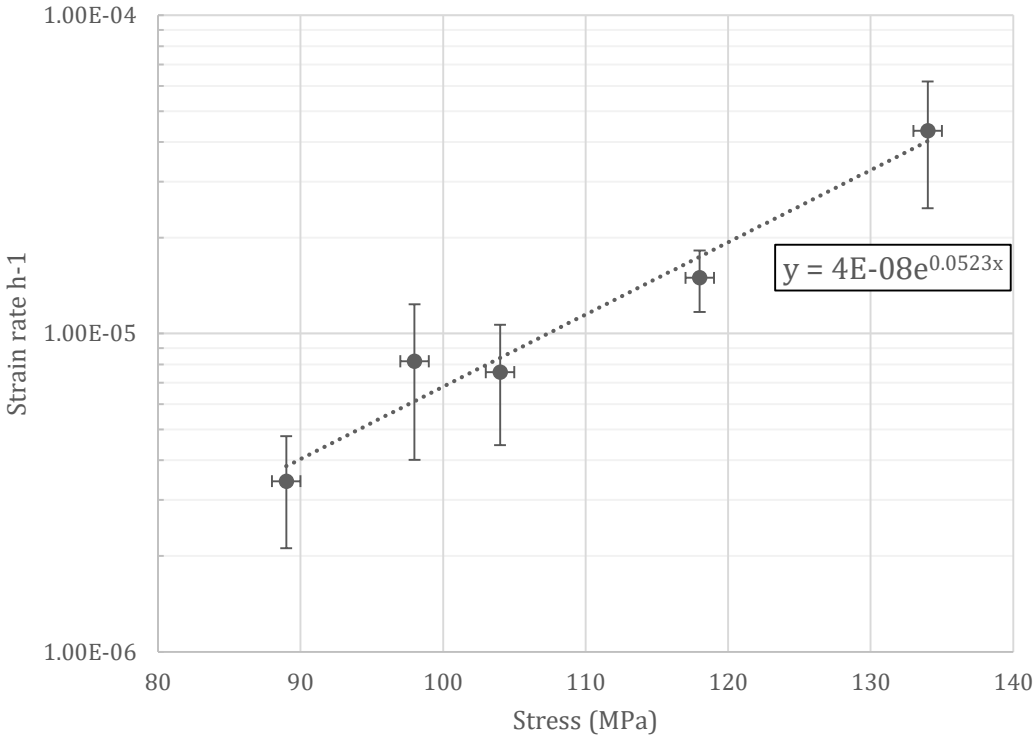


Figure 38: Best fit and calibration line for future test rigs and standard deviations at each stress level

CHAPTER 5

PRE-STRAINING EFFECT ON THE CREEP BEHAVIOUR OF IMPRESSION CREEP TESTS FOR A P91 STEEL AT 600^{o}C

5.1 BACKGROUND/MOTIVATION

Material subject to pre-straining may incur a change to its high temperature properties such as creep. Previous work in this area is related to the hot/cold work effect that remains in components post manufacture that then subsequently enter into high temperature service and to the possible optimization of materials through pre-straining to enhance their creep properties [101]. The technique used to bend pipelines involves raising the temperatures of the material in the region that needs bending and then closing the outer edges of the pipe, which creates a variation in thickness of the pipe between the extrados and the intrados, the former will have been subjected to thinning and plastic straining. It therefore maybe useful to test materials post manufacture using small specimen test methods for creep strength property variation if they are to enter high temperature service. There have been a few studies in recent years on the effect of pre-straining on stainless steel 316H [102]–[104], where it has been shown to increase creep resistance, nickel based alloys have also been tested where the opposite effect has been present [105]. It has been shown that depending on the material composition the effect of pre-straining may have enhancement and deleterious effects on the creep strain rate, creep ductility and rupture life of the material [106]. The nature of the effect is composition specific, although it is not known how much the microstructure plays a role. Previous work on pre-straining has focused on testing pre-strained uniaxial specimens in the creep regime. However, in these studies the engineering strain is used as a measure for pre-hardening whereas the true strain is to be used in the proposed work. In order to get creep data at specific true strain levels, impression creep testing of sections of a plastically deformed

uniaxial test specimen is presented in this work. This will aid the description of more localised creep behaviour in systems where the pre-straining is not uniform, similar to the way the test method has been used to characterise weldments [107]. The novelty in testing is the ability for the impression specimens to be removed from the necked region of a failed tensile specimen and for that particular strain to be tested. However the necked region strains are difficult to measure due to the lack of a uniform uniaxial strain in the region and so strains in that region are approximate values. It also tends to reason that material deformed past its tensile strength may not be used in service.

5.1.1 Small Scale Creep Testing – Impression & Small Punch

Two of the most widely used non-standard small mechanical test samples for use in power plant component material characterisation are the Impression and Small Punch creep tests. The impression specimen is usually 10x10mm rectangle 2.5 mm thick and the small punch specimen is usually a 8mm diameter disc which is 0.5mm thick according to the CEN workshop agreement [33]. The impression specimen is loaded with a flat rectangular indenter which has a contact area 10x1mm. The small punch specimen is loaded by a hemispherical punch head usually 5mm in diameter. An example of the specimen geometries and loading set up can be seen in Figure 39. The impression creep test is the simpler of the two tests in that the sample is deformed in uniaxial compression meaning the test can only produce the primary and secondary portion of the creep curve. A benefit of this simplicity is that it is a pure creep curve. Even though a failure life is not be produced, the test can be used in the capacity of a strength ranking tool [57]. The small punch test on the other hand is capable of producing all three portions of the creep curve, primary, secondary and tertiary including rupture of the specimen. However, this comes at a cost of increased complexity in the deformation mechanisms. Before the specimen has crept the specimen undergoes an initial plastic deformation including local thinning around the crown of the punch head [36]. The deformation of the sample is analogous to membrane stretching and is far from uniaxial in nature, including shearing

around the bottom clamp of the receiving hole. The specimen is also prone to failure in two separate locations, near the crown of the punch head and near the bottom clamp of the receiving hole. The initial plasticity present in the small punch test has a varied effect on the creep life [36] due to the non-uniform nature of the hot tensile pre-straining in the test. In the present work, the technique of pre-straining material and creep testing is to be investigated using the impression creep test mis-heat treated P91 and regular P91. The aim is to find a correlation factor between the two test techniques.

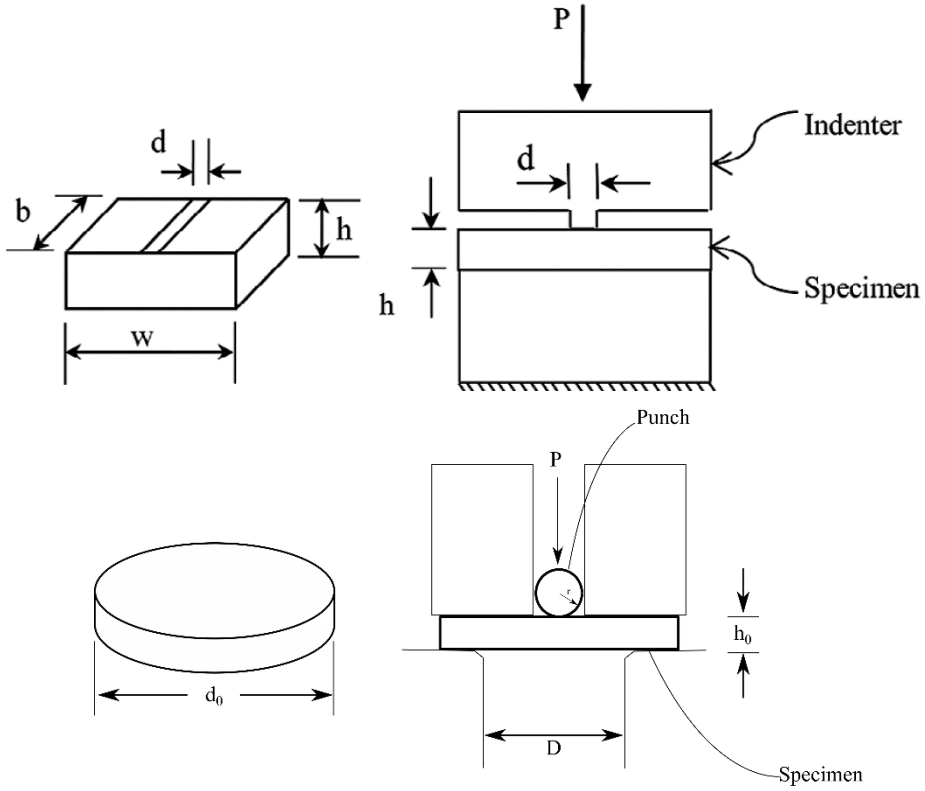


Figure 39: Top left impression specimen, top right impression loading arrangement, bottom left small punch specimen and bottom right small punch loading arrangement

5.1.2 P91 Steel – Normal and Aberrant Microstructural Conditions and Implications for Operating Power Plant

P91 steel is a 9-12% chromium power plant steel with significant additional creep strengthening from fine niobium vanadium carbo-nitride precipitation. It is characterised by its martensitic microstructure as a result of heat treatment

which involves austenizing at 1040-1080^{o}C, air-cooling and then tempering at 730-800^{o}C [89]. It is used primarily in forgings, tubing, pipes and headers. Mis-heat treated P91, also referred to as Aberrant P91, is a form of the steel that has failed to form a fully martensitic microstructure and instead has a ferritic one, in the worst cases 100% ferrite. This has the effect of greatly reducing the creep strength. If found in-service presents a risk to power plant operators because the strength of the material is not well evaluated. It is often detected in service because of its low hardness, typically 160HV or less in comparison to 200-250HV for normal P91.

5.2 MATERIAL AND EXPERIMENTAL SET-UP

5.2.1 Material and Heat Treatment

Although it is not always possible to establish how the aberrant microstructure has formed in individual cases, an absence of Martensite implies that, at some stage, temperature has risen into the Austenite range. The most likely way this can occur is by overshooting the tempering temperature either during the tempering stage of parent material production or during the post weld heat treatment of a weld. If the temperature rises sufficiently into the Austenite range before falling back to the correct tempering temperature, the Martensite can disappear. The tempering or post weld heat treatment will then be carried out on a Ferrite microstructure, which will be retained on final cooling to ambient.

A series of trials by Heywood [108] has shown that one particular heat treatment sequence can successfully reproduce the aberrant microstructure observed in service, and this was used in the present work.

This involved austenizing a sample of martensitic P91 at 910^{o}C for 30mins, skipping the air-cooling phase and dropping the temperature of the furnace to 760^{o}C and then holding at this temperature for 3.5hrs. This is done to ensure that the ferritic microstructure is fully formed through the thickness of the specimen.

After the 3.5hr period the furnace is left to slowly cool down to room temperature with the specimen inside to resist any sharp thermal changes to the material. Once complete, hardness testing of the sample must be conducted in order to confirm that there is no portion of the material that has the martensitic phase present.

5.2.2 **Large Uniaxial Specimen and Hot Tensile Testing**

In the interest of testing impression samples at different pre-strain levels and to simulate the possible effects of pre-strain during the small punch test or manufacture, hot tensile testing was carried out on the aberrant and normal P91. The testing was done to failure and true strain values calculated using FE analysis. An oversize specimen was tested, with identical gauge length/diameter ratio of the standard uniaxial creep specimen of 5/1. Modifications were made to the specimen so that the gauge diameter would be large enough to host impression creep samples after failure in the regions that experience necking. The sample was limited by the size of the grips at the Lab with a thread size M20 being the largest available meaning that the gauge diameter was designed to be 16mm. Details of the uniaxial specimen used can be seen in Figure 40.

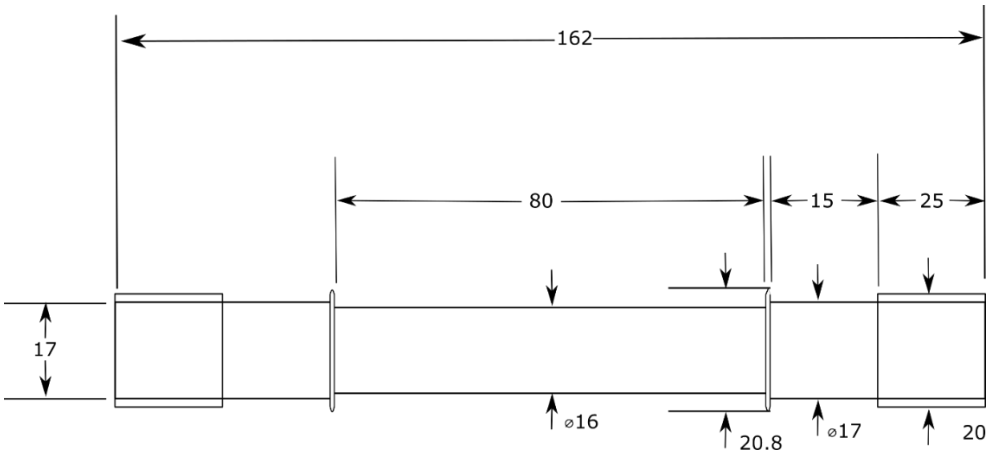


Figure 40: Oversize uniaxial specimen (dimensions in mm)

5.2.3 Removal of Impression Specimen and Creep Test Conditions

Once the uniaxial specimen fractured samples, impression were removed from four locations including the grip as a reference (Table 7). Samples were taken as close to the failure site as possible giving test samples with large strains, beyond what would be usable in practice. The specimen removed from the grip of the sample is the un-strained control sample. The sample strains were estimated preliminarily using diametral measurements, calculated using Equation 5.1, and calculated by the FE Model:

$$R_A = 1 - e^{\varepsilon_t} \qquad (5.1)$$

where R_A is the reduction in area ratio and ε_t is the true strain at failure. During removal of samples, it was ensured that witness marks were left on the sample in order that the surface facing the fracture site could be used as the loading surface. Subsequently the samples were tested at a converted impression test load of 98 MPa which has been set as standard for P91, falling in the power law creep regime, at a duration of ~250hrs for each test.

Table 7: Strain levels and locations of removed material for both specimens

Aberrant		**Martensitic**	
True strain (abs)	**Distance from failure site (mm)**	**True strain (abs)**	**Distance from failure site (mm)**
0	50	0	50
0.13	46	0.14	13
0.41	11	0.31	9
0.60	7	0.60	6

5.3 EXPERIMENTAL RESULTS

5.3.1 Uniaxial Tensile Test at 600°C

The aberrant material is shown to have increased ductility at the test temperature than the martensitic version of the steel as to be expected, the increase in engineering strain is 1.5x larger. However the necking is more localised around the failure region than the normal steel. This makes it more difficult to remove samples with large strains.

The relationship between engineering stress and strain can be easily derived:

$$\varepsilon_t = \int_{l_0}^{l_t} \frac{dl}{l} = \ln\left(\frac{l_t}{l_0}\right) = \ln\left(\frac{A_0}{A_t}\right) = \ln(1 + \varepsilon_{eng}) \quad (5.2)$$

And the true stress σ_t:

$$\sigma_t = \sigma_{eng}(1 + \varepsilon_{eng}) \quad (5.3)$$

These relationships hold up until the ultimate tensile stress of the material from which point the material is said to obey the simple isotropic hardening law:

$$\sigma_t = K\varepsilon_t^m \quad (5.4)$$

The constants *K* and m can be obtained by taking the logs of the plastic portion of the true stress-strain curve and taking the intercept and gradient respectively, in this case they were found to be *K*=329.7 and *m* = 0.1272, for aberrant and *K*=518.7 and *m*=0.1002 for martensitic. It is clear from Figure 41 and Figure 42 that the martensitic material is considerably stronger in tension and has a much lower ductility compared to the aberrant (ferritic) material.

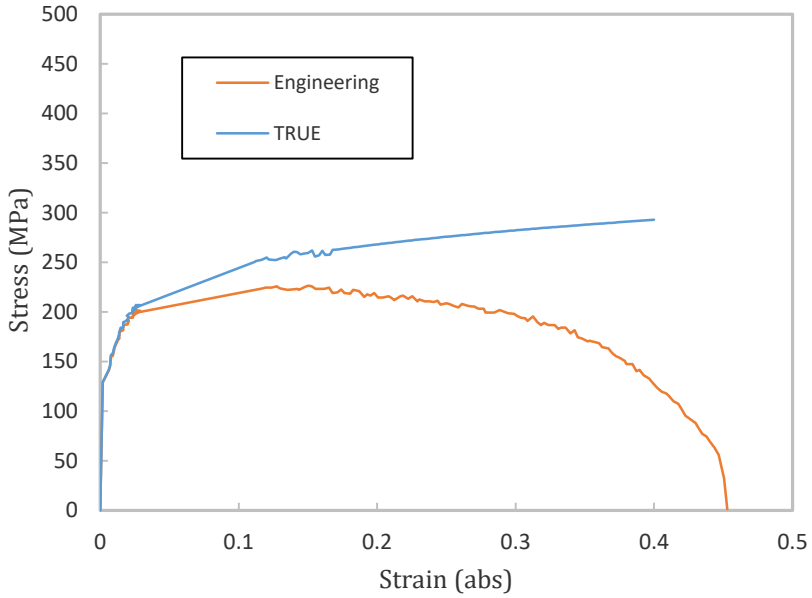


Figure 41: Engineering and true strain curves for aberrant material at 600°C

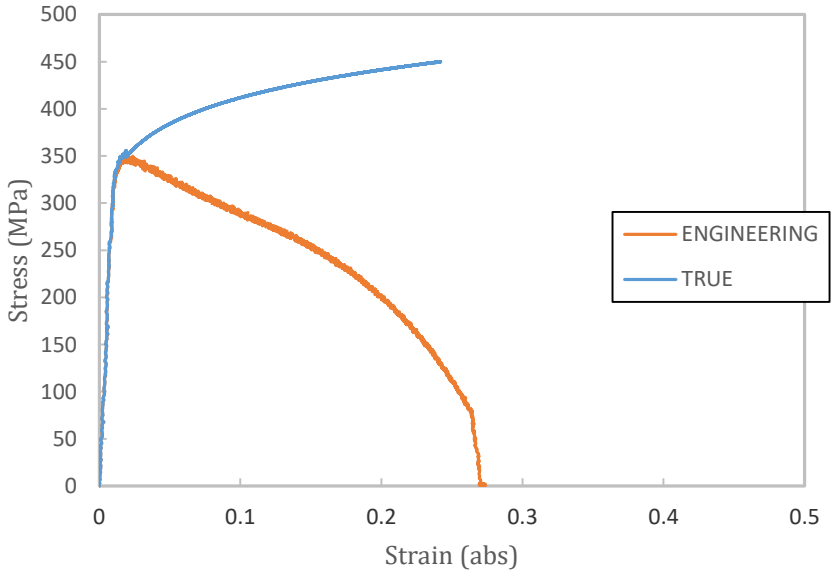


Figure 42: Engineering and true strain curves for martensitic material at 600°C

5.3.2 EBSD and Hardness Mapping of Tested Tensile Specimen

Hardness mapping of the failed specimen was used in this case to identify the regions of strain hardening as a preliminary method to evaluate the strain within the sample for specimen removal. As expected for the type of pre-straining employed the hardness of the specimen at the grip and away from the failure site are comparatively low and show little variation. Approaching the necked region as you start to see large changes in cross-sectional area there is a sharp increase in the hardness with the highest values appearing at the failure site. This is the case for both the aberrant and martensitic specimen, the straining is greater with the aberrant specimen, which can be attributed to the higher ductility of the sample owing to larger distortion of grains and increased sub-grain formation as shown in the EBSD images (Figure 43). Images are taken from the necked region of the specimen away from the failure site. Grain distortion and fragmentation is greater towards the failure site and can be linked to the increase in hardness for both specimens due to grain size reduction. This is in contrast as to what would be found in a long term creep specimen, which would have similar hardness values at the grip and failure site [109], owing to thermally activated deformation and damage mechanisms, however short term creep due to higher loads may show increased ductility at the failure site. The EBSD maps were taken at approximately the 25-30mm points shown on the plot in Figure 43.

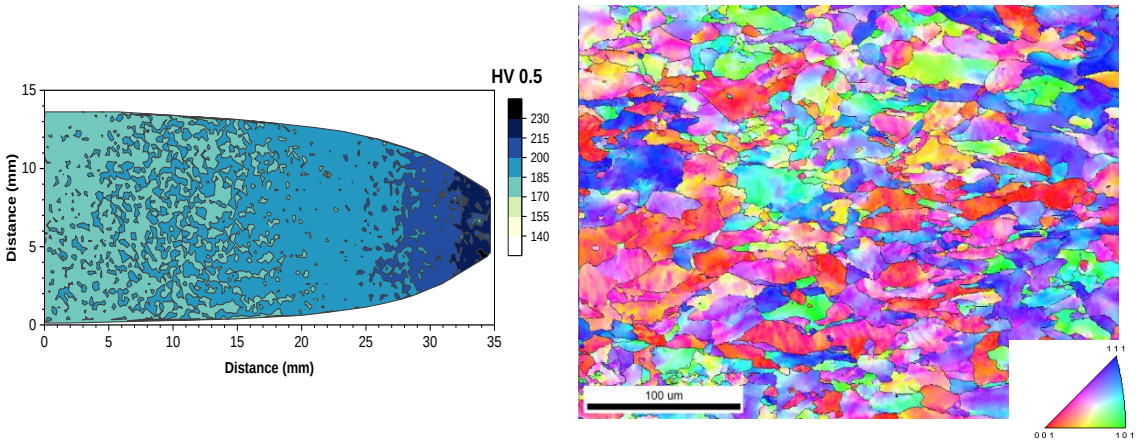
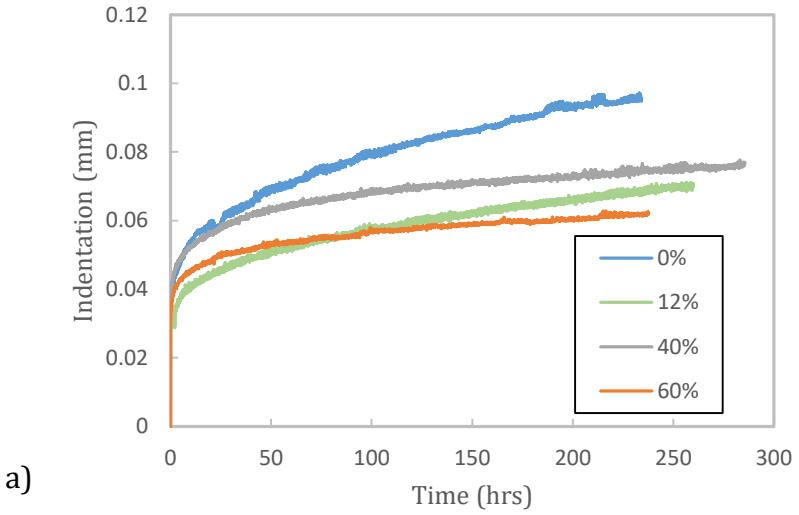


Figure 43: Hardness map of failed aberrant specimen (left) and SEM-EBSD images showing granular distortion orientation map (right)

5.3.3 Impression Creep Tests at 600°C Using Un-Strained and Pre-Strained Specimens

Results in general were consistent, showing a decreasing strain rate with increased pre-straining, see Figure 44. Generally for impression creep tests the creep strain rates in the secondary phase tends to decrease with time as with the 12% and 40% results, the 0% shows a sharp decline toward the end of the test and the 60% shows an increase in strain rate. The changes in the 0% and 60% strain rates can be attributed to instabilities in the lab temperature, which occurred during testing. Martensitic results are over on the next page.



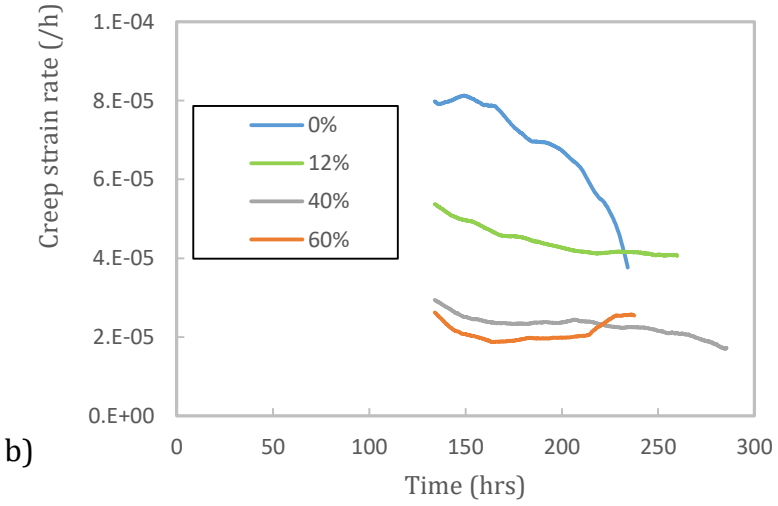


Figure 44: Impression creep test results for pre-strained P91 at 600°C a) indentation traces and b) equivalent creep strain rates

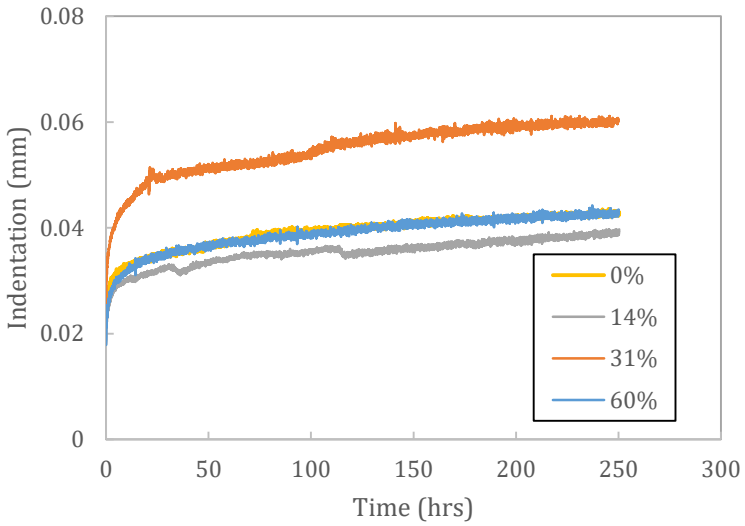


Figure 45: Martensitic pre-strain indentation cases

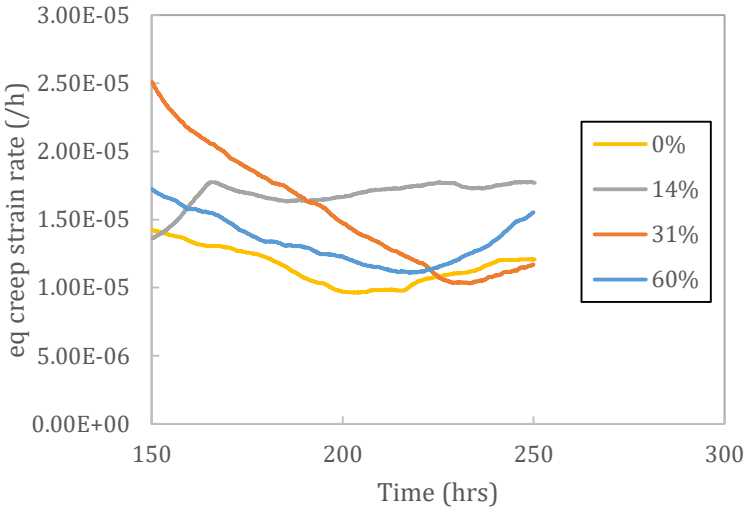


Figure 46: Martensitic strain rates

5.4 MODELLING OF LARGE UNIAXIAL TENSILE TEST

5.4.1 Finite Element Modelling of the Uniaxial Tensile Test

The hot tensile test specimen was simulated using the finite element method in order to accurately calculate the strains within the specimen at failure using an elastic-plastic analysis. A basic constitutive relation was used based on the material constants obtained in the tensile tests to describe the plastically deformed specimen. The total strain is described as a combination of elastic and plastic strains in three dimensions:

$$\varepsilon_{ij} = \varepsilon_{ij}^{el} + \varepsilon_{ij}^{pl} \tag{5.5}$$

where ε_{ij}^{el} and ε_{ij}^{pl} are the elastic and plastic components of the strain tensor. The material experiences hardening when the yield stress is exceeded subject to the von Mises yield criterion following a power law relationship:

$$\dot{\bar{\varepsilon}}^{pl} = D_p(^{\sigma_{eq}}/_{\sigma_y} - 1)^{n_p} \tag{5.6}$$

where $\dot{\bar{\varepsilon}}^{pl}$ is the equivalent plastic strain rate, σ_{eq} is the equivalent stress, σ_y is the material yield stress and D_p, n_p are temperature dependant material parameters. The hardening law is necessary to model the large deformations present in a uniaxial test to failure.

However, in the necked area of the sample, seeing as there is local thinning and notch formation, the stress state is altered from a simple uniaxial one to a multiaxial one. The stresses and strains would then need to be calculated and is done using the flow rule for conversion, the plastic strain tensor increment which is also the deviatoric strain increment is calculated as follows:

$$\Delta\varepsilon_{ij}^{pl} = \Delta\,\bar{\varepsilon}^{pl}\,{}^{3}/_{2}\,{}^{S_{ij}}/_{\sigma_{eq}} \tag{5.7}$$

where, S_{ij} is the deviatoric stress tensor and $\bar{\varepsilon}^{pl}$ is the scalar equivalent plastic strain, which describe both the direction and the magnitude of the plastic deformation. The full numerical implementation can be observed in the Abaqus theory manual [110]. The commercial numerical software Abaqus was used to simulate a quarter of the specimen (Figure 47) with the in-built plasticity model

and with the help of a mesh convergence study (Figure 48) an element size of 0.5mm was used in the gauge section. Axisymmetric quad reduced integration elements (CAX8R in Abaqus) were used in order to allow for smooth deformation of the elements. The geometry non-linear feature was also used to account for the large deformations near the failure site and the accompanying necking in the sample. During this mode the Jacobian is constantly updated as the elements undergo severe stretching around the centre of the specimen and the stress state of the specimen transforms from purely uniaxial to a triaxial state of stress. The simulation is run to the engineering strain at which the experimental sample failed as no failure criterion is employed, Figure 49 shows a comparison of numerical and experimental results.

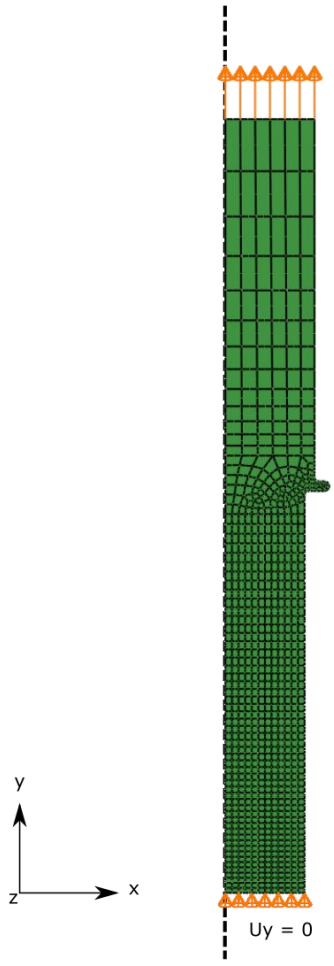


Figure 47: Un-deformed uniaxial mesh and boundary conditions

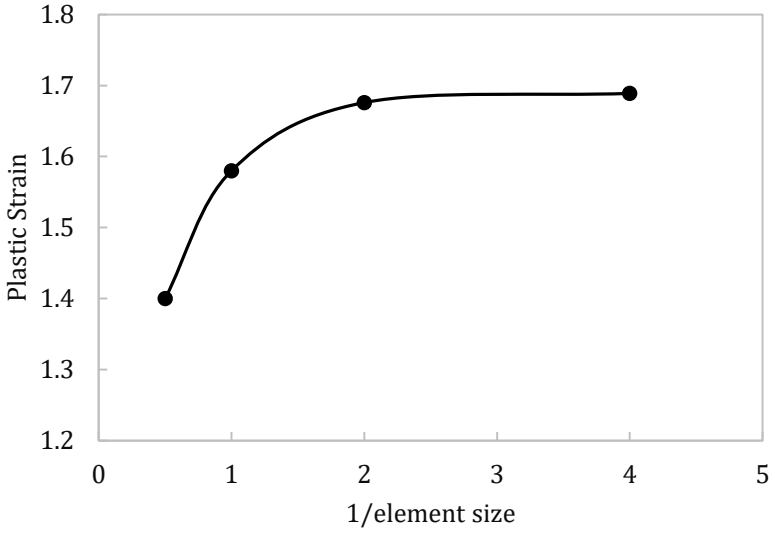


Figure 48: Study used to select the appropriate mesh

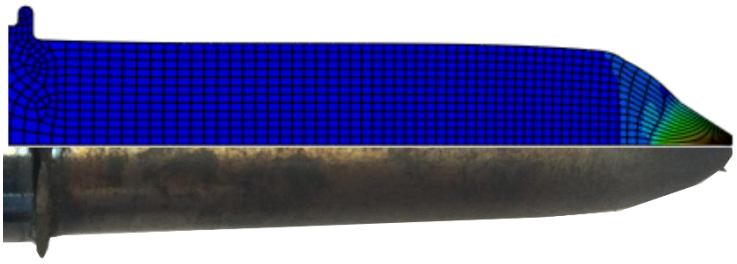


Figure 49: Plastic equivalent strain contours

The true strain at the base of the specimen was correlated to the engineering strain after fitting a power law curve to the data with constants a = 270.4, b=3.861 and c=0.03373:

$$\varepsilon_t = a\varepsilon_{eng}^{b} + c \qquad (5.8)$$

Fitting results can be seen in Figure 50, change in the shape of the curve is a result of the onset of necking – the ultimate tensile stress of the steel is exceeded and apparent softening of the material is observed at ~14% engineering strain.

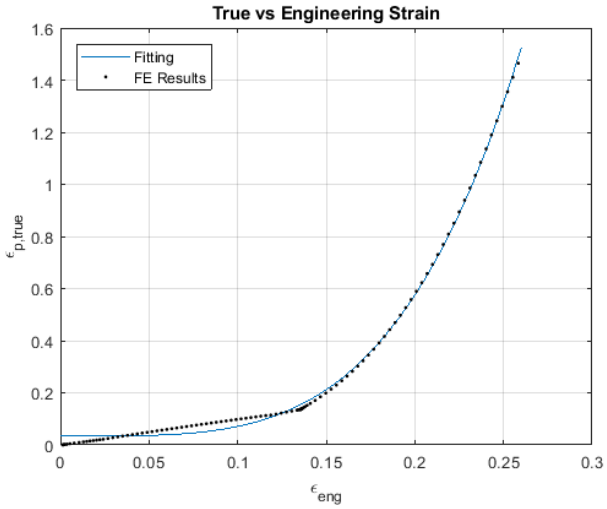


Figure 50: Tensile test at 600°C and true vs engineering strain finite element results and power law fitting

5.5 DISCUSSION

5.5.1 Capability of Impression Creep Testing

Impression creep has been shown to produce strain rates that are equivalent to those of uniaxial ones by Sun et al[58]. Creep strain rates are lower for the pre-strained specimens in relation to the as-received un-strained specimen. Generally, the trend according to the strain data for 98MPa indicates an increase in creep life with an increase in true strain, for this test type on the aberrant (ferritic) P91 material. EBSD images point to elongated grains along the loading axis of the test specimen, the elongated grains in this instance are orthogonal to the applied load from the impression indenter. The combinations of the mode of loading, dislocation movement due to plastic straining and locations and sizes of precipitates in the matrix lead to an increased difficulty in dislocation movement. It has been observed in previous work [36]that in uniaxial tension creep tests the effect of pre-straining is not always creep enhancement and that the effect is load dependant. Creep strength reduction in this instance may be as a result of void nucleation and cavity density within the specimen and so the load carrying cross-section may be reduced in this instance resulting in an increased nominal stress and hence creep rate. However in this case an increase in cavity density may not

have the same effect and creep may depend mainly on dislocation mobility and grain boundary sliding effects.

Previous work have shown that at pre-straining levels >20% the Monkman-Grant correlation for the material starts to break down [106]. So even though the reduced strain rates are observed it is unclear whether the creep ductility remains the same or is reduced as is the case for pre-straining above 20%. However the derived Φ parameter ($\Phi = \dot{\varepsilon}_{pmin}/\dot{\varepsilon}_{omin}$) [111] although is decreasing for the ferritic (aberrant) case, in the case of the martensitic material it behaves in a highly non-linear manner, however the behaviour is similar to that seen for the uniaxial case for engineering strains as seen in the literature [36].

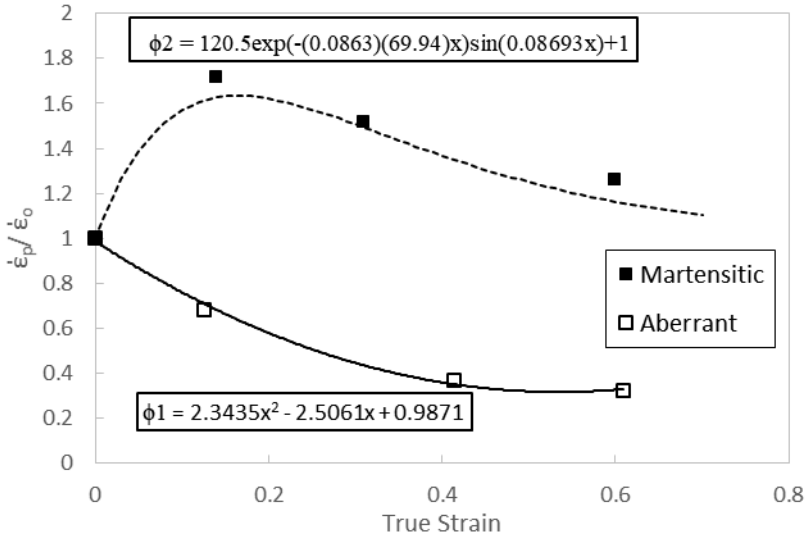


Figure 51: Derivation of the phi parameter for aberrant and martensitic cases at 98MPa 600°C

5.6 CONCLUSIONS

- Capability for impression creep testing and mechanical characterisation of fine changes in material property has been realised along with several previous studies of a similar nature.
- A predictive function for the secondary creep behaviour of grade 91 shows that there is a decrease in strain rate when material hardening is

increased, but is inconclusive as to whether at large strains this results in an increase in creep life (strains>20%).

- Although there is an increase in creep strength with the aberrant material, even with a pre-strain value of 60% (for which the increase in creep life isn't assured) the minimum equivalent creep strain rate is still larger than that of the martensitic material in all cases at this stress level.
- The test may be used in post manufacture sampling and testing.

CHAPTER 6
SCOOPING EFFECT OF POWER PLANT PIPES USING CONTINUUM DAMAGE MECHANICS

6.1 INTRODUCTION

Large chemical plants and power plants usually operate at high temperatures and pressures at which creep degradation can be the dominant mechanism for failure in the components subjected to these conditions. In sub-critical fossil-fired power plants, operation temperatures and pressures can exceed 550^{o} and 170 bar respectively, the plants may be expected to operate continuously under these conditions for periods extending (in the UK) forty years – well beyond the original design life of the components, which is in the region of 25 years. In such cases it is necessary to be able to conduct condition monitoring exercises to ensure the structural integrity of the at risk components. Creep condition monitoring usually consists of cold assessments which may include diametrical surveys, hardness surveys, non-destructive testing measurements which may include ultrasonic and potential drop techniques (sonic or electric signal is reflected through the wall of the component, disturbances in signal indicate voids or damage) [112] as well as the use of metallographic techniques alongside creep replicas for microstructural assessment. Innovative test techniques for the assessment of components include scoop sampling and small specimen creep testing of in-service components. This involves the removal of button shaped samples from in-service components during scheduled outages. An example of a tool that accomplishes this is the Rolls-Royce Ssam-2 scoop sampler (Figure 11-chapt2) [53] which through the use of a hemispherical cutting head and a flexible drive shaft effectively grinds out button shaped scooped samples (approx. 30mm diameter 5mm depth depending on wall thickness) from the surface of the component. This leaves behind a dimple on the surface of the component, which must be polished and deburred to remove any surface roughness introduced by the cutting process. The material removed by this process can then be machined into small sample test specimens [28], which include the small punch creep test

specimen, the impression creep test specimen, the small two bar creep test specimen, the ring creep test and the miniature uniaxial specimen (see chapt2 as reference). So far these test methods have been useful in the ranking [1], [25] of similar components by creep strength which aids in the prioritisation of components for inspection and possible removal. There has also been an effort to use the removed material to obtain the material constants for more complex constitutive damage models like the Kachanov-Robotnov creep damage equations [62] in cases where there may be aberrant or mis-heat treated material, which may be weaker than the normal material in service and hence needs identification.

The effect of the remaining dimple on the structural integrity of the component has been investigated before; elastic and steady state creep analysis have been conducted by Rouse et. al [113] and Dedov et. al [114] which illustrate the stress risers that appear below the base of the dimple. Resulting stress concentrations were used to calculate the effective creep life reduction in a variety of loading configurations according to PD5500 [115] [113]. The loading conditions and dimple placements where designed in a worst-case scenario highlighting the requirement for careful selection of sampling sites so as not to intensify damage growth. The natural progression from linear steady-state models is to use non-linear damage models which include a variable that accounts for macroscopic (or microscopic) material degradation, this allows for the modelling of the tertiary phase of creep and for a more accurate prediction of the remaining life of the material.

Continuum creep damage modelling as a life prediction tool for three dimensional or complicated structures has gained popularity over the past 20 years, which can be attributed to the numerical capabilities of modern PC's. As a result the failure modes of simple components with notches and defects can be examined in more detail using one damage state variable [116] and two damage state variable equations [117]. Furthermore as it is of interest to investigate the effect that the dimple would have on the failure of a component, the effects of

small spherical notches or defects have been investigated numerically for single crystal materials [118] in which the accumulation of inelastic strains (ductility exhaustion) is used as an indicator for damage in the material. This analysis however was conducted at the meso scale and was used to simulate void growth in and around the defect using a micromechanical material model, the macro or continuum effects are not considered in this particular work when considering creep crack initiation. The aim of the present study is to acquire an accurate representation of the percentage of allowable material to be removed from in service components and to further understand the accumulation of damage (growth of voids) in instances where material is removed according to different loading conditions. The model is verified using a pair of novel test specimens capable of obtaining the multiaxiality parameter 'α_m' (see Chapter 2 Equation 2.3). This is also done in a manner which greatly reduces the time taken for testing as the notch strengthening behaviour is not as pronounced as that of a Bridgeman notch specimen [119]. In this case an asymmetric spherical notch and an elliptical notch are used to simulate multiaxial effects and in the latter case complex loading effects, in the aim of simulating out of plane damage accumulation. Traditionally a Bridgeman notch specimen is used to simulate the effects of a multiaxial stress state of a material.

The chapter is structured in a way that illustrates the methods used to make creep life predictions in pipes, starting from steady-state Norton's law and reference stress methods and progressing to creep continuum damage mechanics. The damage laws are then used to make predictions for the scoop-sampled pipe, which are later verified by the two novel test specimens.

6.2 MATERIALS AND METHOD

6.2.1 Material Composition

9-12% chromium steels are most commonly used in fossil-fired power plants with many plants in Europe and the USA containing headers and piping made from the material. The chemical composition and typical uniaxial rupture life are shown below in Table 8.

Table 8: Chemical Composition of P91 steel (wt %)

C	**Si**	**Mn**	**P**	**Si**	**Cr**	**Mo**	**Ni**
0.387	0.382	0.463	0.003	0.005	10.1	1.02	0.315
Al	**Co**	**Cu**	**Nb**	**Ti**	**V**	**W**	**Fe**
0.0395	0.0091	0.055	0.0544	0.0059	0.239	0.309	Balance

6.2.2 Material Behaviour Model

The reproduction of creep strain curves for a uniaxial condition is an area of significant importance when it comes to understanding creep behaviour. Several models have been suggested over the years [120]. The most robust solution to this problem is continuum damage mechanics, which employs a power law or sinh function coupled with a material deterioration equation to simulate mechanical degradation and hence the three stages of creep. Kachanov and Robotnov [9] formulated the first widely used one-state variable suite of equations which were generalised by Leckie and Hayhurst [10], [121] to produce the multiaxial equivalent (Chapter 2 Equation 2.29). The damage term is in the denominator of the strain function (representing void coalition and growth, effectively reducing the load carrying area of the material) and tends from 0 to 1, 0 being undamaged material and 1 being material that is unable to carry load. The formulation results in an infinite strain rate if the max value is set to 1. In order to circumvent this the maximum damage value may be set to 0.99, however the strain rate still approaches infinity leading to very small time steps during the latter stages of FE simulation and lengthy solution times. Liu and Murakami

proposed a new model [14] which circumvents this problem and so is more suited to problems where damage localisation occurs. The Liu and Murakami creep damage equations take the form:

$$\frac{d\epsilon_{ij}^{c}}{dt} = \frac{3}{2} A \sigma_{eq}^{n} \frac{S_{ij}}{\sigma_{eq}} \exp\left[\frac{2(n+1)}{\pi\sqrt{(1+3/n)}}\left(\frac{\sigma_1}{\sigma_{eq}}\right)\omega^{3/2}\right] \tag{6.1a}$$

$$\frac{d\omega}{dt} = D_{LM} \frac{(1-e^{q_2})}{q_2} \sigma_r^{p} e^{q2\omega} \tag{6.1b}$$

where ε^{c}_{ij} and S_{ij} are the creep strain components and the deviatoric stress components respectively; σ_{EQ} and σ_1 are the equivalent stress and maximum principal stress respectively. ω is the damage parameter which indicates the growth of voids. A, n, B, $q_2$and p are material constants and the rupture stress σ_R is described as:

$$\sigma_r = \alpha_m \sigma_1 + (1-\alpha)\sigma_{eq} \tag{6.2}$$

where α_m is a material constant that determines the multiaxiality of a material and falls in the range $0 \leq \alpha_m \leq 1$, this determines whether failure will be dependent on the maximum principal stress or the von mises equivalent stress.

The material constants reported here are based on uniaxial creep data for P91 at 600°C at a number of stresses. A and n are the Norton's law constants and can be obtained by retrieving the slope and the intercept of the linear plot of $\log(\sigma)$ vs $\log(\dot{\varepsilon})$ of the creep data. The intercept and the gradient give $\log(1/B)$ and p when $\log(t_{rLM})$ and $\log(\sigma)$ are plotted against each other. Once determined all that remains is q_2, which is determined by optimising its value to give the model the best fit to the experimental data (see Figure 58 in Appendix for fitting). Values for this model were taken from the literature [11] and a detailed account of how the material constants are determined can be found here [13].

6.2.3 Pipe Geometry and Loading

The components taken into consideration in this work are pipelines that undergo the severest operating conditions within sub-critical power plants, which are the main steam lines. Often the length of the pipe is much larger than the diameter and so the closed end condition is used which simulates an infinitely long pipe, a dimple is added to replicate a removed scoop and generate the required stress concentrations. The internal diameter of the pipes is 240mm along with a range of wall thicknesses ranging from 30mm-60mm. Based on British standards PD5500 the mean diameter hoop stress (σ_{MDH}) can be calculated for each the aforementioned geometries with the following relationship:

$$\sigma_{MDH} = \frac{p_i(R_0/R_i + 1)}{2(R_0/R_i - 1)} \tag{6.3}$$

where p_i is the internal pressure loading and R_0 and R_i are the external and internal pipe radii respectively. For most cases, the mean diameter hoop stress is 59.5 MPa, except three cases where the stresses are 50, 55 and 70MPa. The axial load (σ_{ax}) used is derived from the closed end condition due to the assumption of an infinitely long pipe:

$$\sigma_{ax} = p_i/[(R_0/R_i)^2 - 1] \tag{6.4}$$

The axial load is varied in accordance with maximum and minimum allowable system loading conditions based on a loading factor k ($0 \leq k \leq 1$), with 0 representing the axial load which represents the closed end condition and 1 representing that maximum permissible additional axial load according to PD5500. The loading factor k is used alongside the axial stress to generate the equivalent moments to be applied to the system [122], where:

$$\sigma_{ax} = \frac{M_x R_0}{I_x} \tag{6.5}$$

$$M_x = \frac{\pi}{8} k p_i \left[\left(\frac{R_0}{R_i} + 1\right)^2 - 2\right] \frac{R_i^3}{R_0/R_i} \left[\left(\frac{R_0}{R_i}\right)^2 + 1\right] \tag{6.6}$$

The moments are applied about the x-axis in Figure 52, where M_x is the applied moment and I_x is the second moment of area of the pipe. Full test parameters are shown in Table 9.

Table 9: Test parameters selected for analysis

WT(mm)	h(mm)	Internal Pressure (MPa)	MDH (MPa)	k
30	3.00	13.22	59.50	0
35	3.00	15.15	59.50	0
40	3.00	17.00	59.50	0
50	3.00	20.52	59.50	0
60	3.00	23.80	59.50	0
30	2.25	13.22	59.50	0
35	2.63	15.15	59.50	0
50	3.75	20.52	59.50	0
60	4.50	23.80	59.50	0
40	2.00	17.00	59.50	0
40	4.00	17.00	59.50	0
40	5.00	17.00	59.50	0
40	3.00	14.29	50.00	0
40	3.00	15.71	55.00	0
40	3.00	20.00	70.00	0
40	3.00	17.00	59.50	0.5
40	3.00	17.00	59.50	1
40	3.00	17.00	59.50	0*
40	3.00	17.00	59.50	0.5*
40	3.00	17.00	59.50	1*

*Loading due to moment

6.2.4 **FE Modelling**

The commercial FE package ABAQUS was used to create and model an elastic-creep analysis of the component, using the package's strain-hardening model for steady-state creep analyses. For creep damage modelling a CREEP sub-routine was used to implement the Liu-Murakami damage effect. A half pipe global 3D model was set up with a relatively coarse mesh; the front axial face of the model was constrained with a displacement boundary condition, as was the face of symmetry. The rear axial face was loaded with the closed end condition axial force along with an equation constraint to keep the load direction constant. The inner surface is subjected to internal pressure loading. A refined mesh selected through mesh convergence is used in and around the notch in order to carefully study the stress concentration and damage which is initiated in that area. A quadratic reduced integration brick element (C3D20R) was used in all cases. The analysis produced small deformations overall so the geometry non-linear feature was left unticked. The pipe length was selected so as to be double the size of the damaged area affected due to notch stress localisation. The bending moment was applied about a reference point at the centre of the pipe (directly below the notch) and constrained to the face on which the axial load would normally be applied through a multipoint constraint.

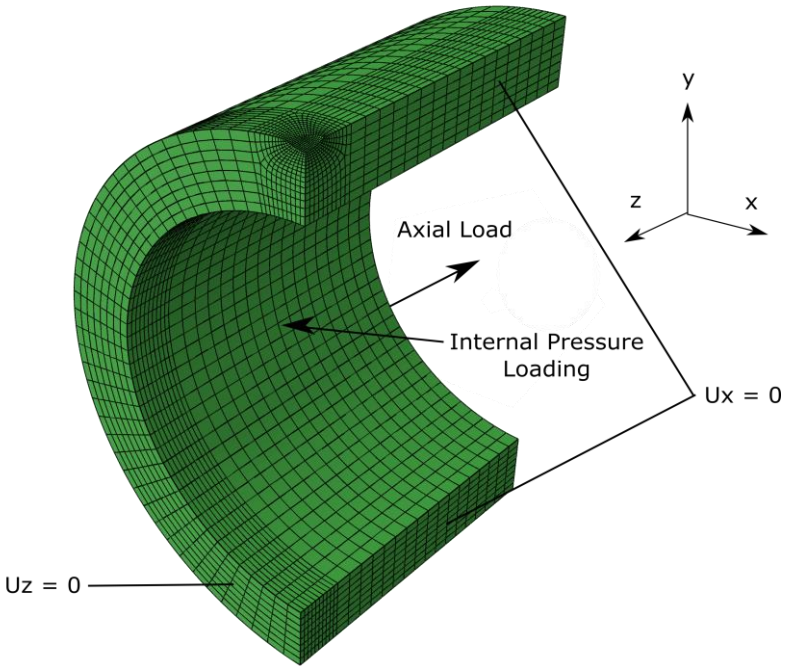


Figure 52: FE Model and Boundary Conditions

6.2.5 **Life Prediction**

The life prediction of a plain pipe can be estimated analytically and numerically [123]. The analytical and steady-state numerical solutions use similar methods for prediction. Using the reference or skeletal point stresses across the thickness of the pipe, the uniaxial life prediction equation can be used (Equation 6.7). The equation is found by integrating equation (6.1b) between the limits of the start and end of life [13].

$$t_{rLM} = \frac{1}{D_{LM}\sigma_r^p} \tag{6.7}$$

where σ_r is the reference stress and B and p are constants from the Liu-Murakami creep damage equations. Alternatively, is it possible to obtain similar results using creep damage analysis. Failure life is then determined when damage reaches a critical value within the model, which in this case would be 0.99. Analyses are done on 2D axisymmetric models [123].

6.3 PRELIMINARY RESULTS

6.3.1 **Illustrative Behaviour**

6.3.1.1 Steady State Life Prediction

Steady-state life prediction is achieved through two separate methods at any given alpha (α_m) value. The first is done by taking the peak rupture stress [56]and the second can be done by using the reference rupture stress [123] of the pipe from the base of the notch radially to the inner surface of the pipe. The rupture stress (σ_R) is described by Equation 6.2 and is a combination of the von mises and maximum principle stresses acting on the structure at any time. Once the peak value is found, the value can be inserted into Equation 6.7 as the stress value for estimate of life prediction. The reference rupture stress is calculated by running the analysis at several Norton's law '*n*' values (typically, 1, 2, 5 and 9). The rupture stress contour is obtained for each *n* value along the thickness of the pipe (if a notch is present, across that plane). Superimposing the normalised

rupture stress contours for each *n* value on the same plot shows the reference rupture stress as the point at which all the lines meet, this stress is independent of *n*. The stress obtained with Equation 6.7 makes an estimate of the failure life.

6.3.1.2 Continuum Damage Life Prediction

Non-linear analysis can be executed in order to obtain failure life and with multi-core computing more accessible can be now be simulated relatively quickly. To estimate the time to failure using this method observe the time at which an element within the finite element model has reached the peak damage value (0.99) for the current analysis. This is an indication that the element has lost its load carrying capacity, effectively signally significant component weakness in that region. A CREEP sub-routine using the Liu-Murakami creep damage equations was used in this manner and a comparison of the three techniques used can be seen in Figure 53. The peak rupture stress method consistently gives conservative failure times whereas the reference rupture stress method overestimates the time in comparison with the CDM method.

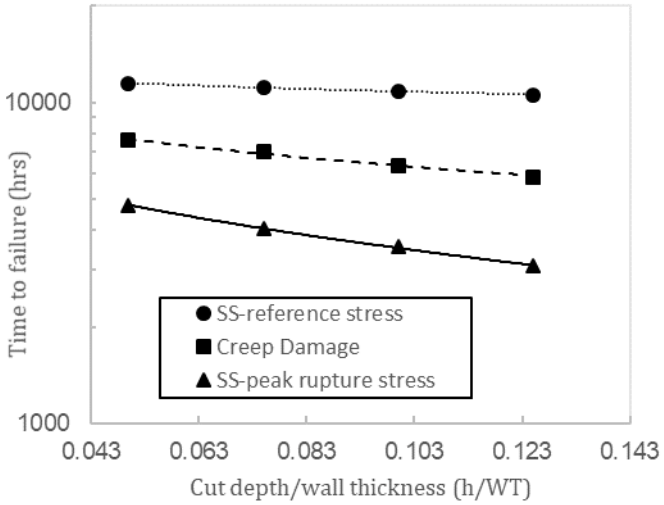


Figure 53: Life estimations, comparison of different methods.

6.3.2 **Parametric Behaviour**

The scoop depth *h*, the wall thickness *WT,* and the mean diameter hoop stress were varied in order to determine what effect the scoop to wall thickness ratio,

scoop size and load in reducing creep life. The comparisons of the scooped pipe were made alongside results of a plane pipe as a reference.

6.3.2.1 Effect of Scooping Dimensions

A scoop depth (h) of 3mm was selected as the reference for most analyses as this is the scoop size that would be selected for use in practice as it constitute enough material for the removal of recommended impression creep specimen sizes (10x10x2.5mm) and small punch specimen (10mm diameter and 0.5mm thickness). At a fixed scoop depth of 3mm, analyses were conducted for pipes of varying wall thickness (30-60mm). A reference wall thickness (WT) of 40mm was used giving the ratio h/WT = 0.075 as the reference ratio. Keeping the ratio h/WT constant, the scoop depth was modified to fit the change in wall thickness for subsequent analyses using the same range of pipe dimensions (see Figure 54).

It has been shown in previous work [123] that the mean diameter hoop stress is a conservative measure for use in remaining life predictions and that with the same σ_{MDH} and increasing wall thickness the reference stress decreases (showing increase in life). For scoops of the same geometry, the same reduction in life in absolute terms regardless of wall thickness is displayed, provided the σ_{MDH} is the same (Figure 54). Once the ratio is fixed for h/WT, an increase in wall thickness results in an increase in life reduction in absolute terms. For the range of pipe

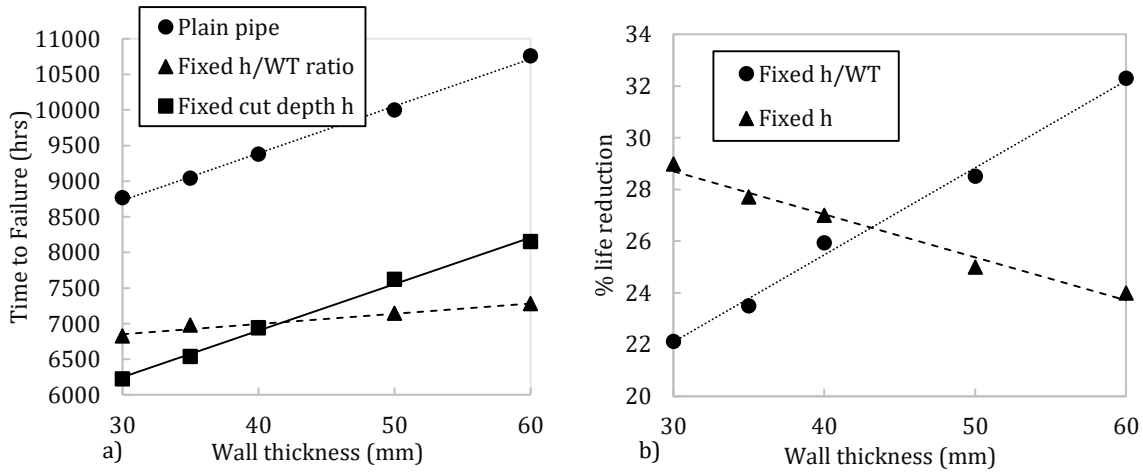


Figure 54: a), b) Geometric effects on failure life

wall thicknesses and sampling dimensions, the percentage life lost is observed to be 20-30% for the material in the present study (Figure 54b).

6.3.2.2 Effect of Loading

System loads acting on the pipelines tend to create loading conditions that vary from the closed end condition contributing to additional axial loads or moments, calculation of these loads are shown in sect 2.3. The effect of loading conditions was investigated on the model with a wall thickness of 40mm at scoop depth of 3mm. Loads studied were additional axial loads permissible in British standards PD5500, scaled through a loading factor k which varies from 0 to 1 (1 being the maximum additional axial load and 0 being the closed end condition axial load). A bending moment was also studied alongside the axial load, as it is common in power plants that straight pipes experience bending moments due to the hangers supporting the pipe systems. The bending moments were calculated according the equivalent axial load using Equation 6.4. The loading factors are the same as those used for the additional axial load, Figure 55 shows that for corresponding moment and axial loads the additional moment has a greater effect on life reduction primarily because the moment was set-up in a way that it caused maximum damage by opening the scoop. The maximum permissible moment (loading factor 1) created a life reduction in the region of 60% as seen in Figure 55.

6.3.2.3 Failure Orientations

The plane in which the most damage has accumulated is not orthogonal to the hoop direction, but is actually at a 45^{o} angle to the radial direction at the tip of the scoop for the closed end condition load, k = 1 (Figure 56). This is an unexpected result, as the crack plane would be assumed to be at right angles to the maximum principal stress. However, the 45^{o} angle would suggest that crack growth would propagate in the maximum shear stress direction. The triaxial state of stress reveals the material dependency on the driver for damage. The rupture stress (Equation 6.2) describes this effect on the damage path so for a low multiaxility parameter (α_m) the resulting areas experiencing the most

damage will be dependent on the effective stress, eluding to the aforementioned result. When the additional axial load is increased there is a shift in the orientation of the failure plane, most pronounced at loading factor 1 where it is greatest in the y-z plane rather than the x-y plane for loading factor 0 (Figure 56). The larger additional axial load becomes the driver for damage rather than the mean diameter hoop stress.

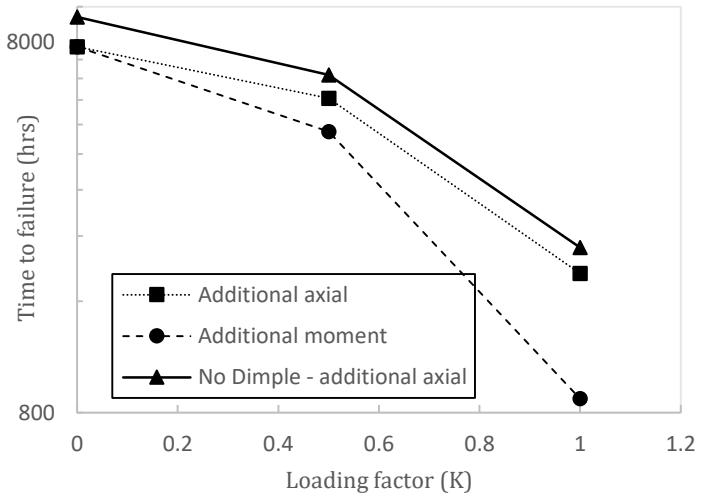


Figure 55: Life reduction caused by different loadings, cut depth h=3mm

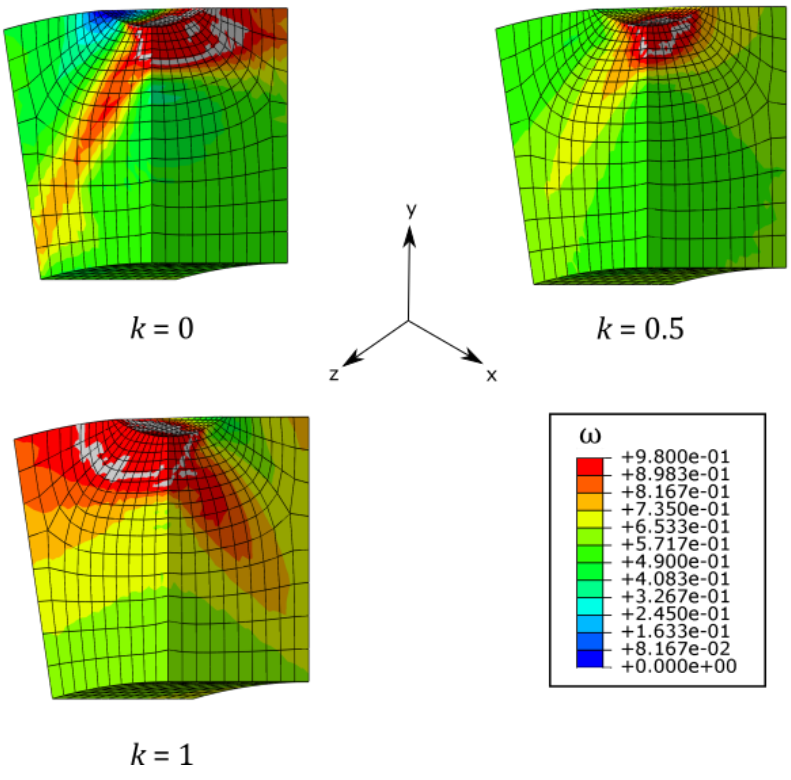


Figure 56: Accumulated damage (ω) due to extent of loading

6.4 VALIDATION OF PIPE RESULTS

6.4.1 FE Simulations

6.4.1.1 Geometry and Loading

Two novel specimens were used to validate and replicated the damage in section 6.3.2 of the present work. The test specimens used are a modification of standard uniaxial creep specimens of circular gauge to ones that have a square cross-section of 7x7mm. Notches have been carved out of one of the surfaces of the specimens using a ball nose slot drill. Two notch geometries were selected for the present study, a spherical one and an elliptical one. The curvature of the spherical profile is derived from a sphere of radius 3mm, the depth of the notch is 2mm, and so the projected circle on the specimen has diameter of 5.75mm. The elliptical notches have a curvature which is derived from a prolate spheroid of major radius 6mm and minor radius 3mm and has a depth of 2mm. The projected ellipse on the surface of the specimen is tilted at an angel of 70^{o} from the normal vertical axis. The geometries of the notches were calculated by fitting a surface through the points generated from the surface characterisation of the machined specimens and then imported into an ABAQUS model. For the specimen with a

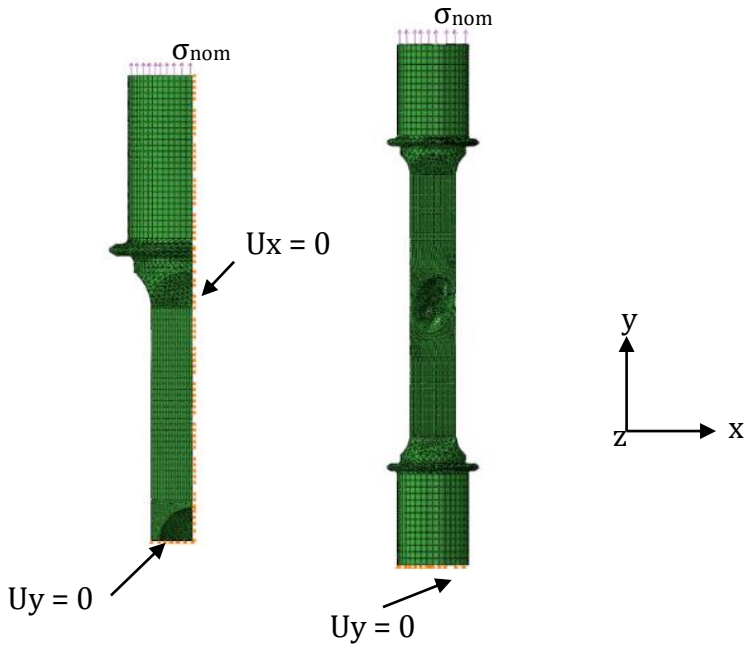


Figure 57: FE model set-ups for spherical and elliptical specimens

spherical notch a quarter model was used, as planes of symmetry were observed in vertical and horizontal planes, displacement boundary conditions were applied to the planes of symmetry of the model and were applied as U_x= 0 on the vertical face and U_y=0 on the horizontal face. A uniaxial distributed load was applied to the top surface of the specimen see Figure 57. The specimen with an elliptical notch was modelled in full, due to lack of symmetry. So a displacement boundary condition set U_y=0 was set at the base of the specimen and a distributed load was applied to the top surface of the specimen. A mesh sensitivity study was conducted and it was found that an element size of 0.25mm was sufficient in the areas of interest in and around the notch, any lower gave vanishingly smaller increases in accuracy. Material constants were determined using the method in section 3.2.1 for P91 at 600C (Table 10), with good agreement between model and experiments as seen in Figure 58.

6.4.1.2 Material Sensitivity to Dimple

The dimple due to its curvature introduces a multiaxial stress state in and around it causing a distribution of the load. However, unlike in a Bridgeman notch specimen the curvature is asymmetrical and so the induced multi axial stress state is not as pronounced. Nonetheless, there is a response to changing the alpha value on the failure life using both dimple types (Figure 59). Since the alpha value of the material is unknown, it will be calculated with the new specimens. This is calculated in the same way is it would with a Bridgman notch, where finite element analysis are performed at alpha values of 0, 0.5,1 for the same material properties. Alpha is determined by finding the point of agreement between the experimental and numerical time to failure. The noticeable fact is that the asymmetrically notched specimens produce a significantly shorter failure life at an alpha value of 0, when the multi-axial effects are at their maximum and failure is determine by the von Mises stress and not the maximum principal stress. This is attributed to the magnitude of the rupture stress at the skeletal point, which in both of the asymmetric notches can be seen as greater than that of the Bridgeman notch. Normalising the rupture stress against the nominal stress also reveals an

increase in the rupture stress for the asymmetric notch and a slight increase in the Bridgeman notch.

Table 10: Liu-Murukami materials constants for P91 at 600C

A	n	D_{LM}	p	q_2
5.28E-36	14.28	2.95E-31	12.74	3.55

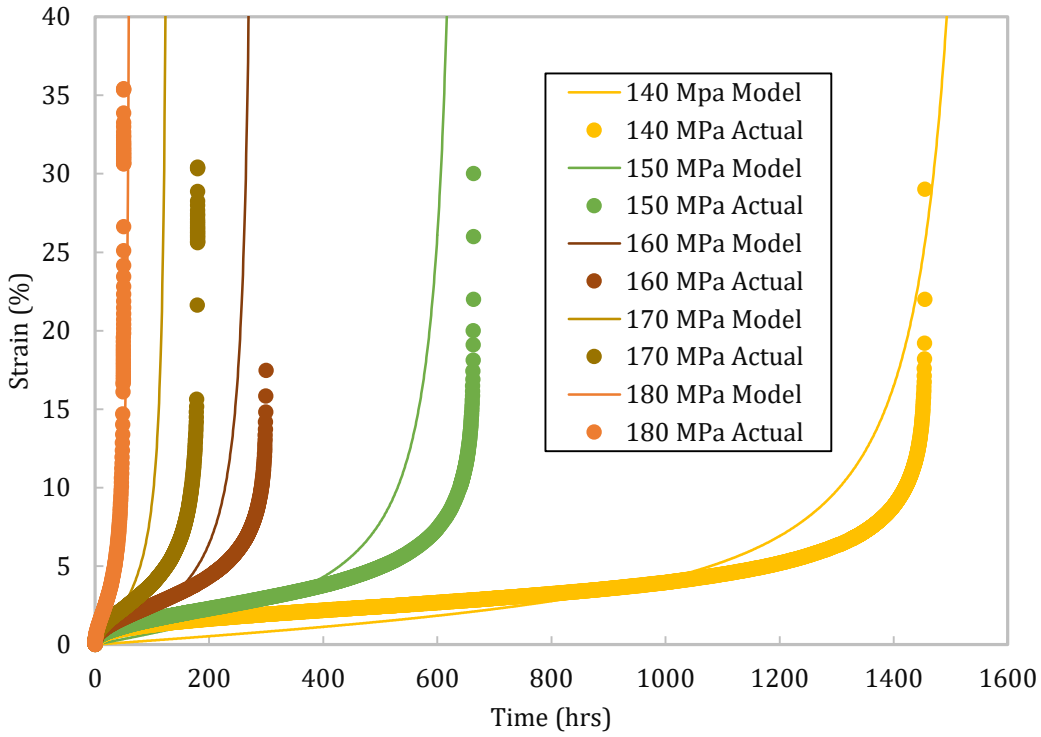


Figure 58: Liu and Murakami model fitting to P91 uniaxial data at 600C

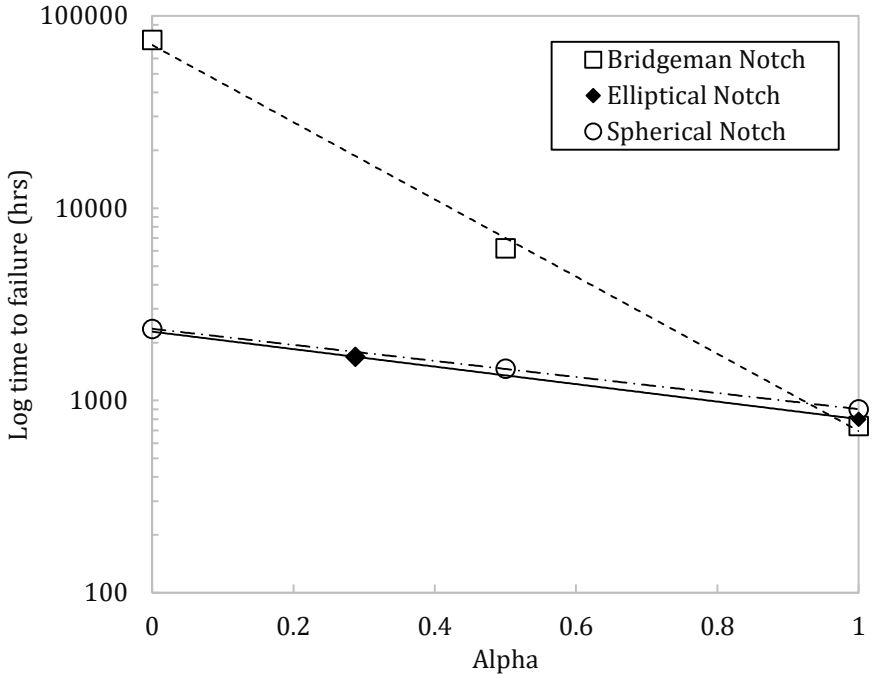


Figure 59: Specimen Notch sensitivities

6.4.1.3 Effect of Notch Geometry on Failure life

Further analyses were conducted on the elliptical specimen in which the aspect ratio of the ellipse was varied as well as is the angle φ that the major axis of the ellipse makes with the horizontal axis through the centre of the specimen. This was conducted in order to observe the angle φ that the maximum damage plane made with the same axis (Figure 60). These changes in elliptical configuration can be attributed to changes in the loading in and around the notch area, contributing to changes in the interaction between the principal stresses and the shear stresses. The critical plane labelled in Figure 60 is the plane through which the material damage is the most advanced, points from the z-axis (into the page) are superimposed in order to form a simplified 2D image of the plane. The methodology used to obtain the maximum damage plane is as follows. Failure at element centroid is obtained using a python script (appendix), which terminates at the frame and element at which damage has reached the critical value for maximum damage. The element centroid coordinates in x and y and their corresponding damage values are extracted, then exported to and plotted in MATLAB. A weighted linear least squares fit (Equation 6.8) is fitted to the data

with the weights w_i being the associated damage value of each data point, a schematic can be seen in Figure 60. The tangent of the gradient of the fitted line is φ, the angle of the maximum damage plane. The weighted sum of squares S_w is described as:

$$S_w = \sum_{i=1}^{n} w_i (y_i - \hat{y}_i)^2 \tag{6.8}$$

where

$$\hat{y}_i = p_1 x + p_2 \tag{6.9}$$

and y_i is the response data at that point.

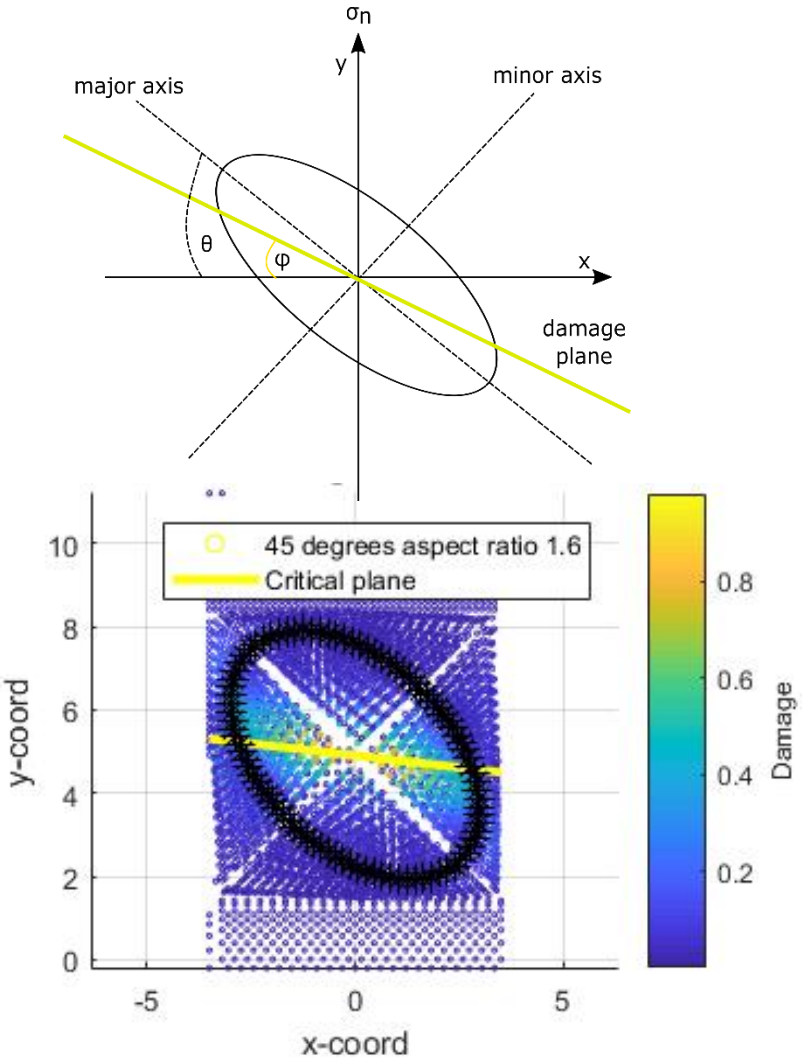


Figure 60: (Top) Angles and orientation of failure plane (Bottom) Example plot θ = 45°

A parametric study was conducted which varied three parameters, the material (alpha value), the aspect ratio a_r of the ellipse and the angle θ that the major axis of the ellipse made with the x – coordinate axis. In general, an increase in the alpha value results in an increase the angle φ, this can be attributed to the increased dependence on the maximum principal stress in the value of the rupture stress Equation 6.2. The maximum principal stress is at its maximum below the notch in the z-direction (into the page), whereas the von mises stress is at its greatest near the surface of the ellipse near the narrowest corners of the wall of the specimen. The results are presented in Table 11 and visualised in Figure 61.

Table 11: Maximum damage plane angles obtained from parametric study

Aspect ratio a/b	**Ellipse angle (°)**	**Maximum damage plane angle for alpha value (°)**		
		0	**0.5**	**1**
1.4	45	8.36	10.8	13.65
1.6	45	11.6	14.41	16.62
1.8	45	16.129	17.37	20.46
1.4	70	14.08	15.21	16.05
1.6	70	15.13	15.61	16.18
1.8	70	18.26	19.11	18.86
1.4	30	4.5	5.50	6.724
1.6	30	5.85	6.56	8.77
1.8	30	6.6	7.96	9.36

The relationship between the alpha value ellipse angle and aspect ratio is represented by a polynomial fit of the data, where $R^2 = 0.9788$. The plot shown in Figure 61 is the fitting of the data at an aspect ratio of 1.6; the function was generated at these parameters to compare with experimental data of similar parameters.

$$\varphi = -24.26 + 5.154\alpha_m + 1.293\theta + 0.6572\alpha_m^2 - 0.0582\alpha_m\theta - 0.01049\theta^2 \quad (6.10)$$

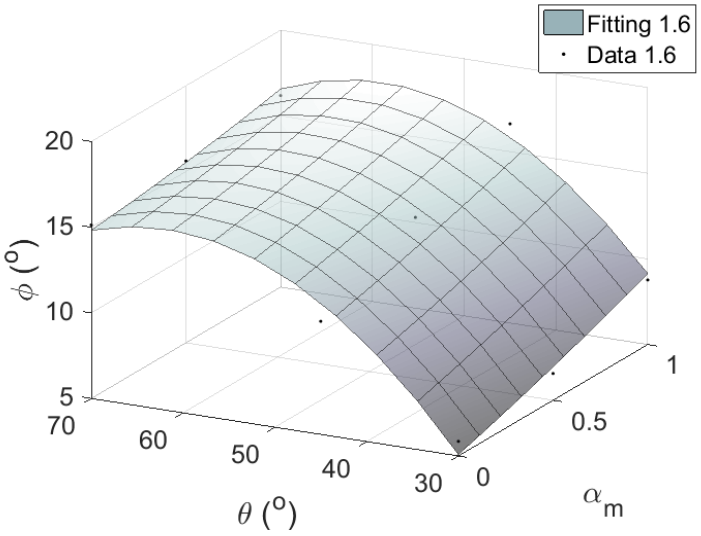


Figure 61: Fit of failure plane dependence

6.4.2 **Experimental Testing**

6.4.2.1 Specimen Preparation and Creep Testing

The notches were machined using a ball nose slot drill, which achieved a surface finish of ~3.5µm. The surface of the specimens where characterised with an Alicona infinitely variable microscope (Figure 63) to ensure the finish stated above, the data was imported to matlab and the surface finish was verified by running a Fourier transform (function fft) on detrended data applied on a line segment of data collected through the dimple of the specimen (Figure 64). Specimens can be seen in Figure 62.

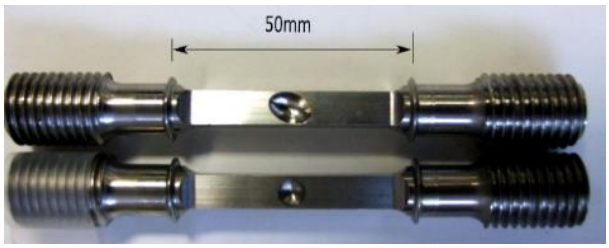


Figure 62: Elliptical notch top and spherical notch bottom

The specimens where creep tested using a dead load Denison creep rig at loads of 140,150 and 160 MPa (net section stress) for each specimen type (Figure 65), and testing was done at 600C in accordance with the uniaxial testing used to

calibrate the creep damage model. The specimen with the elliptical notch failed earlier than the spherical one at all loads, this was attributed to bending induced by the notch in the x-y plane as an addition to the bending caused by the asymmetry of the notches in the y-z plane (z-direction is into the page). The Bridgeman notch is known to have exceptional notch strengthening behaviour and is off the chart for this particular comparison shown in Figure 66. The failure life of 1599hrs for the spherical notch corresponds to an alpha value of 0.288 for the studied material when checked alongside the finite element values obtained in Figure 59. The results were then corroborated by checking failure lives of the models against those of the tested specimens at 0.288 for alpha, as in Figure 66.

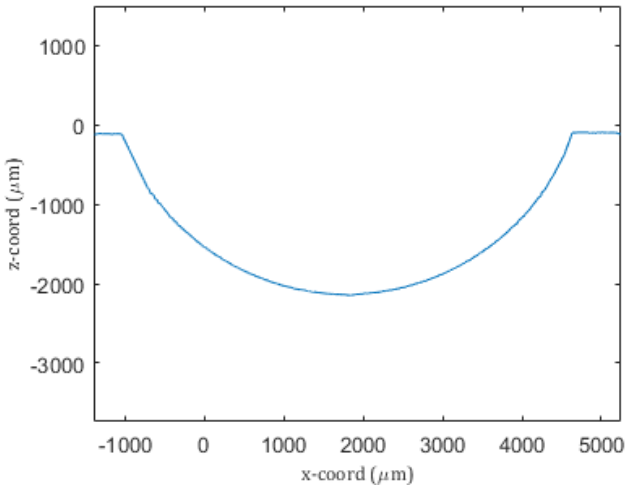


Figure 63: Segment taken from Alicona measurements of spherical dimple

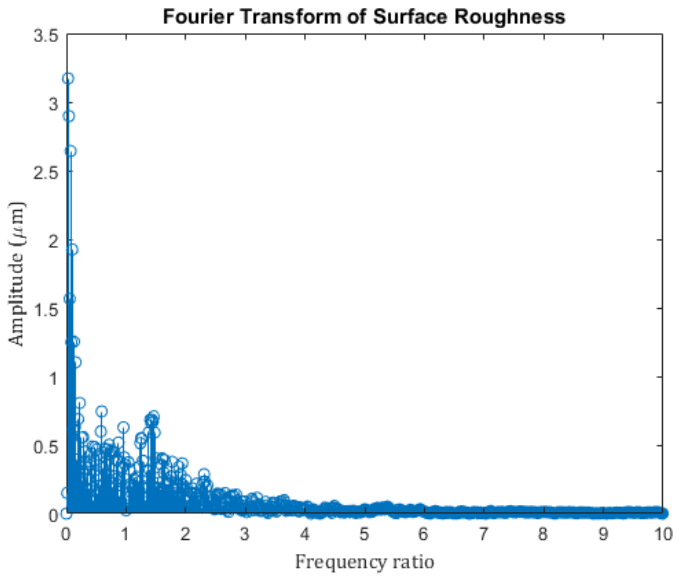


Figure 64: Fourier transform of surface roughness of spherical dimple

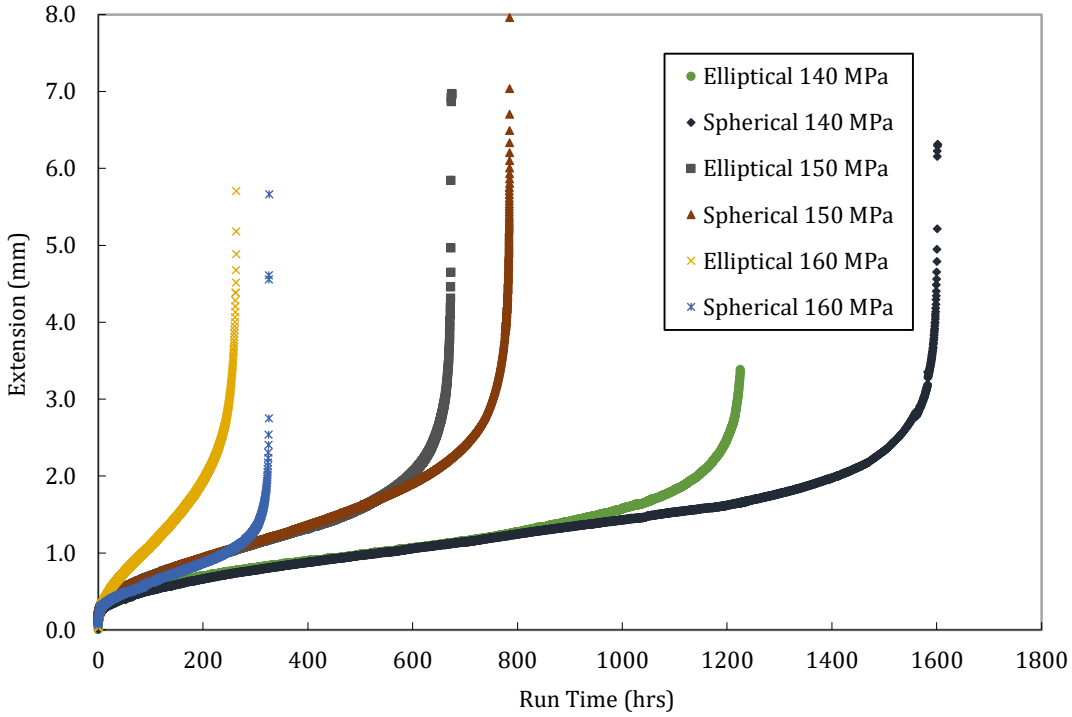


Figure 65: Creep rupture tests for the P91 notched bars at 600°C

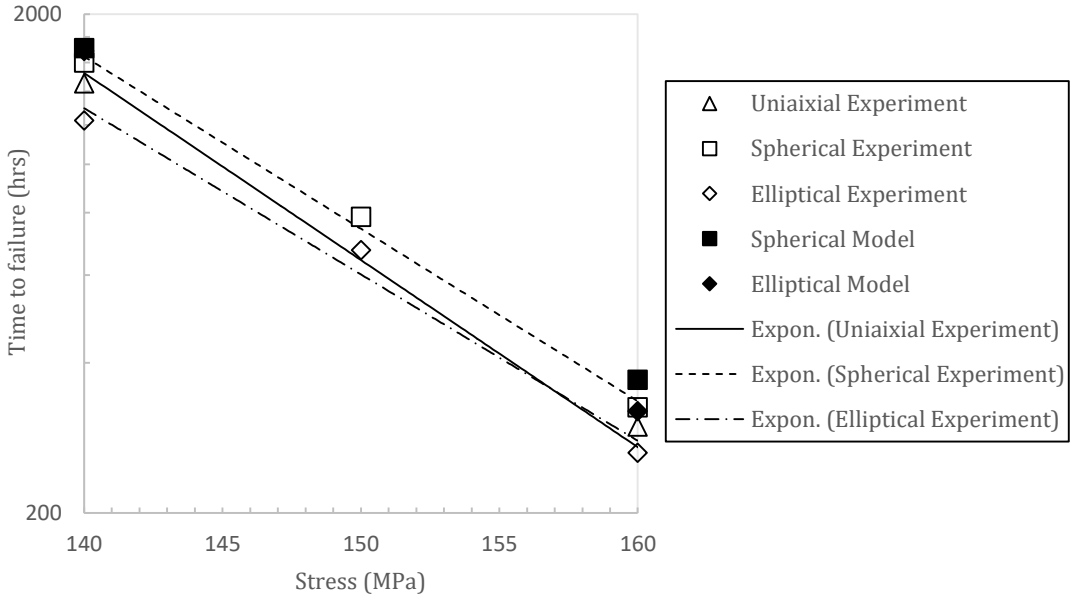


Figure 66: Comparison of Experimental and modelling failure times alpha 0.288

6.4.2.2 Creep Failure Investigations

Further validation of the damage results was done by comparing the approximate angle of failure of the tested specimens. After taking an image of the failed specimens, the specimen was aligned so that the vertical faces were at 90 degrees, a least squares line was fitted through the visible fracture surface by taking the coordinates of the pixels in which the fracture surface lay. The gradient of the resulting line was used as the failure plane angle. The angle found was within 0.2 degrees of the predicted angles (using Equation 6.10) showing good agreement between the model and the experiment (Figure 67). The specimens failed by ductile fracture characterised by elongation around the failure site and a jagged fracture surface, which was to be expected at net section stresses > 140MPa for the tested material.

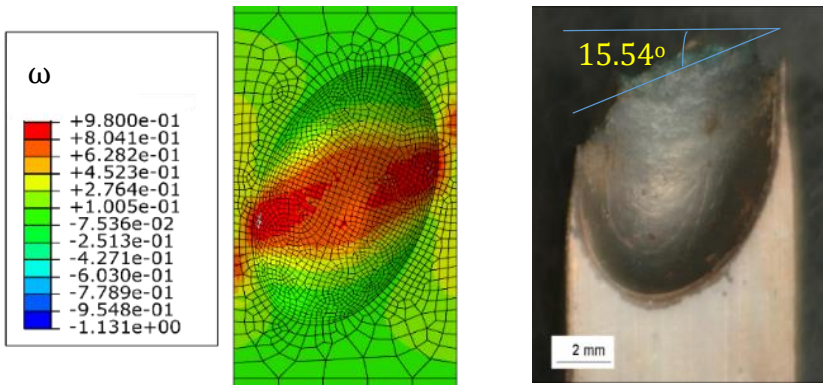


Figure 67: Model and specimen failure 140MPa (net section stress), aspect ratio a/b = 1.6 alpha 0.288.

6.5 DISCUSSION

A parametric study of different pipe geometries and scoop sample depths using creep continuum damage mechanics was done. The cost of longer computational times against steady state methods was leveraged by the increase in accuracy of creep failure lives obtained using these methods, along with a discernible point of failure displayed by the model which is when elemental damage reaches a critical value signalling a loss in load carry capacity.

For a hemispherical cutter of diameter 50mm scoop removals of 3mm is depth were shown across all pipe wall thicknesses (30-60mm) to have a life reductions effect of less than 30% in conditions where the axial load according to loading factor k is 0, see Figure 54. Meaning that even for narrow wall thicknesses removing 10% of material in the pipe wall would be allowable considering that sampling for component assessment would occur in the later stages of a plants life (small specimen testing has mainly been used as a remaining life assessment technique) and that most components would have a safety design factor of 2. The cost of reducing a components life by less than 50% in the case that it may be a faulty component (due to defects or faulty microstructure), would be a reasonable cost in that the component would still be likely to complete its time in service without needing to be replaced. This is assuming the components behave as designed and allowing for the safety factor.

The conditions warranting concern would be in locations where a bending moment with a loading factor k=1 is present. In these cases the reduced life would be greater than 50% at the minimum cut depth putting the sampled component in danger of failing prematurely if found to be strong. This can be observed in Figure 55.

The stress state dependent damage accumulation (Figure 56), shows the expected peak planes for material damage to occur and so it was of interest to replicate this behaviour experimentally. The design of two specimens were chosen as an analogue to a scooped power plant straight pipe, with the elliptical notch chosen so as to replicate loading conditions that included bending and in order to try and control the effect of the accumulation of damage after sampling.

The two notched samples were also used to obtain the material properties of the material being tested. In this area, the two notches are seen as capable of accomplishing the task but are not as sensitive as the Bridgman notch as eluded to earlier due to an increased reference rupture stress over the Bridgeman notch

and a reduced stress triaxiality. This means that the alpha sensitivity of the Bridgeman notch is far greater than the samples new samples tested.

However the main aim was to control the direction of the accumulation of damage at it has been shown that at an ellipse angle (in reference to maximum principle stress) of 45 degrees has the greatest effect on the direction of damage accumulation with increased control obtained when the aspect ratio of the notch is increased from 1.4 to 1.8.

The limitations of the model used are the inability of the model to simulate the deformations in the specimen in the final stages of creep. Although there is good agreement between the results, the current model did not incorporate any failure of elements. However, for the present application i.e. controlling the effect of damage evolution, it has been observed that the model can effectively predict the direction of macro damage evolution.

6.6 CONCLUSIONS

An alpha value of 0.288 was determined for the given material. The specimens are not intended to be a replacement for the Bridgeman notch and were used in this study as determining alpha was a useful by-product of the geometry of the specimen.

As shown previously by Hyde et al [13] the current model is capable of predicting within 0.2 degrees the angle at which a macro crack would form and hence a prediction of the plane of crack growth.

The advised scooping allowances for straight pipes with an additional load, factor 0 and 0.5 is 10% of the wall thickness, to ensure life reduction is well below 50% for a hemispherical cutter of diameter 50mm and may be greater for cutters with a larger diameter. Furthermore, sampling of components subject to the maximum permissible axial load should be kept to 3mm and sampling should be avoided for cases subject to the maximum permissible bending moment.

CHAPTER 7
DISCUSSION, CONCLUSIONS AND FUTURE WORK

7.1 DISCUSSION

7.1.1 Small Specimen Creep Testing and Life Management

The requirements for the work presented in this thesis relates to the application of small-scale sampling and miniature specimen testing of high temperature and high pressure components. The methods presented are related primarily to fossil-fired power plants due to the material tested (Grade 91 steel). However, it is possible that the methods developed will be applicable to other plants that experience severe operating conditions, which may need monitoring and managing e.g. chemical plants. The small specimen testing method focused on in this thesis was the impression creep test. It was selected due to its simplicity; a flat-ended indenter is loaded onto a flat square specimen measuring 10x10x2.5mm. It's conversion to uniaxial creep data as per Hyde et al [27], has a sound mechanical basis in the reference stress approach (see Chapter 2). It has one main shortfall, which is the lack of creep rupture life data, due to it being a compressive indentation creep test. However, the minimum creep strain rate data is of a high quality and tests lasting only a few hundred hours give data that would otherwise need a thousand hours plus using full size uniaxial creep tests [58] notwithstanding the reduced amount of material required. In addition, it has already been partially uptaken in industry having been extensively tested on CrMoV piping by Brett et al [25] for which it was used as a ranking tool. For future uptake, a standard procedure for use and operation was needed along with a methodology to sample and assess ageing components.

A test database was developed for Grade 91 steel at 600^{o}C by four independent labs (University of Nottingham, VTT, EPRI and AMEC FW), specifically BAR 257, material that sits towards the weak end of the Grade 91 creep strength scatter band. Using stepped stress tests applied to one specimen per test rig, creep data

at five load levels was obtained for each lab (steady-state creep for a minimum of 200hrs). The rigs were not identical; one employed a dead-weight loading system as opposed to servo-mechanical. Another had a reverse loading system, with the specimen sitting above the indenter rather than below and fine temperature control (±0.3°C). The two quantities assessed during the testing where the stability of the indentation trace and the resulting creep strain rate taken from the final 100 hrs at each stress level during steady-state creep. The stability of the indentation traces was found to be lowest with the dead-weight rig, temperature control ±0.5°C and best with the servo-mechanical rig with temperature control (±0.3°C) over the five stress levels. Although there was a discrepancy in stability of indentation traces between rigs, the minimum creep strain rates were in agreement. Cost conscious operators may opt for the cheaper dead-weight rigs provided there is adequate temperature control, at the loss of indentation trace stability.

Small specimen testing as a life management tool would be one of a suite of tools and techniques used in modern power plants for condition monitoring, life management and remaining life assessment. An example of the strategies used in a modern plants life monitoring include EPRI's three level assessment [50] Figure 68, where small specimen testing is best suited for the later stages of

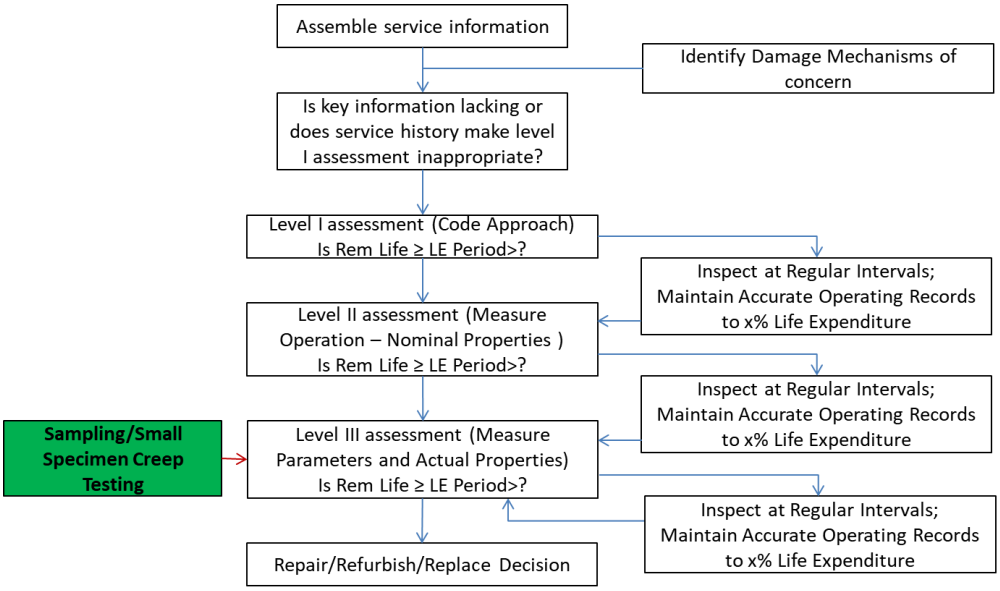


Figure 68: Generic procedure for component life assessment according to EPRI [50], with stage incorporating small specimen testing.

assessment as can be seen in green and bold. The state of a component's structural integrity is assessed with increasing levels of sophistication depending on the level of component degradation. Impression creep may be used in this way as a remaining life assessment tool along with the Monkman-Grant approach provided predictive stress-time to failure design curves for the tested material exist. Using the impression creep minimum strain rate along with the Monkman-Grant correlation ($\dot{\varepsilon}.t_f = C$) the remaining life of the component can be assessed depending on whether the material falls within the strength scatter band for that material, alluding to whether the material would be on course to age according to design or fall short of the prediction. The use of this data in light of the fact that the components being sampled will usually be under combined states of stress and would have undergone other forms of damage due to perhaps chemical or stress corrosion remains to be seen. However if a material were to fall well below the limits of the strength scatter band there would be obvious indicators as to whether to repair or replace the component in question.

It also follows that the component having been tested would have had material removed from its surface further complicating its stress condition. For straight pipes the scooping allowances are: with an additional load factor 0 and 0.5 is, 10% of the wall thickness to ensure life reduction is well below 50% for a hemispherical cutter of diameter 50mm and may be greater for cutters with a larger diameter. Scooping is not advised from components with a load factor greater than 0.5.

7.1.2 **Pre-Straining and Impression Creep Testing**

The use of impression creep testing for the assessment of material property variation is not a new concept, Sun et al [124] have used the technique for the characterisation of the different metallurgical zones in welds. Pre-straining and uniaxial creep testing has also been studied showing both creep enhancement and reduction effects depending on the material tested [103]. Cortellino et. al [36] used the technique to develop an enhanced Liu-Murukami creep damage model for the interpretation of the small punch test. In this work, the application

is more suited to the post manufacture creep testing of strained components. Using the data from the impression creep tests, tolerances for the pre-strain levels in manufactured components may be pushed to their limits based on the true pre-strain creep life predictions from the impression creep test.

7.2 CONCLUSIONS

- An impression creep database was developed using grade 91 for standardisation purposes.
- Dead weight impression test rigs may be used commercially (due to reduced capital cost) provided temperature control is in the ±0.5^{o}C range.
- Power plant component strength can be determined using the impression creep test in combination with the Monkman-Grant correlation and material design curves
- Round Robin testing finalised conditions required for standardization, including a calibration line for future test rigs.
- Impression creep testing may be used on prospective high temperature components post manufacture for creep strength assessment of strained areas, being optimized to the possible non-linear creep behaviour.
- Scoop sampling must not exceed 10% of the component wall when a 50mm diameter hemispherical scoop sampler is used. Components experiencing system loads with loading factors k greater than 0.5 should be avoided.
- Using a novel asymmetric elliptically notched specimen, the material triaxiality (α value) may be obtained and the maximum damage evolution plane may be predicted using finite element analyses within 0.2^{o}.

7.3 FUTURE WORK

Concerning impression creep testing the relevant authorities and standards bodies will need to be contacted to finalise the standardisation procedure. Improvements have been made to draft a code of practice in which the important parts are mentioned in Chapter 4. The suggested calibration material is BAR 257 (P91) the material used in the 'Round Robin' testing. The line of best fit of the

averages of all the data through the tested load levels is the calibration line and can be found in Figure 38.

The remaining work in the quantification of the effect of high levels of pre-straining and subsequent creep testing requires further testing at more load levels. The creep life enhancement effect has been shown to be load dependant for other materials tested in other work.

Concerning scooping assessment, the requirements are to model pipe bends as they may be the most challenging to sample. Furthermore, the current energy market requirements for fossil plants means that they are constantly experiencing start up and shut down. In order meet the needs of the capacity market filled by renewable energy sources, fossil energy sources are used to fill the capacity gap left by renewable sources during peak energy demand. With specific attention to ageing plants, it would be of interest to know the impact on remaining life a scooped component would experience under cyclic loading conditions.

In addition, it may be useful to characterise and understand the behaviour of pre-strained materials entering high temperature service by conducting full size low-cycle fatigue and creep-fatigue interaction tests.

REFERENCES

[1] S. J. Brett, "The Application of Small Scale Sampling and Impression Creep Testing to Power Plant," *ECCC Conf. Creep Fract.*, 2014.

[2] I. MacLeay, K. Harris, A. Annut, and Department of Energy and Climate Change (DECC), "Digest of UK Energy Statistics (DUKES) 2014," *Dig. UK Energy Stat.*, 2014.

[3] Naveena, V. D. Vijayanand, V. Ganesan, K. Laha, and M. D. Mathew, "Application of impression creep technique for development of creep resistant austenitic stainless steel," *Procedia Eng.*, vol. 55, pp. 585–590, 2013.

[4] M. D. Mathew, J. Ganesh Kumar, V. Ganesan, and K. Laha, "Small punch creep studies for optimization of nitrogen content in 316LN SS for enhanced creep resistance," *Metall. Mater. Trans. A Phys. Metall. Mater. Sci.*, vol. 45, no. 2, pp. 731–737, 2014.

[5] M. C. Elliotis, "A Finite Element Approach for the Elastic-Plastic Behavior of a Steel Pipe Used to Transport Natural Gas," in *Conference papers in energy*, 2013.

[6] K. Naumenko, "Modeling of high-temperature creep for structural analysis applications," Martin Luther University of Halle-Wittenberg, 2006.

[7] R. K. Penny and D. L. Marriott, *Design for Creep*, 2nd Edition. Chapman and Hall, 1995.

[8] J. Betten, *Creep mechanics (Third Edition)*. Springer, 2008.

[9] Y. N. Rabotnov, *Creep Problems in Structural Members*. Elsevier, 1969.

[10] F. A. Leckie and D. R. Hayhurst, "Constitutive Equations of Creep Rupture," *Acta Metall.*, vol. 25, no. 9, pp. 1059–1070, 1977.

[11] J. P. Rouse, W. Sun, T. H. Hyde, and A. Morris, "Comparative assessment of several creep damage models for use in life prediction," *Int. J. Press. Vessel. Pip.*, vol. 108–109, pp. 81–87, 2013.

[12] M. Yatomi, A. D. Bettinson, N. P. O'Dowd, and K. M. Nikbin, "Modelling of damage development and failure in notched-bar multiaxial creep tests," *Fatigue Fract. Eng. Mater. Struct.*, vol. 27, no. 4, pp. 283–295, 2004.

[13] C. J. Hyde, T. H. Hyde, W. Sun, and A. A. Becker, "Damage mechanics based

predictions of creep crack growth in 316 stainless steel," *Eng. Fract. Mech.*, vol. 77, no. 12, pp. 2385–2402, 2010.

[14] Y. Liu and S. Murakami, "Damage Localiztion of Convential Creep Damage Models and Proposition of a New Model for Creep Damage Analysis," *JSME Int. J.*, vol. 41, no. 1, pp. 57–66, 1998.

[15] T. H. Hyde, C. J. Hyde, and W. Sun, "A Basis for Selecting the Most Appropriate Small Specimen Creep Test Type," *J. Press. Vessel Technol.*, vol. 136, no. 2, p. 024502, 2014.

[16] T. H. Hyde and W. Sun, "Some considerations on specimen types for small sample creep tests," *Mater. High Temp.*, vol. 27, no. 3, pp. 157–165, 2010.

[17] T. H. Hyde, C. J. Hyde, and W. Sun, "Theoretical basis and practical aspects of small specimen creep testing," *J. Strain Anal. Eng. Des.*, vol. 48, no. 2, pp. 112–125, 2013.

[18] A. Garzillo, C. Guardamagna, L. Moscotti, and L. Ranzani, "A technique for the residual life assessment of high temperature components based on creep-rupture testing on welded miniature specimens," *Int. J. Press. Vessel. Pip.*, vol. 66, no. 1–3, pp. 223–232, 1996.

[19] M. Askins, "Estimating the remnant life of boiler pressure parts," 1988.

[20] Y. Kadoya, T. Saida, S. Date, T. Yamauchl, and T. Goto, "Assessment of Remaining Life of Fossil Power Plant Parts by means of a Miniature Creep Rupture Test," *ISIJ Int.*, vol. 30, pp. 854–861, 1990.

[21] T. H. Hyde, W. Sun, and A. A. Becker, "Analysis of the impression creep test method using a rectangular indenter for determining the creep properties in welds," *Int. J. Mech. Sci.*, vol. 38, no. 10, pp. 1089–1102, 1996.

[22] W. Sun, T. H. Hyde, and S. J. Brett, "Application of Impression Creep Data in Life Assessment of Power Plant Materials at High Temperatures," *J. Mater. Des. Appl.*, vol. 222, pp. 175–182, 2008.

[23] T. H. Hyde and W. Sun, "Evaluation of conversion relationships for impression creep test at elevated temperatures," *Int. J. Press. Vessel. Pip.*, vol. 86, no. 11, pp. 757–763, 2009.

[24] T. H. Hyde, W. Sun, and S. J. Brett, "Some Recommendations on the Standardization of Impression Creep Testing," in *Creep & Fracture in High*

Temperature Components Design & Life Assessment, 2009, vol. 1, no. 2, pp. 1–9.

[25] S. J. Brett, "Small Scale Sampling and lmpression Creep Testing Applied to Aged 0.5CrMoV Steam Pipework Systems," *EPRI Int. Conf. Adv. Condtion an dRemain Llife Assess. Foss. Power Plants - Coal, Gas HRSC*, 2012.

[26] S. J. Brett, B. Kuhn, J. H. Rantala, and C. J. Hyde, "Impression Creep Testing for Material Characterization in Development and Application," *Mater. Adv. Power Eng.*, no. 10th, 2014.

[27] T. H. Hyde, K. A. Yehia, and A. A. Becker, "Interpretation of impression creep data using a reference stress approach," *International Journal of Mechanical Sciences*, vol. 35, no. 6. pp. 451–462, 1993.

[28] W. Sun, T. H. Hyde, and S. J. Brett, "Small Specimen Creep Testing and Application for Power Plant Component Remaining Life Assessment," in *Integrity, Reliability and Failure of Mechanical Systems*, 2013.

[29] T. H. Hyde and W. Sun, "Multi-step Load Impression Creep Tests for a 1/2Cr1/2Mo1/4V Steel at 565C.," *Strain*, vol. 37, no. 3, pp. 99–103, 2001.

[30] B. Gülçimen and P. Hähner, "Determination of creep properties of a P91 weldment by small punch testing and a new evaluation approach," *Mater. Sci. Eng. A*, vol. 588, pp. 125–131, 2013.

[31] J. P. Rouse, F. Cortellino, W. Sun, T. H. Hyde, and J. Shingledecker, "Small punch creep testing: review on modelling and data interpretation," *Mater. Sci. Technol.*, vol. 29, no. 11, pp. 1328–1345, 2013.

[32] P. Dymacek and F. Dobeš, "Small Punch Testing of Exposed High-Pressure Steam Pipelines," in *Pressure Vessels & Piping*, 2013, no. i, pp. 1–7.

[33] CEN, "CEN-Workshop agreement 2006."

[34] J. Chakrabarty, "A theory of stretch forming over hemispherical punch heads," *Int. J. Mech. Sci.*, vol. 12, no. 4, pp. 315–325, 1970.

[35] T. H. Hyde, M. Stoyanov, W. Sun, and C. J. Hyde, "On the interpretation of results from small punch creep tests," *J. Strain Anal. Eng. Des.*, vol. 45, no. 3, pp. 141–164, 2010.

[36] F. Cortellino, J. P. Rouse, B. Cacciapuoti, W. Sun, and T. H. Hyde, "Experimental and Numerical Analysis of Initial Plasticity in P91 Steel

Small Punch Creep Samples," *Exp. Mech.*, vol. 57, no. 8, pp. 1193–1212, 2017.

[37] Z. Yang and Z. wen Wang, "Relationship between strain and central deflection in small punch creep specimens," *Int. J. Press. Vessel. Pip.*, vol. 80, no. 6, pp. 397–404, 2003.

[38] K. Kobayashi, I. Kajihara, H. Koyama, and G. C. Stratford, "Deformation and Fracture Mode during Small Punch Creep Tests," *J. Solid Mech. Mater. Eng.*, vol. 4, no. 1, pp. 75–86, 2010.

[39] D. T. Blagoeva and R. C. Hurst, "Application of the CEN (European Committee for Standardization) small punch creep testing code of practice to a representative repair welded P91 pipe," *Mater. Sci. Eng. A*, vol. 510–511, no. C, pp. 219–223, 2009.

[40] W. Sun and T. H. Hyde, "Determination of Secondary Creep Properties Using a Small Ring Creep Test Technique," in *Metallurgical Journal*, 2010, vol. LXIII, pp. 185–193.

[41] C. J. Hyde, T. H. Hyde, W. Sun, S. Nardone, and E. De Bruycker, "Small ring testing of a creep resistant material," *Mater. Sci. Eng. A*, vol. 586, pp. 358–366, 2013.

[42] T. H. Hyde and W. Sun, "A novel, high-sensitivity, small specimen creep test," *J. Strain Anal. Eng. Des.*, vol. 44, no. 3, pp. 171–185, 2009.

[43] T. H. Hyde, B. S. M. Ali, and W. Sun, "Analysis and Design of a Small, Two-Bar Creep Test Specimen," *J. Eng. Mater. Technol.*, vol. 135, no. 4, p. 041006, 2013.

[44] B. S. M. Ali, "Development of Non-Destructive Small Specimen Creep Testing Techniques," University of Nottingham, 2013.

[45] A. C. Mackenzie, "On the use of a single uniaxial test to estimate deformation rates in some structures undergoing creep," *Int. J. Mech. Sci.*, vol. 10, pp. 441–453, 1968.

[46] R. G. Sim, "Reference Stress Concepts in the Analysis of Structures During Creep," *Int. J. Mech. Sci.*, vol. 12, pp. 561–573, 1970.

[47] B. Dogan and T. Hyde, "Industrial Application of Small Punch Testing for In-Service Component Condition Assessment: An Overview," in *Pressure*

Vessels and Piping, 2012, pp. 1–11.

[48] A. Tonti, "Residual life evaluation techniques, defect assessment procedures and monitoring in coal power plants," *Coal Power Plant Mater. Life Assess. Dev. Appl.*, pp. 199–228, 2014.

[49] J. Janovec, D. Poláchová, and M. Junek, "Lifetime assessment of a steam pipeline," *Acta Polytech.*, vol. 52, no. 4, pp. 74–79, 2012.

[50] EPRI, "Generic Guidelines for the Life Extension of Fossil Fuel Power Plants," 1986.

[51] J. D. Parker and J. Purmenski, "Assessment of performance by monitoring in service changes," in *Reliability and Integrity of Advanced Materials*, 1992, pp. 1051–1056.

[52] A. Dedov, I. Klevtsov, T. Lausmaa, and D. Neshumayev, "Method of small samples for assessment of properties of power plant components: Sampling devices and stress concentration in dimples," *VTT Symp. (Valtion Tek. Tutkimuskeskus)*, vol. 2, no. 247, pp. 180–192, 2007.

[53] Rolls-Royce, "Scoop Sampling Extraction of Material Samples for Examination and Analysis." 2010.

[54] T. H. Hyde, W. Sun, and S. J. Brett, "Application of Impression Creep Test Data for the Assessment of Service Exposed Power Plant Components," *Metall. J.*, vol. 58, pp. 138–145, 2010.

[55] B. Dogan, "Sampling and Small Punch Testing in the Power Generation Industry," *Determ. fo Mech. Prop. Mater. by Small Punch Test. Other Miniat. Test. Tech.*, 2010.

[56] J. P. Rouse, W. Sun, and T. H. Hyde, "The effects of scoop sampling on the creep behaviour of power plant straight pipes," *J. Strain Anal. Eng. Des.*, vol. 48, no. 8, pp. 494–511, 2013.

[57] S. J. Brett, J. H. Rantala, and S. Holmstrom, "Practical Application of Impression Creep Data to Power Plant," in *Baltica IX: Life Management and Maintenance for Power Plants*, 2013.

[58] W. Sun, T. H. Hyde, and S. J. Brett, "Application of impression creep data in life assessment of power plant materials at high temperatures," *Proc. Inst. Mech. Eng. Part L J. Mater. Des. Appl.*, vol. 222, no. 3, pp. 175–182, 2008.

[59] T. H. Hyde, W. Sun, and C. J. Hyde, *Applied Creep Mechanics*. Mcgraw Hill, 2014.

[60] Y. Li and R. Sturm, "Determination of Creep Properties from Small Punch Test," in *Pressure Vessels and Piping*, 2008, pp. 1–12.

[61] D. Blagoeva, Y. Z. Li, and R. C. Hurst, "Qualification of P91 welds through Small Punch creep testing," *J. Nucl. Mater.*, vol. 409, no. 2, pp. 124–130, 2011.

[62] T. H. Hyde, B. S. M. Ali, and W. Sun, "On the Determination of Material Creep Constants Using Miniature Creep Test Specimens," *J. Eng. Mater. Technol.*, vol. 136, no. 2, p. 021006, 2014.

[63] British Standards Institution, "Metallic materials — Uniaxial creep testing in tension — Method of test (ISO 204 : 2009)," 2009.

[64] D. Blagoeva, N. Taylor, and R. Hurst, "State-of-the-Art Report on Application of Miniaturized Testing Techniques to Support Life Management Decisions for Nuclear Plants," 2007.

[65] J. Shan, Z. Z. . Qian, and X. Ling, "Influence of Oxidation to Small Punch Creep Test," *Key Eng. Mater.*, vol. 353–358, pp. 461–464, 2007.

[66] T. H. Hyde and W. Sun, "Application of Impression Creep Test Data for the Assessment of Service Exposed Power Plant Components," *Metall. J.*, vol. 58, pp. 138–145, 2010.

[67] B. S. M. Ali, "Development of Non-Destructive Small Specimen Creep Testing Techniques," University of Nottingham, 2013.

[68] Y. Kadoya, T. Goto, S. Date, T. Yamauchi, T. Saida, and T. Sada, "Assesment of remaining life of fossil power plant parts by means of a miniature creep rupture test," *ISIJ Int.*, vol. 30, no. 10, pp. 854–861, 1990.

[69] S. J. Brett, "Small Scale Sampling and Impression Creep Testing Applied to Aged CrMoV Steam Pipework Systems," in *EPRI International Conference on Advances in Condition and Remaining Life Assessment for Fossil Power Plants Coal, Gas and HRSG*, 2012.

[70] T. H. Hyde, K. A. Yehia, and A. A. Becker, "Interpretation of Impression Creep Data Using a Reference Stress Approach," *Int. J. Mech. Sci.*, vol. 35, pp. 451–462, 1993.

[71] CEN (European Comitte for Standardisation), “Small Punch Test Method for Metallic Materials,” 2006.

[72] J. Chakrabarty, “A Theory of Stretch Forming over Hemispherical Punch Heads,” *Int. J. Mech. Sci.*, vol. 12, pp. 315–325, 1969.

[73] T. H. Hyde, M. Stoyanov, W. Sun, and C. J. Hyde, “On the Interpretation of Results from Small Punch Creep Tests,” *J. Stain Anal.*, vol. 45, pp. 141–164, 2009.

[74] F. Larson and J. Miller, “A Time-temperature Relationship for Rupture and Creep Stresses,” *ASME, Trans. J. Eng. Mater. Technol.*, vol. 74, pp. 765–775, 1952.

[75] T. Izaki, T. Kobayashi, J. Kusumoto, and A. Kanaya, “A creep life assessment method for boiler pipes using small punch creep test,” *Int. J. Press. Vessel. Pip.*, vol. 86, no. 9, pp. 637–642, 2009.

[76] Z. Abdallah, V. Gray, M. Whittaker, and K. Perkins, “A critical analysis of the conventionally employed creep lifing methods,” *Materials (Basel).*, vol. 7, no. 5, pp. 3371–3398, 2014.

[77] S. P. Jeffs, R. J. Lancaster, and T. E. Garcia, “Creep lifing methodologies applied to a single crystal superalloy by use of small scale test techniques,” *Mater. Sci. Eng. A*, vol. 636, pp. 529–535, 2015.

[78] B. Wilshire and P. J. Scharning, “Creep ductilities of 9-12% chromium steels,” *Scr. Mater.*, vol. 56, no. 12, pp. 1023–1026, 2007.

[79] M. Prager, “The Omega Method – An Engineering Approach to Life Assessment,” *J. Press. Vessel Technol.*, vol. 122, pp. 273–280, 2000.

[80] S. J. Brett, “Impression Creep Update,” 2017.

[81] B. Dogan, “Small Punch Testing and Applicaiton in Power Generation Industry,” in *Pressure Vessels & Piping*, 2011, pp. 1–10.

[82] S. J. Brett, “Case Study: Early type IV cracking on two retrofit grade 91 steel headers,” in *OMMI*, 2008, vol. 5, no. 2, pp. 1–13.

[83] S. J. Brett, “The Practical Application of Small Scale Sampling and lmpression Creep Testing to Grade 91 Components,” *7th Int. Conf. Adv. Mater. Technol. Foss. Power Plants*, 2013.

[84] F. Dobeš and K. Milička, “Application of creep small punch testing in

assessment of creep lifetime," *Mater. Sci. Eng. A*, vol. 510–511, no. C, pp. 440–443, 2009.

[85] B. Kim, "Small punch creep behavior and nondestructive evaluation of long term aged AISI 316L stainless steel," *Int. J. Precis. Eng. Manuf.*, vol. 14, no. 7, pp. 1267–1270, 2013.

[86] H. Nobakhti and N. Soltani, "Evaluating Small Punch Test as Accelerated Creep Test Using Larson–Miller Parameter," *Exp. Tech.*, vol. 40, no. 2, pp. 645–650, 2016.

[87] K. Harris and J. B. Wahl, "Improved single crystal superalloys, CMSX-4® (SLS) [La+Y] and CMSX-486®," *Superalloys 2004 (Tenth Int. Symp.*, no. Figure 1, pp. 45–52, 2004.

[88] K. Coleman and I. A. Shibli, "Failures of P91 Steel at the West Burton Plant in England Raise Concerns About the Long Term Behavior of the Advanced Steel," 2003.

[89] F. Abe, "1 - Grade 91 heat-resistant martensitic steel ," in *Coal Power Plant Materials and Life Assessment*, A. Shibli, Ed. Woodhead Publishing, 2014, pp. 3–51.

[90] L. Cipolla and J. Gabrel, "NEW CREEP RUPTURE ASSESSMENT OF GRADE 91," in *Super-High Strength Steels*, 2005, vol. 91, pp. 1–11.

[91] T. M. Pollock and S. Tin, "Nickel-Based Superalloys for Advanced Turbine Engines: Chemistry, Microstructure and Properties," *J. Propuls. Power*, vol. 22, no. 2, pp. 361–374, 2006.

[92] R. C. Reed, *The Superalloys: Fundamentals and Applications*. Cambridge University Press, 2006.

[93] Z. L. Kowalewski, D. R. Hayhurst, and B. F. Dyson, "Mechanisms-based Creep Constitutive Equations for an Aluminium Alloy," *J. Strain Anal.*, vol. 29, no. 4, pp. 309–316, 1994.

[94] S. N. G. Chu and J. C. M. Li, "Impression creep; a new creep test," *J. Mater. Sci.*, vol. 12, no. 11, pp. 2200–2208, 1977.

[95] C. Maharaj, J. P. Dear, and A. Morris, "A review of methods to estimate creep damage in low-alloy steel power station steam pipes," *Strain*, vol. 45, no. 4, pp. 316–331, 2009.

[96] T. H. Hyde and W. Sun, “Evaluation of conversion relationships for impression creep test at elevated temperatures,” *Int. J. Press. Vessel. Pip.*, vol. 86, no. 11, pp. 757–763, 2009.

[97] T. H. Hyde, W. Sun, A. A. Becker, and J. A. Williams, “Creep properties and failure assessment of new and fully repaired P91 pipe welds at 923 K,” *Proc. Inst. Mech. Eng. Part L J. Mater. Des. Appl.*, vol. 218, no. 3, pp. 211–222, 2004.

[98] W. Bendick, L. Cipolla, J. Gabrel, and J. Hald, “New ECCC assessment of creep rupture strength for steel grade X10CrMoVNb9-1 (Grade 91),” *Int. J. Press. Vessel. Pip.*, vol. 87, no. 6, pp. 304–309, 2010.

[99] Standards Measurement & Testing, “The Determination of Uncertainties in Creep Testing to European Standard prEN 10291,” 2000.

[100] F. Monkman and J. Grant, “An empirical relationship between rupture life and minimum creep rate in creep-rupture tests,” in *ASTM 56*, 1956, pp. 593–620.

[101] S. Chaudhuri and R. N. Ghosh, “Creep behavior of 2.25Cr1Mo steel-Effects of thermal ageing and pre-strain,” *Mater. Sci. Eng. A*, vol. 510–511, no. C, pp. 136–141, 2009.

[102] Q. Auzoux, L. Allais, C. Caës, I. Monnet, A. F. Gourgues, and A. Pineau, “Effect of pre-strain on creep of three AISI 316 austenitic stainless steels in relation to reheat cracking of weld-affected zones,” *J. Nucl. Mater.*, vol. 400, no. 2, pp. 127–137, 2010.

[103] A. Mehmanparast, C. M. Davies, D. W. Dean, and K. Nikbin, “Effects of plastic pre-straining level on the creep deformation, crack initiation and growth behaviour of 316H stainless steel,” *Int. J. Press. Vessel. Pip.*, vol. 141, pp. 1–10, 2016.

[104] A. Mehmanparast, C. M. Davies, D. W. Dean, and K. Nikbin, “Material pre-conditioning effects on the creep behaviour of 316H stainless steel,” *Int. J. Press. Vessel. Pip.*, vol. 108–109, pp. 88–93, 2013.

[105] Y. H. Zhang and D. M. Knowles, “Prestraining effect on the creep behaviour of nickel base C263 superalloy,” *Mater. Sci. Technol.*, vol. 18, pp. 917–923, 2002.

[106] D. F. Li, N. P. O'Dowd, C. M. Davies, and K. M. Nikbin, "A review of the effect of prior inelastic deformation on high temperature mechanical response of engineering alloys," *Int. J. Press. Vessel. Pip.*, vol. 87, no. 10, pp. 531–542, 2010.

[107] H. U. Prasanna and K. R. Udupa, "Probing the deterioration of 316L stainless steel welds due to ageing and creep by indentation creep tests," *Nucl. Eng. Des.*, vol. 241, no. 12, pp. 4938–4943, 2011.

[108] R. K. Heywood, "Elevated Temperature Tensile Test and Microstructure/Hardness Examination of P91 Header Material - Results of Test on Material 'As Supplied from the Mill' and after 'Anomolous Heat Treatment'."

[109] W. Sun, T. H. Hyde, and S. J. Brett, "Use of the Impression Creep Test Method for Determining Minimum Creep Strain Rate Data," *Small Sample Test Tech.*, vol. 44, no. 0, pp. 1–9.

[110] Dassault Systems, *Abaqus Theory Guide*, 6.14. 2014.

[111] K. Tai and T. Endo, "Effect of pre-creep on the succeeding creep behavior of a 2.25Cr1Mo steel," *Scr. Metall. Mater.*, vol. 29, no. 5, pp. 643–646, 1993.

[112] G. Sposito, C. Ward, P. Cawley, P. B. Nagy, and C. Scruby, "A review of non-destructive techniques for the detection of creep damage in power plant steels," *NDT E Int.*, vol. 43, no. 7, pp. 555–567, 2010.

[113] J. P. Rouse, W. Sun, and T. H. Hyde, "The Effects of Scoop Sampling on the Creep Behaviour of Power Plant Straight Pipes," *J. Strain Anal.*, vol. 48, no. 8, pp. 494–511, 2013.

[114] A. Dedov, I. Klevtsov, T. Lausama, and D. Neshumayev, "Method of Small Samples for Assessment of Properties of Power Plant Components: Sampling Devices and Stress Concentration in Dimples," in *Life Management and Maintenance for Power Plants*, 2007, vol. 2, pp. 180–192.

[115] British Standards Institution, "PD5500 - Specification for unfired fusion welded pressure vessels," 2012.

[116] X. Du, D. Liu, and Y. Liu, "Numerical limit load analysis of 3D pressure vessel with volume defect considering creep damage behavior," *Math. Probl. Eng.*, vol. 2015, 2015.

[117] J. Yang, J. S. Hsiao, M. Fong, and T. B. Gibbons, "The Application of Physically Based CDM Modeling in Prediction of Materials Properties and Component Lifetime," *J. Press. Vessel Technol.*, vol. 126, no. 3, p. 369, 2004.

[118] E. P. Busso, N. P. O'Dowd, and R. J. Dennis, "A Rate Depend Formulation for Void Growth in Single Crystal Materials," in *IUTAM Symposium on Creep in Structures*, 2000, pp. 41–50.

[119] G. A. Webster *et al.*, "A Code of Practice for conducting notched bar creep tests and for interpreting the data," *Fatigue Fract. Eng. Mater. Struct.*, vol. 27, no. 4, pp. 319–342, 2004.

[120] S. R. Holdsworth *et al.*, "Factors influencing creep model equation selection," *Int. J. Press. Vessel. Pip.*, vol. 85, no. 1–2, pp. 80–88, 2008.

[121] F. A. Leckie and D. R. Hayhurst, "Creep Rupture of Structures," *Proc. R. Soc. A*, vol. 340, no. 1622, 1974.

[122] T. H. Hyde and W. Sun, "Effect of bending load on the creep failure behaviour of a pressurised thick walled CrMoV pipe weldment," *Int. J. Press. Vessel. Pip.*, vol. 79, no. 5, pp. 331–339, 2002.

[123] W. Sun, T. H. Hyde, A. A. Becker, and J. A. Williams, "Steady-state creep reference rupture stresses for internally pressurised pipes for use in life prediction," *Int. J. Press. Vessel. Pip.*, vol. 79, no. 2, pp. 135–143, 2002.

[124] W. Sun and T. H. Hyde, "A potential method for determining the HAZ properties in welds using two-material impression creep test," *Acta Metall. Sin. (English Lett.*, vol. 17, no. 4, pp. 591–596, 2004.

APPENDIX

Python script used to determine frame during which crack initiation occurs

```
from abaqusConstants import * #import abaqus api
from odbAccess import *  # Allows for the access of odb files
import math  #basic mathematical operations

######################################################################


#Creat list of odb names
odb_list_names = ['Model_1','Model_2',……..]

# Initialise text file for data entry

g=open('Global_crack_init.txt','w')                #a to append w to write
g.write('Model\t crack_init\n')

#Cycle through odb list names to analyse each model individually

for vl in range(0,len(odb_list_names),1):
        #
        #Create path and objetcts
        #
        odbPath = odb_list_names[vl]+'.odb'
        #odbPath = "Drive:\Database\Folder\odbname"
        odb = session.openOdb(name=odbPath,readOnly=FALSE)
        #
        #Initialise element directories
        #
        myAssembly = odb.rootAssembly
        myInstance = myAssembly.instances['SECT-1']
        element = myInstance.elements
        node = myInstance.nodes

        allFrames = session.odbData[odbPath].steps['Step-2'].frames.keys()  #list the frames

        damage  = 0 #

        #Find crack initiation point using the element centriod values
        for i in range(len(allFrames)):                    #cycle through frames
          if damage >= 0.98:
            break
          frame = odb.steps['Step-2'].frames[i]              #define frame for iteration
          if 'SDV1' in frame.fieldOutputs:
            dam  = frame.fieldOutputs['SDV1']              #we want to look at damage
            damcent = dam.getSubset(position=CENTROID)         #look at centroid damage
```

```
                for v in damcent.values:                    #cycle through all elements in frame
                  damage = v.data
                  if damage >= 0.99:
                    break                                   #make damage variable the elemental damage value

            initFrame = frame.frameId                       #note the frame at which crack initiation happens

#           print odbPath

#           print "Crack initiation occurs at %s hours, frame %s"%(frame.frameValue,initFrame)

            g.write('%s\t %s\n'%(odb_list_names[vl],frame.frameValue))      #Write model name and life to text file
```

Python script used to extract coordinates of centroids and corresponding damage

```
from abaqusConstants import * #import abaqus api
from odbAccess import *  # Allows for the access of odb files
import math  #basic mathematical operations

######################################################################

odbPath = "Drive:\Database\Folder\Odbname.odb"
odb = session.openOdb(name=odbPath,readOnly=FALSE)

#Initialise element directories

myAssembly = odb.rootAssembly
myInstance = myAssembly.instances['PART-2-1']
element = myInstance.elements
node = myInstance.nodes

allFrames = session.odbData[odbPath].steps['Step-2'].frames.keys()  #list the frames

damage  = 0 #

#Find crack initiation point using the element centriod values
while True:
  if damage >= 0.99:
    break
  for i in range(len(allFrames)):                   #cycle through frames
    if damage >= 0.99:
      break
    frame = odb.steps['Step-2'].frames[i]               #define frame for iteration
```

```
    if 'SDV1' in frame.fieldOutputs:
      dam  = frame.fieldOutputs['SDV1']                    #we want to look at damage
      damint = dam.getSubset(position=INTEGRATION_POINT)      #look at integration point damage
      damcent = dam.getSubset(position=CENTROID)             #look at centroid damage
      for v in damcent.values:                             #cycle through all elements in frame
        damage = v.data
        if damage >= 0.99:
          break                                #make damage variable the elemental damage value

initFrame = frame.frameId                                  #note the frame at which crack initiation happens
print "Crack initiation occurs at %s hours"%(frame.frameValue)

# Initialise text file for data entry
g=open('odbname.txt','w')
g.write('x-coord\t y-coord\t damage\n')

# Write element centroid coordinates and their damage values for the whole model
for v1 in damcent.values:
  xc = 0
  yc = 0
  for v2 in element[v1.elementLabel].connectivity:
    xc = node[v2].coordinates[0] + xc                  #sum up the x-coordinates for the element
    yc = node[v2].coordinates[1] + yc                  #sum up the y-coordinates for the element
  avx = xc/len(element[v1.elementLabel].connectivity)      #obtain the centroid coordinates
  avy = yc/len(element[v1.elementLabel].connectivity)

  if 0 <= avy <= 10:                                 #Only write coordinates in range
    g.write('%s\t %s\t %s\n'%(node[v2].coordinates[0],node[v2].coordinates[1],v1.data))

g.close()
odb.close()
```